11/6/18/90 Sm (1)

#2

SANDIA REPORT

SAND90—0198 • UC—~~434~~ 712
Unlimited Release
Printed April 1990

Calculations for RADLAC, IBEX, and the RLA in 1989

James W. Poukey

Prepared by
Sandia National Laboratories
Albuquerque, New Mexico 87185 and Livermore, California 94550
for the United States Department of Energy
under Contract DE-AC04-76DP00789

Issued by Sandia National Laboratories, operated for the United States Department of Energy by Sandia Corporation.

Available to DOE and DOE contractors from
Office of Scientific and Technical Information
PO Box 62
Oak Ridge, TN 37831

Prices available from (615) 576-8401, FTS 626-8401

Available to the public from
National Technical Information Service
US Department of Commerce
5285 Port Royal Rd
Springfield, VA 22161

NTIS price codes
Printed copy: A04
Microfiche copy: A01

Distribution
Category UC-[redacted] 712

SAND--90-0198

DE90 010394

CALCULATIONS FOR RADLAC, IBEX, AND THE RLA IN 1989

James W. Poukey
Plasma Theory Division
Sandia National Laboratories
Albuquerque, New Mexico 87185

Abstract

This report presents the results of numerical modeling of the electron beam generation, transport, and conditioning in the Sandia accelerators RADLAC, IBEX, and RLA for the year 1989. The codes used were the particle code MAGIC, the trajectory code TRAJ, and some preliminary work with the 3-D code Quicksilver. The results are mostly in the areas of injector design, beam propagation in IFR channels and B_θ cells, and emittance measurements. The energy range of these electron beams is from 1 MeV to 20 MeV.

Outline

I. Introduction
II. RADLAC Injectors
  A. RADLAC 4 MV Injector
  B. RADLAC 8 MV Injector
  C. RADLAC 16 MV Injector
  D. IBEX Large Immersed Diode
III. RLA Injectors
  A. Foil/Aperture Diodes Without B_z
  B. "Laser" Diode
  C. Re-Entrant Non-Immersed Diode with B_z
  D. Small-Radius Immersed Diode

IV. Beam Emittance Measurement Studies
   A. Aperture Method
   B. Whole Beam Methods
      1. Recirc with Foil
      2. RADLAC after Extraction
V. Beam Conditioning and Propagation Studies
   A. B_θ Cell Calculations
      1. IBEX Vacuum Wire Cell
      2. RADLAC B_θ/Gas Cell
      3. Recirc Gas Cell Plus Wire
   B. Recirc IFR Shape and Foil Studies
   C. Recirc IFR Accelerating Gap
   D. Hermes III Beam Propagation with Foils and Wire Cells
   E. Hermes II Diode Plus Gas Cell
VI. RHEPP Diodes
VII. Preliminary Quicksilver Studies of Off-Center Beams
   A. Wire Guiding
   B. Gap Effects

I. Introduction

As in previous years it seems appropriate to summarize the recent computer work relevant to Sandia's electron beam accelerators RADLAC, IBEX, and RLA.[1-6] As before, the purpose is to organize and document the large number of simulations with MAGIC and TRAJ which were done in support of the ongoing experimental research and development for these devices. The work was done in collaboration with a number of people, primarily M. G. Mazarakis and C. A. Frost (1242), who suggested many problems and provided much input and feedback. Others who provided suggestions and input include M. Buttram (1248), R. C. Platt (SAI), T. W. L. Sanford (1231), J. T. Crow (1241), S. Shope (1242), J. R. Freeman (1241), and R. Coats (1241).

The continuing quest for a good RADLAC injector is discussed in Sec. II, where the emphasis is on going to higher voltages via the Helia/Hermes III technique of voltage addition. In Sec. III we discuss calculations for all four of the present candidate diodes for RLA; the main new feature here is the use of ions to control the electron focus in B_z-free apertured diodes.

Since the goal of these machines is to produce a good-quality beam, methods to measure beam emittance are of great interest; in Sec. IV we discuss calculations which illustrate the advantages and difficulties of several of these methods.

The complex issues of beam propagation and acceleration in IFR channels and B_θ cells are considered in Sec. V. Some MAGIC simulations for the high-current Hermes II and Hermes III beams are also discussed in this section.

Some early simulations of a possible RHEPP diode are summarized in Sec. VI. Only some basic diode designs are discussed; rep-rate considerations are not included.

Finally, in Sec. VII a few preliminary runs of off-center electron beams near current-carrying wires and passing through accelerating gaps are shown. The results here are somewhat inconclusive, partly because some aspects of the code needed for such problems are still under development, and partly because of the considerable expense of running realistic geometries.

II. RADLAC Injectors

There are several advantages to using a higher-voltage diode in RADLAC, including a stiffer beam and fewer accelerating gaps and field coils. We begin with the present 2-feed, 4 MV system and then consider the upcoming 4-feed, 8 MV injector. Then we show some runs (diode only, individual feeds not calculated) for a 16 MV injector which would eliminate the accelerating gaps entirely; this is sometimes referred to as the "SMILE" RADLAC. Finally, a large-radius immersed IBEX diode is briefly discussed.

A. RADLAC 4 MV Injector

The setup for the MAGIC runs is shown in Fig. 1a. The goal here is to match the experiment as closely as possible, including the applied B field of 12 kG in the beam region, the measured input V(t) in each feed (Fig. 1b), and a 200 kV/cm emission threshold on the cathode. An electron map at t = 37.5 ns, when V(diode) is peaked at about 3.5 MV and is slowly varying, is given in Fig. 1c.

The simulation in Fig. 1 used 46,000 cells, 24,000 electron rings (at a typical timestep), and 9 hours of Cray time. One of the goals is to study the time-dependence of the leakage current (7 kA in Fig. 1c); to aid in this a particle movie over the whole pulse was produced. The movie shows no loss to the insulators in the feeds, although electrons at early times do hit the left-hand metal prong near feed 1. That there must be some leakage in this type of injector is due to the fact that B_z decreases back from the cathode tip (Fig. 1a), so that there is a region between B_z-insulation and self-B_θ-insulation where the B lines spiral outwards, allowing electrons to follow these lines to the metal separator (Fig. 1c).

Although the A-K gap (1.6 cm) region is not very well resolved, the simulation and movie do show production of a reasonably good 40 kA beam exiting the rhs of Fig. 1c. The beam emittance, due to cyclotron oscillations, can be improved with a stronger applied B.

B. RADLAC 8 MV Injector

The problem setup is given in Fig. 2, which shows the 4 feeds and a B line for a "steady-state" run with 2 MV/feed, 8 MV total diode voltage, 6 cm A-K gap, a 50 kA beam (not annular) with 25 kA leakage to a metal divider. The time-dependent runs used the V(t) in Fig. 3, where (a) is the input per feed and (b) is the total V(diode). The results are summarized in Table I and illustrated in Figs. 4 and 5. The main variations are in applied B strength and cathode emission threshold. As seen in Fig. 3, the 4 feed voltages, which peak at 2 MV at 30 ns, add up at the A-K gap to give

Table I. Summary of RADLAC Injector 4-feed MAGIC runs; all cases with A-K gap = 6 cm. E_{thr} = cathode emission threshold

Case	E_{thr}	V(t)	B_z^{gap}	I_b^{max}	I_{leak}^{max}	Output beam quality	Early leakage
3	10 kV/cm	Steady 8 MV	20 kG	50 kA	25 kA	ok	
4	10 kV/cm	Fig. 3, Peak 7 MV	20 kG	43 kA	24 kA	ok	~1 kA max
5	10 kV/cm	Peak 6.7 MV	13 kG	50 kA	18 kA	Poor	~1 kA max
7	200 kV/cm	Peak 6.4 MV	20 kG	43 kA	24 kA	ok	300 A max(insul)

a peak of 7 MV at 43 ns (this is a large system). In Fig. 4a for B_z = 13 kG (at A-K gap) and low emission threshold (case 5, Table I), note that at early t = 7.5 ns about 1 kA is being lost to various places because the beam current I_b has not grown enough to establish self-B_θ insulation on the shank. This loss only lasts a few ns, however; by 15 ns the only loss is to the metal divider as in Fig. 2. The movie for case 5 shows the fast onset and decay of this early loss, and also shows a nearly

unchanging flow pattern after about 20 ns; the late-time flow is shown in Fig. 4b (compare Fig. 2).

If B_z (gap) is increased to 20 kG (case 4, Table I), nearly the same result is obtained (compare Figs. 5a and 4b) except the loss is increased slightly during the main part of the pulse, and the output beam has better quality (lower $\beta_\perp$). The leakage during the main part of the pulse is 24 kA, again to the metal divider. The most realistic case (run 7, Table I) at 200 kV/cm, 20 kG is shown at 30 ns in Fig. 5b. The basic result near peak voltage is about the same as case 4, Table I, but in this case a careful analysis of the early-time leakage was done, calculating losses to insulators and metal dividers, as shown in Table II.

Table II. Details of early-time leakage for run 7, Table I (Fig. 5b) with threshold 200 kV/cm

Δt	Leakage to insulator	Leakage to metal
0 - 10.5 ns	none	none
10.5 - 12 ns	307 A	none
12 - 13.5 ns	285 A	1.0 kA
13.5 - 15 ns	none	2.2 kA
15 ns -	none	24 kA max

The maximum electron energy to the insulator is about 600 keV. The rearmost part of the cathode shank never turns on for this threshold (compare Figs. 5b [case 7] and 5a [case 4]). Again, a movie made the details easier to visualize.

A numerical problem with these "whole injector" runs is that the A-K gap region is not well resolved, so that the output beam properties may not be calculated accurately. To check this, a model for part of the injector was developed, and a case for B_z (gap) = 19 kG is shown in Fig. 6. This model is a compromise between simulating the whole injector, Figs. 1-5, and simulating only the diode (see below). Only feed #3 (Fig. 4a) is explicitly included; the other voltages are applied from the ends (4 MV lhs, 2 MV rhs) as shown. The time-dependent aspects are not included; these cases were simply run until an 8 MV steady-state was reached. In Fig. 6, the output beam is 57 kA with $\beta_\perp$ = 0.07 and the leakage is 26 kA. Comparing Fig. 5a, the results are qualitatively the same, but there are some differences: in the better-resolved Fig. 6, the V(max) = 8 MV is higher, leading to higher I_b = 57 kA and consequently a thinner sheath on the shank. The output $\beta_\perp$ is slightly lower (but the beam is not phase-mixed). Reducing B_z to 12 kG has the effects of increasing I_b to 63 kA while decreasing the leakage to 20 kA (same V and I[total]); while beam quality suffers somewhat, the difference is not drastic and the emittance is better than in Fig. 4b (13 kG), showing that some of the output emittance there was numerical in origin. Finally the case in Fig. 6 was repeated with smaller gap = 4 cm and lower applied V = 6 MV (total); the flow appears almost identical but I_b decreases to 45 kA (steady state), and the leakage also decreases (20 kA); beam quality improves slightly.

The best possible resolution of the A-K gap is obtained by simulating the diode alone with a uniform applied B_z. Figure 7 shows the results for B_z = 19 kG (7a) and 13 kG (7b). Figure 7a agrees well with Fig. 6, suggesting that the resolution (spatial) in the latter "partial" model is adequate for predicting beam properties. However, some care must be used in comparing output beam emittance (i.e., $\beta_\perp$ and radius) in these figures, because the beams are not yet phase-mixed. Figure 7b at the lower B_z clearly has larger radial oscillations and a thicker shank sheath. The contributions of the shank in Figs. 7a and 7b are 60% and 73%.

C. RADLAC 16 MV Injector

The rather complicated setup for MAGIC runs of the 16 MV RADLAC "SMILE" injector is shown in Fig. 8a. Here we assume that the 8 feeds have produced a flat-top voltage of 16 MV. There is an applied B_z, but it is only local, near the cathode tip; its purpose is to focus the beam through the aperture and spin it up so that the angular momentum will prevent beam loss to the wire. The "cell" past the thin anode foil is a combination gas and wire cell; the gas for charge neutralization and the wire (carrying an externally applied current I_ω) for centering and focusing. In MAGIC, the gas was modeled simply by setting E = 0, and the wire by a perfectly conducting metal boundary a few cells in radius which contributes a $B_\theta = \mu_0 I_\omega / 2\pi r$. From P_θ conservation we can estimate the wire size needed so that most of the beam cannot reach the wire surface.

A typical steady-state result is given in Fig. 8b. Here the aperture radius $r_{ap} = r_k = 0.96$ cm. The beam current which propagates through the cell is very sensitive to r_{ap}; in Fig. 8b about 60 kA hits the aperture, while for r_{ap} = 1.14 cm only 1 kA is lost. The total diode current for V = 16 MV, gap = 16 cm is 137 kA; for the case shown we obtain 40 kA beam, 60 kA loss to aperture, 7 kA loss to the wire, and 29 kA radial leakage. The 20 kG field in the A-K gap seems nearly optimal; for 10 kG about 110 kA hits the wire (P_θ too low), and for 30 kG the radial loss is 44 kA. Clearly, larger B_z is better than smaller.

The output beam $\beta_\perp = 0.24$, about as one expects since $(\nu_\omega f/\gamma)^{1/2} = 0.20$, where $\nu_\omega = I_\omega/17$ kA. The value of I_ω = 20 kA in Fig. 8b; this seems sufficient since if I_ω = 10 kA we obtain a beam radius in the cell which is too large (a few electrons scrape the wall); on the other hand the output beam is cooler, $\beta_\perp = 0.16$.

We emphasize that this RADLAC injector is speculative, and there is no plan as of January 1990 to try it in the lab. However, the simulations look promising, and the success of the Helia and Hermes III voltage adders suggest that the SMILE approach is worth pursuing.

D. IBEX Large Immersed Diode

We include this topic here since it is basically similar to the RADLAC diodes (annular and immersed). Figure 9 shows a MAGIC run at B_z = 16 kG (uniform), with V = 3.5 MV and the resulting I_b = 23 kA (out at $\beta_\perp = 0.14$ but not phase-mixed). The output served as a source for some IPROP runs by D. Welch (MRC), to see how such a beam could be conditioned in a B_θ cell.

A problem with this diode is the large P_θ; after extraction from the field the rotation would be c/2. And, we cannot decrease B_z much; rerunning with B_z = 10 kG leads to much larger radial oscillations and a few kA loss on the aperture.

III. RLA Injectors

There are four basic candidate diodes being considered as the injector for the RLA.[7] In this section we describe recent simulation results for each type.

A. Foil/Aperture Diodes without B_z

The MAGIC run in Fig. 10a illustrates the difficulty of explaining the experimental result of 15-20 kA out the IFR channel of a RLA foil/aperture injector. The simulation is set up like the experiment as closely as possible, with a 7 cm A-K gap, 3.7 MV applied, and an aperture (r_{ap} = 1.5 cm) and thin foil separating the vacuum diode from the IFR channel (needed to transport the beam to the racetrack[7]). Only 5 kA is produced as beam current (out of 56 kA total).

One possible explanation is that there is somehow a plasma formed in the A-K gap. Figure 10b and Table III show that if this plasma density is 1.5 X 10^{12} cm^{-3} to 2.0 X 10^{12} cm^{-3}, then I_b(rhs) will match the experiment.

Table III. Effect of gap plasma on output beam for experimental RLA-IBEX injector
Parameters: gap = 7 cm, V = 3.7 MV, r_{ap} = 1.5 cm, I(total) = 57 kA

n_{plas}^{gap}	I (to aper.)	I(rhs)	$\beta_\perp$ (at foil)
0	28 kA	5 kA	0.12
1 X 10^{12}	34 kA	10 kA	0.27
1.5 X 10^{12}	35 kA	14 kA	0.32
2 X 10^{12}	36 kA	18 kA	0.36
1 X 10^{13}	42 kA	35 kA	0.45

The effect of the plasma ions, after the plasma electrons have been blown away, is to reduce the radial E field, allowing B_θ to focus more of the beam through the thin foil. Another possible explanation is shown in Fig. 10c; here we have merely reduced the A-K gap, causing more current to be emitted from the cathode tip and pass through the foil. Physically, it is difficult to justify either explanation: there is no obvious mechanism for producing a gap plasma during the voltage pulse, and the physical gap is 7 cm, with presumably negligible closure.

Inclusion of the complete shank does not seem relevant to the main issue here, so we now look only at emission near the small-radius cathode tip. The run in Fig. 11a (vacuum everywhere) reveals the same problem as Fig. 10a: most of the current (23 kA total at V = 4 MV) hits the aperture. Again, gap closure can resolve the problem (Fig. 11b), but begs the question.

The key here seems to be the emission of ions from the aperture. This seems reasonable since at early times the beam will deposit considerable energy into the aperture surface (Fig. 11a). For the MAGIC run of Figs. 12-14, we used the experimental V(t) as input (Fig. 12a), because the problem is clearly a time-dependent one. The output beam current vs. time in Fig. 12b shows that a peak of 20 to 30 kA can be produced by including ions (protons) emitted from the aperture surface. The details of the system behavior are best seen from the particle movie, showing electrons blowing out radially at early times before the ions have crossed the gap (Fig. 13); then pinching in almost to the aperture opening as in Fig. 11a and holding there until the ions fill the gap; and finally focusing through the opening in the aperture (partially covered by a thin foil) and propagating along the IFR channel (Fig. 14). The beam current fluctuates, then decays with the voltage (Fig. 12b). The maximum beam current is 28 kA, the maximum ion current is 800 A (at 27 ns).

The mechanism for the oscillations seen in Fig. 12b is apparently a relaxation oscillation; after the first beam focusing the ion emission decreases and the beam defocuses, increasing the ion emission again and leading to more focusing. An obvious question concerns how many ions are needed to cause the beam focusing. Several runs were made varying the emission area on the aperture surface; for an outer emission radius of 3.2 cm or greater, the focus occurs; for 2.4 cm or less, it does not. Going to a very large emission radius does not change the results of Figs. 12-14 much; apparently adding ions at large radius does not affect the beam dynamics appreciably.

For this type of diode, ions are generally important, but the details of their effects may vary considerably for different parameters. Figure 15a shows a MAGIC run of the RLA 1 MV diode with A-K gap = 2 cm without ion emission from the aperture. The result is about 8 kA total, with only 700 A down the channel. Adding ion emission from the aperture out to r = 5 cm still does not focus the beam (Fig. 15b), although I (total) increases to 11 kA, I_b (rhs) = 1.3 kA, with I_i = 280 A (steady state run). Opening the A-K gap to 3 cm does not change the result much, whether or not we include a thin foil across the aperture opening, as in Fig. 15c.

Later experiments with the 1 MV RLA diode employed a smaller gap and larger cathode radius. As seen in Fig. 16a (no ions) and 16b (with ions from aperture in $0.8 < r < 2.0$ cm), some current propagates even without ions (simply because of the large cathode tip area and smaller gap), but the ions still have important effects: over twice as much current propagates in Fig. 16b. By going to still larger cathodes one might obtain the desired beam currents without needing ions, as seen previously in Figs. 20 and 21 of Ref. 1, or Fig. 10c here.

B. IFR Diode

By "IFR diode" we mean a system without B_z when the IFR channel is preformed by a laser and extends all the way to the cathode tip. Figure 17 shows an example at 4 MV, 48 kA (total) with an 11 kA beam propagating. Here the A-K gap = 2 cm and r(channel) = r(aperture) = 8 mm, with $n_{ch} = 2.75 \times 10^{11}$ cm^{-3}. Note that Fig. 17 looks much like Fig. 16a; in fact the only real difference is that the plasma (heavy ions) extends into the A-K gap in the "IFR" case. (Of course the latter IBEX case has much higher voltage and current.) From n_{ch}, we expect $f_e = 0.25$ if all

plasma electrons are expelled, and we obtain nearly this value in equilibrium, $f_e = 0.22$.

A variety of parameter variations were performed, including varying the A-K gap, cathode geometry, aperture size, channel density and radius. The basic results are as found for the plasma-in-gap runs, e.g. Fig. 10b; the output beam is quite sensitive to these details (e.g., Table III), because the presence of ions in the A-K gap strongly affects the beam dynamics there. Probably the real question here concerns the experimental "tunability" of such a diode, and we might expect the problems of alignment and azimuthal symmetry to be crucial in producing a good beam.

C. Re-Entrant Non-Immersed Diode with B_z

We turn now to "cold" injectors using an applied B_z to focus the beam into the IFR channel. Probably the most promising non-immersed injector setup is shown in Fig. 18a. This system is under construction as of January 1990. Voltage waves of about 1 MV each are fed into the four feeds. The addition of these waves was studied with and without beam formation and appears to work well; the total diode voltage vs. t using the experimental input feed voltages is shown for a case with beam emission in Fig. 18b. Note that V(diode) is roughly flat and above 4 MV for $30 < t < 60$ ns. According to Jason runs, the electric stresses on non-emitting surfaces are acceptably low. The magnetic field (Fig. 18a) is produced by coils inside the anode stalk. The flux linking the cathode, while not zero, is low enough (< 100 G) to preclude beam rotation problems. The peak B_z on axis is about 1.2 kG, and this field leads to a nice focus for a 10 kA beam (Fig. 18c). The IFR channel into which the beam is focused begins at the thin foil at z = 122 cm. For the case shown, $r_{ch} = 2$ cm and $n_{ch} = 8 \times 10^{10}$ cm^{-3} (sharp-edge, uniform channel).

Although this problem is treated by MAGIC as a time-dependent one (because the input V varies in t, primarily), for 30-60 ns conditions are steady enough that one can reasonably define potential lines, as in Fig. 18d. Note that $\phi(z)$ across the main 20 cm A-K gap is not linear; we will discuss this point further below.

The run shown in Fig. 18, though interesting and perhaps necessary, took over three hours of Cray time. For parameter and optimization studies, it is unnecessary and uneconomical to use MAGIC, so for these we isolate the beam region, apply a steady voltage of about 4 MV, and use the trajectory code TRAJ. A typical case is shown in Fig. 19, where parts (a)-(c) show applied potential lines and general setup, applied B lines, and a set of trajectories (one in five is plotted).

The only electric field boundary condition which is not obvious is the applied gap voltage $\phi_g(z)$; see the upper left corner of Fig. 19a. It was mentioned in connection with Fig. 18d that $\phi_g(z)$ is not linear, so code studies were done concerning the sensitivity to this assumed function. In view of the "Pierce insert" studies of last year (Ref. 1, pp. 4 and 5), it should not be surprising that there is some sensitivity to $\phi_g(z)$; changing it from linear (constant E_z) to a function approximating that in Fig. 18d (potentials compressed toward anode), reduces I_b from 10.5 kA to 8.9 kA for a particular set of parameters; thus for our TRAJ model we used the "realistic" $\phi_g(z)$, as in Fig. 19a.

The applied B lines in Fig. 19b are approximately the same shape as in Fig. 18a. but the magnitude is weaker (628 G in the flat part, on axis; 33 G at the cathode). This is partly because the "focal length" (i.e., distance from cathode emitter to foil) is about twice as long in Fig. 19, and partly to illustrate how the beam expands before focusing if the field is too weak (Fig. 19c). In Fig. 20 we show a trajectory map for conditions matching the MAGIC run of Fig. 18 fairly well, except that f = 1 in the IFR channel, and d = 17 cm. Comparing Figs. 18c and 20, the flows differ slightly, but the current and output beam quality agree rather well. (The beam quality agreement is somewhat fortuitous since the TRAJ run follows the beam in the channel far enough for phase mixing to occur, whereas the MAGIC run clearly does not.) The final TRAJ value of $\beta_\perp = 0.21$ in Fig. 19c is slightly higher than the equilibrium $(\nu f/\gamma)^{1/2} = 0.17$, but the agreement in Fig. 20 is quite good ($\beta_\perp = 0.25$).

The case in Fig. 20 is near optimum in terms of the desired beam produced. Many parameter variations about this case were run, and some variations were made about the longer-length case in Fig. 19. Of course one type of variation is of the numerical parameters, to check zoning, number of trajectories needed, etc. The most significant physical variations were probably of the voltage and applied B. Here we will just summarize some of the main results.

Roughly speaking, the voltage and B_z must be controlled to within 10%. For example, if in Fig. 19c we drop V from 4.0 to 3.5 MV, the beam focuses about 20 cm before the foil (I = 7.6 kA), but the output beam quality is about the same. Raising V to 4.5 MV leads to I = 10.5 kA, and a beam focus inside the channel, leading to subsequent overfocus and a 1.6 kA loss. Voltage errors greater than 0.5 MV give results too poor to consider; generally it seems better to err on the high side. For voltage variations about the shorter-length Fig. 20 we find the same qualitative result, but the voltage tolerance is smaller (because of the shorter focal length, the system is somewhat more sensitive).

In terms of magnetic field variations, increasing B_z by 7% in Fig. 19c causes the first focus at about 15-20 cm before the foil, but the output beam is nearly the same. A 7% decrease, however, leads to a 1.8 kA loss in the diode; again, it is better to err on the high side. For the shorter length case (Fig. 20), the same rough conclusion holds; only small variations in the design B field are permitted if we wish to avoid beam loss.

Between the short and long systems of Figs. 19 and 20, there is no clear choice; either can be made to work by tuning B_z for given (flat-top) voltage. The shorter system is slightly more sensitive to error and requires a larger B_z (roughly, $B_z \propto L^{-1/2}$) but a shorter solenoid. Either system, or any length in between, should be suitable. Note that very fine tuning, even if possible, is not useful, because the beam always pinches tightly past the foil and phase mixes to $r_b \gtrsim r_{ch}$ and $\beta_\perp \gtrsim (\nu f/\gamma)^{1/2}$.

D. Small-Radius Immersed Diode

This last candidate for the RLA injector was briefly discussed in last year's report (Rep. 1, Fig. 31). The main problem with such a diode (besides the inconvenience of making a strong $B_z = 20$ kG over substantial volume) is the non-zero P_θ, leading to rotation of the final extracted beam. However, if the cathode is

sufficiently small in radius, then P_θ and the final β_θ can also be kept small, even at 4 MeV. The beam in Fig. 31 of Ref. 1 has parameters 12 kA, $\beta_\perp = 0.17$ in the field, and a final $\beta_\theta^{max} = c/6$ after extraction. Of course a small drift tube must be used to avoid space-charge-limit problems, and a rotating beam may not be as good for racetrack transport. Nevertheless, this immersed diode has advantages in terms of sensitivity to parameter variations and perhaps reproducibility, and remains a viable option.

IV. Beam Emittance Measurement Studies

The basic idea of this measurement is to use vacuum expansion of an electron beam to deduce its initial $\beta_\perp$.[8,9] In a situation where space-charge and B_θ effects nearly cancel so that the expansion is emittance-driven, the rms radius vs. distance z is given by[8,9]

$$r_{rms}^2 = r_0^2 + \left(\beta_{\perp 0}^2 + \left. \frac{dr}{dz} \right|_0^2 \right) z^2 - 2 r_0 \left. \frac{dr}{dz} \right|_0 z \qquad (1)$$

where r_0 and $dr/dz|_0$ are initial radius (rms) and absolute slope of the beam envelope, and $\beta_{\perp 0}$ is the initial transverse velocity/c. We divide the studies into two types: expansion of an apertured beam and expansion of the entire beam after passing through a foil or being extracted from a B_z.

A. Aperture Method

Figure 21 illustrates the problem for an IBEX-type beam in an IFR channel (f = 1/2). The 10 kA, $\gamma = 8$ beam (e.g., the output of a RLA injector) with equilibrium $\beta_\perp = 0.18$, $r_b = 1.5$ cm (rms) is incident on an aperture with a hole of radius $r_{ap} = 3$ mm. About 400 A passes through the hole and expands in vacuum for a short distance, then hits a target where r_{rms} is measured. Knowing r_0 and $dr/dz|_0$ at the hole, $\beta_{\perp 0}$ can be found from Eq. (1). For the case in Fig. 21, TRAJ was used with 200 trajectories; the input beam is uniform in density out to r(edge) = 2.1 cm. There is no B_z or net beam rotation.

An obvious problem here is statistics. In Fig. 21a, only 5% of the trajectories pass through the hole. Another issue is that this method only measures the "axial" emittance; electrons with large V_θ cannot reach the hole due to P_θ conservation. This is shown most clearly by phase space plots before and after the hole. Thus, while the $r_{rms}(z)$ plot in Fig. 21b can be used to deduce a $\beta_{\perp 0}$, there is considerable uncertainty in relating this $\beta_{\perp 0}$ to the real rms $\beta_\perp$ of the whole beam. Note, incidentally, the foil-pinch effect[4] in Fig. 21b; although small, it yields a $dr/dz|_0 \neq 0$, and must be evaluated to find $\beta_{\perp 0}$.

TRAJ runs with Gaussian radial profiles, perhaps more physically realistic, were also made. This adds the uncertainty of the cutoff radius, and necessitates following many low-weight trajectories in the "wings". An example is shown in Fig. 22, again for 10 kA, $\gamma = 8$, $\beta_\perp = 0.18$, f = 1/2 (note the parameters yield equilibrium). Only 3% of the 320 trajectories (Fig. 22a) pass through the hole, a current of 576 A. This is enough to yield a small electric field past the hole (Fig. 22b), but the expansion there is

still emittance dominated. The $r_{rms}(z)$ plot (Fig. 22c) yields a value at the target of r_{rms} = 5.4 mm, agreeing with Eq. (1) to within 10%, perhaps somewhat fortuitous.

We can vastly improve the accuracy of the calculation by just simulating the vacuum-expansion region. Of course this assumes we know the input beam parameters (in the hole), and begs the question of measuring $\beta_\perp$ for the whole beam. Figure 23a shows such a TRAJ run, for a 395 A, γ = 8 beam with $\beta_\perp$ = 0.18; note that 55 A scrapes off on the aperture itself. Comparison with Eq. (1) is excellent: the code value of r_{rms} at the target is 5.0 mm, while Eq. (1) yields 4.9 mm. Figure 23b shows the same system with a cold input beam; note that space-charge expansion is completely negligible, verifying that the expansion in part (a) is indeed emittance driven. Further comparisons between code and theory can be found in Table I, Ref. 9, including cases with non-zero $dr/dz|_0$. An example of the latter is given in Fig. 24. The initial focus is given by $\beta_r = -0.15r/r_{ap}$. As seen in Fig. 24b, the beam focuses slightly before expanding. Agreement with Eq. (1) is good but not perfect: about 7% difference in r_{rms} at z = 2.5 cm. We used 240 trajectories here.

B. Whole Beam Methods

1. RLA with foil

Can the same vacuum expansion technique be used to measure $\beta_{\perp 0}$ for a whole beam? Under some conditions, the answer is yes. Figure 25 shows a 10 kA, γ = 8 (IBEX/RLA) case with an input Gaussian beam (r_0 = 1.5 cm, rms; r(cutoff) = 4 cm), no B_z or rotation, and $\beta_{\perp 0}$ = 0.18. The IFR channel on the left of the foil has f_e = 1/2; the beam is in equilibrium until the foil pinch[4] begins a few cm from the foil (Fig. 25c); the wall loss (Fig. 25a) is negligible. The code result for r_{rms} (target) is 3.0 cm, to be compared with 3.1 cm from Eq. (1). It is perhaps surprising that space-charge effects are not contributing for the expansion length of 15 cm (foil to target). As shown in Fig. 25b, the potential well depth is 1 MV, small but not negligible for a γ = 8 beam, but recall that the space charge E_r tends to be canceled by $V_z B_\theta$ to $1/\gamma^2$, leaving emittance as the main expansion force. An analytic estimate of the space-charge doubling length is 47 cm.[6] The method appears to work.

If we run the same case except $\beta_{\perp 0}$ = 0.26, we must increase f to 1.0 for equilibrium before the foil. After the foil (very small foil pinch effect here) we obtain r_{rms} (target) = 4.4 cm, vs. 4.3 cm from Eq. (1). Thus the measurement should work for warmer beams. For cooler beams such as $\beta_{\perp 0}$ = 0.09, Fig. 26, we need f_e = 0.11 for equilibrium, and a very large foil pinch is found, dr/dz(foil) = 0.1 from TRAJ. The agreement with Eq. (1) is surprisingly good, but as seen in Fig. 26 the pinch effect is so large that the expansion length of 15 cm only allows the beam to expand to 1.47 cm (theory 1.36 cm), less than the input r_0 = 1.5 cm(rms). Clearly for a good measurement a longer expansion length is needed, and the space-charge correction will become non-negligible.

Thus the whole-beam/foil method seems better for warm beams. Another problem is that if $\beta_\perp$ is a function of r, the method gives no information about this dependence; perhaps concentric apertures or "pepper pots" would be more appropriate diagnostics. Finally, there is the drawback that to use Eq. (1) to find $\beta_{\perp 0}$, dr/dz(foil)

must be calculated; the semi-empirical formulas[9] may be helpful, but the only certain way is to use TRAJ. In short, measurements must be supplemented with code runs to deduce the emittance in the general case, and the geometry must be chosen carefully.

2. RADLAC After Extraction

To use vacuum expansion to measure the emittance of the RADLAC beam, we must take into account some different effects (see Fig. 27). The RADLAC beam is annular, higher energy, and must be extracted from a guide B_z, so that VXB_z forces and rotation also contribute, besides emittance. Thus Eq. (1) cannot be used.

In Fig. 27a we plot the B lines at the end of RADLAC, i.e., the extraction region. The goal is to deduce $\beta_{\perp 0}$ of the equilibrium beam in the field (15 kG in this example) from the beam pattern on the target (i.e., the rhs conductor). Assuming a 40 kA, 15 MeV annular beam, Figs. 27b and 27c show the TRAJ equilibria for $\beta_{\perp 0} = 0$ and 0.156. Note from Fig. 27b that a cold beam expands and becomes thicker; this is not due to E_r and B_θ forces, which cancel due to the high $\gamma = 30$ ($\gamma_{in} = 26$, since some of the 15 MeV is in potential energy). The expansion is due to rotation (centrifugal and $V_\theta B_z$ forces); the Eqs. of motion and P_θ conservation can be written and solved, but the result is much more complex than Eq. (1), so we have constructed a technique based on TRAJ runs (typical run takes 30 sec. on Cray).

Table IV shows the beam expansion results r_{rms}^{out}, Δr^{out}, and I_b^{out} vs. $\beta_{\perp 0}$ for the system of Fig. 27. Note that as $\beta_{\perp 0}$ increases, r_{rms}^{out} decreases (compare Figs. 27b and c). Δr^{out}, on the other hand, increases rapidly with $\beta_{\perp 0}$, and it is this which should be used to measure $\beta_{\perp 0}$. However, note that for $\beta_{\perp 0} > 0.117$ some beam hits the outer wall, and for $\beta_{\perp 0} > 0.234$ the beam covers the target, putting limits on the technique for a given expansion length. Nevertheless, for typical expected output RADLAC $\beta_{\perp 0}$ values 0.15, the method seems viable. Two serious questions remain: (1) How does one actually determine Δr^{out}? and (2) Can a thin foil be inserted in the full-field region to determine the input beam parameters necessary for the TRAJ model?

Figures 28a-c show a $\beta_{\perp 0} = 0.08$ case using 200 trajectories. The $j_z(r)$ current density profiles at input ($z = 0$ in Fig. 28a)

Table IV. RADLAC beam: Vacuum Expansion after extraction from 15 kG vs. $\beta_\perp^{in}$

$\beta_\perp^{in}$	r_{rms}^{out}(cm)	Δr^{out}(cm)	I_b^{out}(kA)
0.0	3.6	1.4	40
0.078	3.6	1.9	40
0.117	3.5	2.7	38
0.156	3.4	3.2	35
0.234	3.0	4.8	28
>0.24	--	4.8	--

Parameters: 40 kA, 15 MeV, annular 8,12 mm,
R_{wall} = 4.8 cm, B_0 = 15 kG
β_θ(final), theory and code: 0.044 @ r_b(final) = 3.5 cm

Conclusion: must use Δr^{out} to deduce $\beta_\perp{}^{in}$, not r_{rms}^{out}

---

and output (z = 32 cm) are given in Figs. 28b and c. In Fig. 27 and Table IV, Δr^{out} was simply obtained from trajectory plots and a ruler; to correlate with a laboratory measurement we need to use some width in the $j_z(r)$ plots. The width at 25% of maximum seems to agree well with the cruder method; but presumably it does not really matter exactly how Δr^{out} is defined, provided we are consistent. Again, note that Δr^{out} cannot have meaning if some beam is lost to the outer wall at r = 4.8 cm; in this event a shorter expansion length must be used, and a new TRAJ table generated. Figure 28d shows that using more trajectories (400 instead of 200) does not buy much; however, dropping to 100 trajectories yields too much "noise" in $j_z(r)$ out.

Some parameter variations were made to check sensitivity. Varying I_b showed that the method is not sensitive to beam current (and that space-charge effects are not important). Increasing Δr^{in} merely increased Δr^{out} by the same amount (approx). Varying $B_z(z = 0)$ showed considerable sensitivity, so this must be known accurately.

The second question raised above concerns the possibility of inserting a thin foil in the full-field in order to measure all the required quantities on a single shot. The answer for the type of parameters being considered is negative, as shown in Fig. 29, which is nearly like Fig. 27b except for the foil inserted. The foil causes the beam to pinch and expand at smaller z. To compensate, one would have to move the target into the field region, and the increased sensitivity would probably demand that the input beam parameters be measured with prohibitive accuracy.

In summary, a method has been suggested to measure the emittance of the RADLAC beam just before extraction. The method hinges on careful measurement of the input beam $j_z(r)$, shot-to-shot reproducibility, and constructing a TRAJ table to deduce $\beta_\perp$.

V. Beam Conditioning and Propagation Studies

A variety of simulations with MAGIC and TRAJ were made to help understand beam conditioning and equilibria in IFR and B_θ cells. The studies were done for a wide range of parameters including those appropriate for RADLAC, IBEX, RLA, and Hermes II and III. We emphasize that in the gas cell/IFR calculations we do not include collisions, conductivity, or chemistry, except perhaps implicitly through given charge and current neutralization fractions. In this sense our simulations complement the IPROP runs of D. Welch (MRC) in which full self-consistent chemistry is included.

A. B_θ-Cell Calculations

Some preliminary work on this topic, including an analytic theory, was given in Ref. 1, pp. 24-31. This year's work continued, extended, and refined the older results.

1. IBEX Vacuum Wire Cell

Although the vacuum wire cell was abandoned in favor of gas-filled cells in the IBEX experiments in early 1989, considerable effort was expended trying to understand this system, so we summarize the results here. For orientation and review, Fig. 42 of Ref. 1 is suggested. Essentially, the beam is extracted from a guide B_z through a foil into a B_θ-cell, i.e., a region where all forces tend to cancel except the attraction of the wire current I_0, applied to flow in the same direction as the beam. Two other salient points are that the charge and current neutralization induced on the wire are equal except near the ends, and the equilibrium $\beta_\perp$ of the beam in the cell is about $(2\nu_\omega/\gamma)^{1/2}$.

Figure 30 shows the case for the experiments done in early 1989, with a 27 kA, 3.5 MeV, $\beta_{\perp 0} = 0.11$ beam extracted from 16 kG into a wire cell with $I_0 = 16$ kA. In this TRAJ run, the assumed current neutralization $f_m = 0.3$, agreeing well with the calculated charge neutralization $f_e = 0.28$. Note that the beam is heated and expanded in the B_θ cell, as seen previously.[1] In the experimental setup there was an end foil and a vacuum gap where the beam expands very quickly to the wall.[10] As pointed out in Sec. IID, a problem with the immersed IBEX is the large P_θ; the final rotation $V_\theta(\max)$ in Fig. 30a is 0.6c. The equipotentials are shown in Fig. 30b. As shown by theory (Ref. 1 and the IPROP work of D. Welch, MRC) and experiment (C. A. Frost), the system is improved by adding gas to neutralize these large electric fields, and leading to fewer foil replacements.

2. RADLAC B_θ/Gas Cell

The experimental setup as modeled with TRAJ is shown in Fig. 31a. The main differences from the IBEX case of the previous section are that the B_θ cell is filled with gas so that the space-charge is neutralized and the beam current partially neutralized, and the input beam is much higher energy. The goal of the calculations, besides trying to understand the experiments (yet to be performed), is to try to optimize cell performance by varying the many parameters. In particular, we varied γ, I_b, I_0, foil position, B_z(applied), f_e, f_m, $\beta_{\perp 0}$, Δr^{in} of the beam. Figure 31b shows a typical result for $\gamma = 30$, $I_b = 30$ kA, $I_0 = 15$ kA, foil F_1 in "standard" position, $B_0 = 20$ kG, $f_e = 1$, $f_m = 1/2$, $\beta_{\perp 0} = 0.08$, and $\Delta r^{in} = 3$ mm (7, 10 mm annulus). When we write $I_0 = 15$ kA here, we mean either that the wire carries an applied current of 15 kA with no return current (all return current in gas), or that the net current in the wire, I(applied) - I(return), is 15 kA with some return current in the gas. The output beam in Fig. 31b is slightly smaller than the input, but much hotter: $\beta_\perp = 0.3$.

Of some interest is the time-dependence of the B_θ cell behavior. In an attempt to model this, we ran four TRAJ cases for (γ, I_b) = (10, 10 kA), (20, 20 kA), (30, 30 kA), and (40, 40 kA), as shown in Table V. Note that $\beta_\perp$(out), which is mostly in β_θ but some β_r, steadily decreases as the γ, I_b increases. The rms beam radius r_b is a minimum at (30, 30 kA), Fig. 31b. Of course, the best way to approach this problem is with MAGIC and a finite risetime; in fact this has been done for nearly the same parameters in Ref. 1, Fig. 48, except that the cell contains no gas ($f_e^{gas} = f_m^{gas} = 0$, $f_e^{wire} = f_m^{wire} = 0.57$), the resulting final beam after a 15 ns rise to (40, 40 kA) is surprisingly like the TRAJ result. In fact, the TRAJ result without gas

(otherwise like Fig. 31b) is shown in Fig. 32, where the lack of neutralization in the small gap between foils leads to a somewhat thicker annulus but about the same $\beta_\perp$. Comparing Figs. 31b and 32a shows that the gas has lowered the emittance by about a factor of 2/3.

We will summarize some of the other parameter studies. Varying the foil position by moving into the full B_0 = 20 kG does not change the results much (provided the space between foils is an f_e = 1 region). Reducing I_0(wire) by a factor two also makes only a small change (beam is slightly cooler but larger). Reducing I_0 to zero leads to a still cooler ($\beta_\perp$ = 0.16) but definitely larger beam (r = 1.13 cm rms). Of course the real problem with I_0 = 0 is that the centering force is lost, but in 2-D the gas alone keeps the beam from expanding much.

Injecting a hotter, fatter beam annulus (5, 15 mm) give Fig. 33a; comparing Fig. 31b shows as expected that fatter input yields larger r_b(out), and a 1 kA loss to the wire, although $\beta_\perp{}^{out}$ is the same.

Table V. Time Dependence of Output from RADLAC B_θ/Gas Cell (TRAJ)

Input:	$\beta_\perp$ = .08		r_b = .87 cm		(rms)
Input:	I_ω^{net} = 15 kA		Δr = (7, 10) mm		B_0 = 20 kG
Output:	γ	I(kA)	$\beta_\perp$	r_b(cm)	β_θ
	10	10	.45	1.5	.39
	20	20	.31	.95	.27
	30	30	.30	.63	.27
	40	40	.25	.75	.23

For the same thick beam and I_0 = 15 kA but $\beta_{\perp 0}$ halved (Fig. 33b), the resulting final emittance is only slightly smaller. Varying f_m^{gas} in Fig. 33a to 0 makes very little difference, but setting f_m^{gas} = 1 (Fig. 33c) causes the beam to fill the cell; for a hot beam the wire focusing alone is not enough.

3. RLA Gas Cell Plus Wire

The present plan calls for pure IFR transport between injector (Fig. 14a or 18c) and racetrack. We briefly considered another option, where the IFR channel guides the beam only part of the way, and a wire cell takes it the rest. Figure 34 shows the TRAJ model and a sample run. An 11 kA, 4 MeV, $\beta_{\perp 0}$ = 0.24 beam is injected into an IFR channel (f_e = 1, f_m = 1/2). After traveling 1.4 m, the beam encounters a foil and a B_θ cell. There is no I_0 in the wire since we wish to inject onto the racetrack at about 1.8 m (wire is grounded at only one end). As suggested by the figure, this is probably not a good scheme. No matter which type of injector is selected, the mean rotation is

zero (Secs. III A-C), or the beam is small (Sec. IIID); most of the beam will be lost on the wire (possible exception: transparent wire, e.g., axial discharge). In Fig. 34, only 4 kA is transported to the end; these are high $-V_\theta$ electrons (although there is no net rotation, the input $\beta_\perp$ is assumed to be isotropic in r and θ). For a cold input beam, of course, all the beam is lost. Such a scheme is only feasible for a large-radius immersed diode (Fig. 9), but there the rotation will be very large, leading to problems in the racetrack.

B. RLA IFR Shape and Foil Studies

For propagation in the racetrack, an IFR channel with some profile $n_{ch}(r)$ will be used. The question here concerns the effect of this shape on the beam. In using TRAJ to model IFR channels, there are two possibilities: (1) we may use neutralization fractions f_e and f_m, implying that the background plasma can shift quickly to accommodate changes in beam fields; or (2) we may add a fixed background ion density $n_i(r, z)$ to the calculation. For the studies here, option (2) is the only sensible one, but it is unphysical in the sense that over long time scales the ions would move, or background electrons would neutralize some of the ion charge.

Figure 35a shows the trajectories for a RLA-type beam (4 MeV, 10 kA) with uniform $n_i = 2 \times 10^{11}$ cm^{-3} out to $r_{ch} = 1$ cm (sharp edge), implying a (global) $f_e = 0.3$. Normal derivative end boundary conditions on potential ϕ were used, i.e., no end-foils. As seen in the figure, an equilibrium is set up with some electrons getting well outside $r_{ch} = 1$ cm. The output rms $\beta_\perp = 0.11 \approx (\nu f/\gamma)^{1/2}$. Figure 35b shows the same case except the channel is peaked on axis: $n_i = 6 \times 10^{11}$ cm^{-3}, $0 < r < 0.4$ cm; $n_i = 1.24 \times 10^{11}$ cm^{-3}, $0.4 < r < 1$ cm. This profile is a crude model of the measured profiles which tend to be peaked on axis with half-width about 0.5 cm. Again, $f_e = 0.3$ globally. The equilibrium beam has $\beta_\perp = 0.20$, and is somewhat smaller than the uniform-channel case. Overall, the emittance of the uniform case is 75% of the emittance of the peaked case, suggesting that uniform channels, if they could be made, are slightly better. Rerunning Fig. 35a with n_i tripled ($f_e = 0.9$) yields a slightly smaller but hotter beam, the emittance is 1.6 times as large, and 1.2 times the peaked case, showing that lower f may be preferable to making n_i uniform.

On the other hand, adding a lhs foil to the problem, so that the entering beam immediately pinches, shows that higher f is better in terms of beam size and propagation. In fact, for f = 0.2, 0.5, and 1.0 the percent of a 14 kA, 3.7 MeV, $\beta_{\perp 0} = 0.3$, $r_b = 1.1$ cm (rms) beam transported down a 1.22 m pipe is 12, 64 and 100%. Further variations show that for fixed f, larger r_{ch} is better (more beam transported). Of course, these "with-foil" results are more relevant to the channel between injector and racetrack, than to the racetrack itself.

In short, one wants large f in the source-to-racetrack channel, and lower f and uniform n_i in the racetrack. Of course these simple equilibrium studies do not account for turns, instabilities, the difficulties in making the channel, or the 3-D problem of capturing the beam on the racetrack, being studied by J. Wagner (1241).

C. RLA IFR Accelerating Gap

The work discussed here is preliminary, and the problem is still unsolved. The "problem" here is the effect of the gap voltage on the IFR channel. An experiment (pulsing a gap in an IFR channel) is being done by M. G. Mazarakis (1242), as of January 1990. The results show a long current pulse at all locations, even meters from the gap; these results have not been fully understood yet.

As seen by MAGIC, there are several possible models, the main differences coming in how the ends z = 0 and z = L are treated, and whether or not a beam is injected (here we assume no beam). If we simply let the ends be open and apply a voltage to the gap, the electrons will be cleared out by axial motion and then the ions will expand to the wall, for typical densities, e.g., $n_{ch} \approx 10^{11}$ cm^{-3}; for higher densities we have complications such as field penetration, etc.-see Ref. 4, Fig. 17. Adding electrons from the ends is realistic, if we knew the appropriate current and distribution. Several such models were tried, but the results seem inconclusive and somewhat arbitrary.

Periodic boundary conditions are appropriate for a long series of identical gaps around the racetrack; an example is shown in Fig. 36. Here a 2 ns-rise pulse which levels off at 1.5 MV is applied to the gap; the IFR is initially characterized by $n_{ch} = 8.3 \times 10^{10}$ cm^{-3}, $r_{ch} = 2$ cm, $m_i = \infty$. The electrons at 7.5 ns are nearly filling the pipe (Fig. 36a), the ions have not moved here (Fig. 36b), but for $m_i = 2$ amu would have expanded partway to the wall. The electrons in the gap region are accelerated first, so ion expansion is greatest there (for finite m_i). In Fig. 36, however, the ions are just a neutralizing background for the electrons, which accelerate and expand until at 7.5 ns there are several "beams" at different energies (Fig. 36c); the E_z field is still localized near the gap (Fig. 36d). The basic result is that within 10 ns the channel will be seriously perturbed by the gap voltage; of course the main e-beam may in some ways improve things, e.g., retard the ion expansion.[4]

A longer, non-periodic open-ended system is presently being simulated, to better match conditions in the experiment. For an L = 2 m system, the results have some of the same features as the periodic runs, but of course multiple beams are not seen. The electrons quickly accelerate and expand on a few -ns timescale, for the experimental $V_{gap}(t)$ which rises in 20 ns to 800 kV. The ions slowly expand ($m_i = 40$ amu), over several tens of ns. The electron current peaks downstream of the gap at about 1 kA at about 20 ns. The model is still being developed and the implications for the main beam propagation have yet to be simulated.

D. Hermes III Propagation with Foils and Wire Cells

For foil propagation[6,11,12] we may estimate a desirable foil separation from

$$L = \frac{16 r_b}{\pi} \frac{\nu}{\gamma} \left(1 - \frac{r_b}{R} \right)$$

where R = wall radius.[4] For typical Hermes III parameters, this gives about L = 40 cm. The problem is that one can estimate the space-charge limit, and the Hermes III beam of 700 kA is far above it. Nevertheless, several MAGIC runs were

made. Figure 37 shows a simulation for L = 20 cm with 3 foils. The diode calculation is included also, since the $v/\gamma \sim 1$ beam is very nonlaminar. As pointed out several times in earlier reports, e.g., Ref. 12, the problem is that the strong E_z fields near the foils perturb the radial force balance considerably. Of course, if one is above the space-charge limit, the perturbation takes the form of a virtual cathode, seen in Fig. 37 past foil #1. One could place many foils very close together, but this seems impractical for the desired propagation length of ~10 m.

The use of a long B_θ cell, or a series of them, seems more promising. Unfortunately, a vacuum B_θ cell also has space-charge-limit problems. Figure 38 shows a 700 kA annular beam injected through a foil at 20 MeV, with $\beta_{\perp 0} = 0.3$ and $11 < r_b < 20$ cm, R(wall) = 32.6 cm (no B_z or net rotation). The wire (2 mm radius) carries 100 kA, and the induced $f_e \approx 0.1$. As shown in Fig. 38a, the beam expands to fill the pipe; as shown in Fig. 38b, a VK (virtual cathode) forms near the foil.

There are two possible space-charge limits here. Using the standard type of 1-D estimate we obtain[13]

$$z_s = \gamma^{1/2} c/\omega_p \tag{2}$$

where γ is beam energy/mc^2, ω_p = plasma frequency associated with rest-frame beam density, and z_s = stopping length. For the parameters above we obtain z_s = 8 cm, roughly agreeing with Fig. 38b. In this result, the wire plays no role; Eq. (2) is simply based on the charge near a foil needed to dig a potential well of depth = beam energy. For the "2-D" calculation, we solve a 1-D (radial) Poisson equation with conductors at $r = r_\omega$ and R, with a thin annular beam at $r = r_b$ in between. The result is

$$I_{scL}^{2\text{-}D} = 2\pi\varepsilon_0 cV \frac{\ln R/r_\omega}{(\ln R/r_b)(\ln r_b/r_\omega)} \tag{3}$$

which reduces to the correct limit when there is no wire. For Fig. 38, we obtain $I_{scL}^{2\text{-}D}$ = 590 kA. Since only 270 kA reach z = 1 m in Fig. 38, we conclude that the 1-D limit is the operative one here; this is also verified by the potential plots showing a huge retarding E_z field near the beam injection region.

To make this scheme work, we need some charge neutralization. In fact, a gas cell is found to work well (without needing the wire) in both simulations (IPROP runs by D. Welch)[14] and experiment.[15] The calculations found 80% transport over 10 m, and the experiments agree reasonably well.

E. Hermes II Diode Plus Gas Cell

This work was done in early 1989 in support of the Hermes II air-propagation experiments of C. A. Frost et al., and to provide input to the IPROP runs (D. Welch, MRC). A sample MAGIC run is shown in Fig. 39; for a 30 cm A-K gap and r_K = 7.6 cm we obtain 104 kA at 10 MV in the steady state. At the thin foil separating diode and gas cell (modeled as $f_e = 1$, $f_m = 0.8$) the beam is characterized by $\beta_\perp = 0.22$, r_b = 9 cm, and a $\overline{\theta} = -12^o$ convergence angle. The gas cell calculation

is not self-consistent since a chemistry package is needed, but the f_e, f_m values are probably fairly realistic. Also, for the gas cell calculation to be very meaningful, we would have to follow the beam many more betatron wavelengths. Nevertheless, the diode calculation matches the experiment at peak V and I, and gives an idea of the beam size to be expected. The data at the foil was used as input to IPROP.[16]

Note in Fig. 39 that we attempted to simulate the actual hemispherical shape of the Hermes II diode tip by using the slant-emission option in MAGIC; about 40 kA came from the slant, most of the rest from the shank.

The main parameter variations done were of diode gap and cathode radius (for propagation experiments, the goal was to make a small [$r_b \approx 4$ cm] cool beam). For smaller d and r_K we find roughly the same V and I as above, e.g., at (r_K, d) = (2, 8 cm), (V, I) = (8.8 MV, 115 kA); and the beam at the foil has r_b = 3.5 cm (edge); increasing d to 12 cm yields nearly the same result except a larger beam r_b = 5 cm at the foil. The case (r_K, d) = (1.5, 12 cm) gives (8.8 MV, 99 kA) with r_b = 5 cm at the foil.

In short, for the experimental setup code and measurement agree. By using smaller cathodes and gaps, smaller beams for propagation work may be generated.

VI. RHEPP Diodes

From the MAGIC simulation viewpoint, we treat this as a steady-state diode with or without applied B_z, nominally 5 MV, 5 kA with a small solid cathode and a large gap. The goal is to produce a reasonably uniform beam $j_z(r)$ in $r < 10$ cm on an anode/convertor plate. Typical runs are shown in Fig. 40: in (a), no B_z; and in (b), a uniform 1.5 kG is applied. In both cases (r_K, d) = (2, 40 cm). Since these cases were run on the load line $2V_0 = V + Z_0 I$, where V_0 = 2.86 MV and Z_0 = 180 Ω at r = 20 cm, where the TEM voltage wave is input; in Fig. 40a we obtain 7 kA at 4.45 MV, and in 40b, 5.5 kA at 4.75 MV. The main feature to note in Fig. 40 is the huge effect of adding the B_z = 1.5 kG; the output (rhs) beam on the target changes from r_b = 12 cm(rms) in (a) to r_b = 1.5 cm in (b). The beam in (a) is nearly normally incident, with $\bar{\theta} = +1°$, $\beta_\perp = 0.024$; while in (b) we obtain $\bar{\theta} = -3.6°$, $\beta_\perp = 0.067$.

Besides B_z, we varied gap d and cathode size r_K. Doubling d to 80 cm for r_K = 1 cm and B_z = 1.5 kG changes I from 5.2 kA (4.8 MV) to 2.0 kA (5.0 MV). Both cases produce very small beams, $r_b < 2$ cm. Reducing B_z to zero in the d = 80 cm case causes half the 2.8 kA to hit the outer wall. We emphasize that these are steady-state results and rep-rate considerations are not included.

VII. Preliminary Quicksilver Studies of Off-Center Beams

We have used the new 3-D particle code Quicksilver to take a preliminary look at two off-center beam problems of interest for electron linacs and B_θ cells. In the latter case the issue is centering and guiding of an offset beam; in the former case the issue is the effect of a single accelerating gap on a beam injected off-axis. The results really are preliminary; final conclusions cannot be drawn. The reasons for this are (1) an axis of cylindrical symmetry is not yet included in the code; for the B_θ cell problem this can be finessed since the axis region is a conductor, (2) the diagnostics are still being developed, in particular phase-space, particle-flux counts, and spatial

("range") plots are unavailable, and (3) the long running time and considerable file manipulation required for realistic simulations make parameter-variation studies impractical. Nevertheless, a few runs were made for each problem using the present version of the code, and the results at least illustrate the capabilities of the code and some of the physics issues involved in off-center beam problems.

A. Wire Guiding

The ability of a current-carrying wire to center and guide an electron beam is well-known; the 2-D version of the problem was discussed in Sec. VA and several earlier reports. Some earlier work was done with BUCKSHOT by J. R. Freeman, but the model used is not self-consistent and assumes the electrons are line charges. Thus it seems worthwhile to apply the fully 3-D Quicksilver code to the problem. Cylindrical coordinates could be employed, since the axis (r = 0) is inside the conducting wire (r_ω = 2 mm, R(wall) = 3.2 cm). The 10 kA, 10 MeV beam has a radius of about 0.5 cm, and an initial offset of 1 cm; the result at 4 ns (quasi-equilibrium) is shown in Fig. 41 where, unlike most figures, the beam moves right-to-left. Of course, we gave the beam an initial rotation (as in RADLAC), otherwise it would collapse onto the wire.

The net wire current is about 10 kA; as seen in the figure this guides the beam successfully over a propagation length of 1 m. Note, however, that a corkscrew mode develops which causes the radius of the beam to increase near the output end; the beam there scrapes the wall (not visible in Fig. 41) leading to a 2 kA loss. There is no loss to the wire, however; and the wall radius could be increased.

B. Gap Effects

Before adding an accelerating gap, we first ran cases of beams propagating in uniform B_z through open-ended waveguides. Rectangular (x, y, z) geometry was used, with a square beam typically 1 cm X 1 cm in a square waveguide 5 cm X 5 cm, with guide axis along the z (and applied B) direction. Essentially the result is propagation along the field with the corners of the beam being rounded, and basic trajectories helical. Typical parameters were 20-30 kA, γ = 11, cold input beam; the system z-length was 1 m, with B_0 = 20 or 25 kG. The timestep was usually 2 or 2.5 ps, with (DX, DY, DZ) = (2 mm, 2 mm, 2.5 or 5 mm) and a 1 ns risetime on the injected current. The number of electrons used after the beam crossed the system was varied from 60 to 160 thousand.

For an on-center beam the typical beam begins square near z = 0, then rotates slowly, then rounds off the corners, and finally expands in cross section to roughly double in size. Offsetting the input beam by 5 mm in X leads to the same result except an organized helical wave grows up near the output end. It was checked that: (1) a low-current beam (3 kA) goes straight, with no corkscrew mode or appreciable cross-section enlargement, and (2) a 20 kA case (centered) with B_0 = 0 expands to the wall in a reasonable distance.

Finally, an accelerating gap with d = 10 cm was added (centered on z = 50 cm). Three cases were run (Cray time 4-5 hours each): (1) a 1.2 MV gap, 25 kG, on-center beam, (2) a 1.2 MV gap, 25 kG, 1 -cm offset beam, and (3) a

5.2 MV gap, 15 kG, 1 -cm offset beam. All had I_b = 20 kA, γ = 11, cold input, square cross-section 1 cm X 1 cm. The guide cross-section was 5 cm X 5 cm except at the gap, where the V(t) was applied from all four sides with a 1 ns rise. Figure 42 shows the electron map at 7.5 ns for case (3). The conductors are shown in gray, the particles in black, for 30 < z < 70 cm. The effect of the gap is to increase the amplitude of the wave on the beam, such that about 1 kA scrapes off on the walls over the total 1 -m propagation length.

Thus, even for this high-voltage gap and large beam-offset, the gap effect is not serious. Of course, for traversal of several gaps in series we might expect the disturbance to become more serious, and note that effects such as beam breakup or image displacement instability are not included in our simple 1-gap model. For cases (1) and (2) with weaker V = 1.2 MV and stronger B_z, the effects are much smaller; no beam loss occurs in either case. In all cases, we should mention, a quasisteady state is reached and the self-B_z is negligible.

In summary, these Quicksilver simulations are somewhat primitive and certainly preliminary. Further work on off-center beam problems will surely be done as the code diagnostics improve and better models are developed.

References

1. J. W. Poukey, SAND89-0298, April 1989.
2. J. W. Poukey, SAND88-0039, February 1988.
3. J. W. Poukey, SAND87-3068, January 1988.
4. J. W. Poukey, SAND87-0494, April 1987.
5. J. W. Poukey, SAND87-0384, March 1987.
6. J. W. Poukey, SAND85-2670, February 1986.
7. M. G. Mazarakis et al, Proc. DARPA Review, Monterey, CA, 1989.
8. K. W. Struve, F. W. Chambers, and J. C. Clark, IEEE Trans. Nucl. Sci. NS-32, 1991 (1985).
9. J. R. Freeman and J. W. Poukey, "IBEX Emittance Measurements", memo, November 30, 1989.
10. This was first pointed out by B. B. Godfrey.
11. R. J. Adler, Part. Accel. 12, 39 (1982).
12. J. W. Poukey, SAND83-2511, February 1984.
13. J. W. Poukey and N. Rostoker, Plas. Phys. 13, 897 (1971).
14. D. R. Welch and B. B. Godfrey, MRC Report MRC/ABQ-N-412, May 1989.
15. T. W. L. Sanford et al., paper submitted to Spring Meeting of APS, April 16-19, 1990.
16. D. R. Welch, private communication.

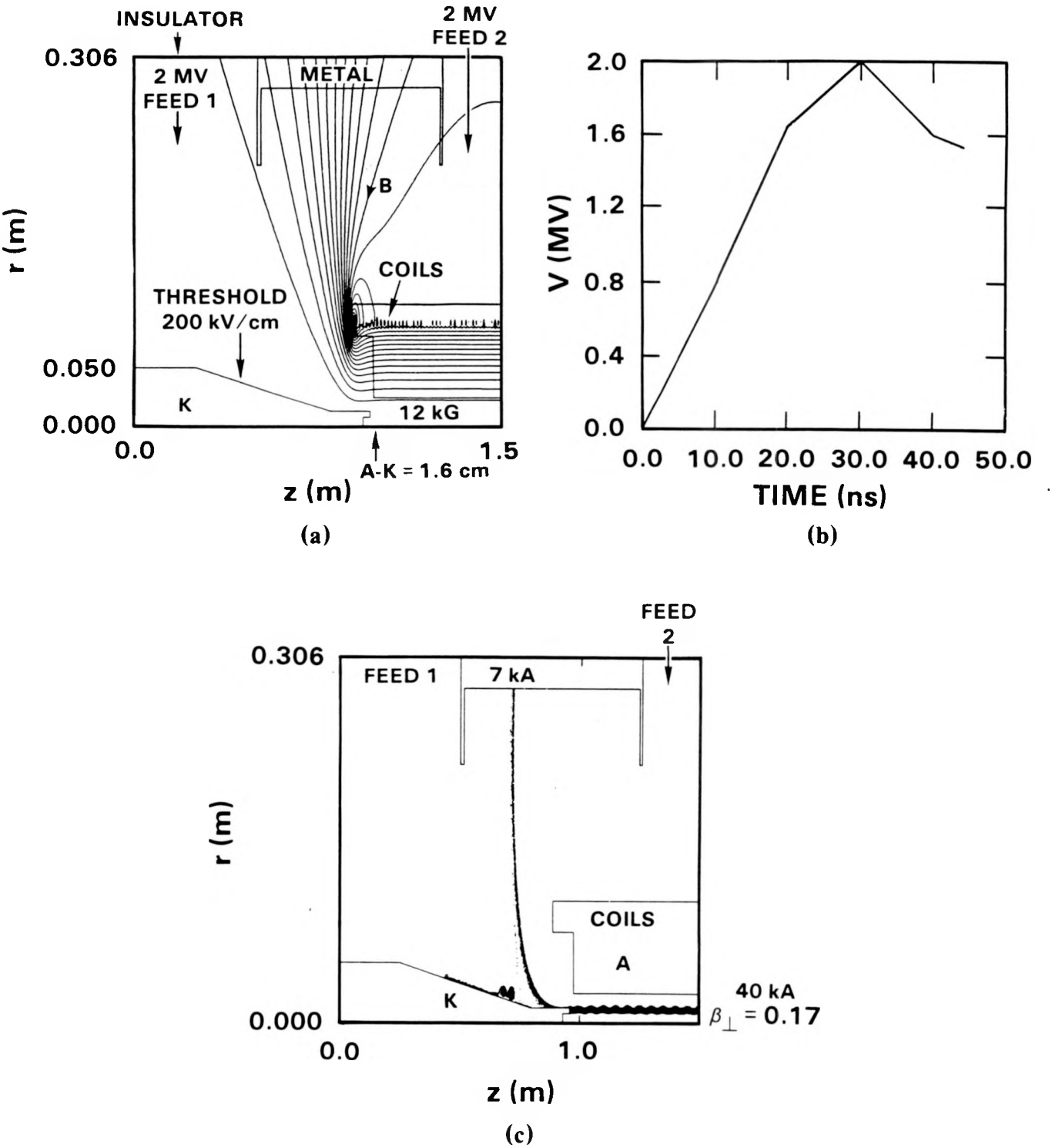

Figure 1. MAGIC simulation of the RADLAC 2-feed injector at B_z = 12 kG.
(a) Problem setup and applied B lines.
(b) Input V(t) for each feed.
(c) Electron flow near peak V and I showing 40 kA beam, 7 kA leakage to metal divider between feeds.

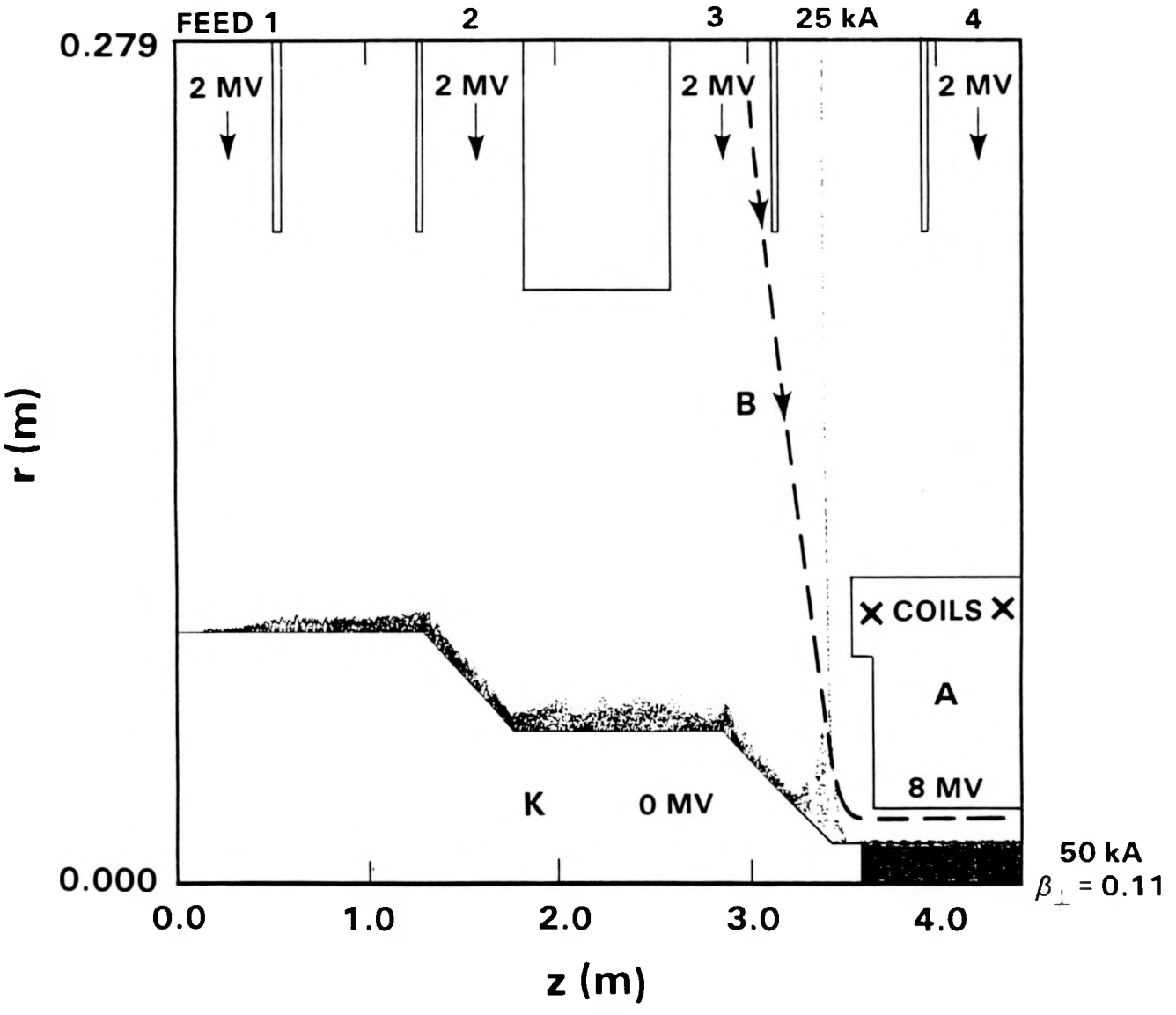

Figure 2. **Setup for MAGIC runs of 4-feed injector. In the case shown, the system was run to a steady state by injecting a constant 2 MV wave into each feed. The applied B is the same as in Fig. 1a except scaled up so the maximum in the A-K gap is 20 kG. For the geometry shown, with d = 6 cm, the 8 MV system produces a 50 kA beam with a 25 kA leakage.**

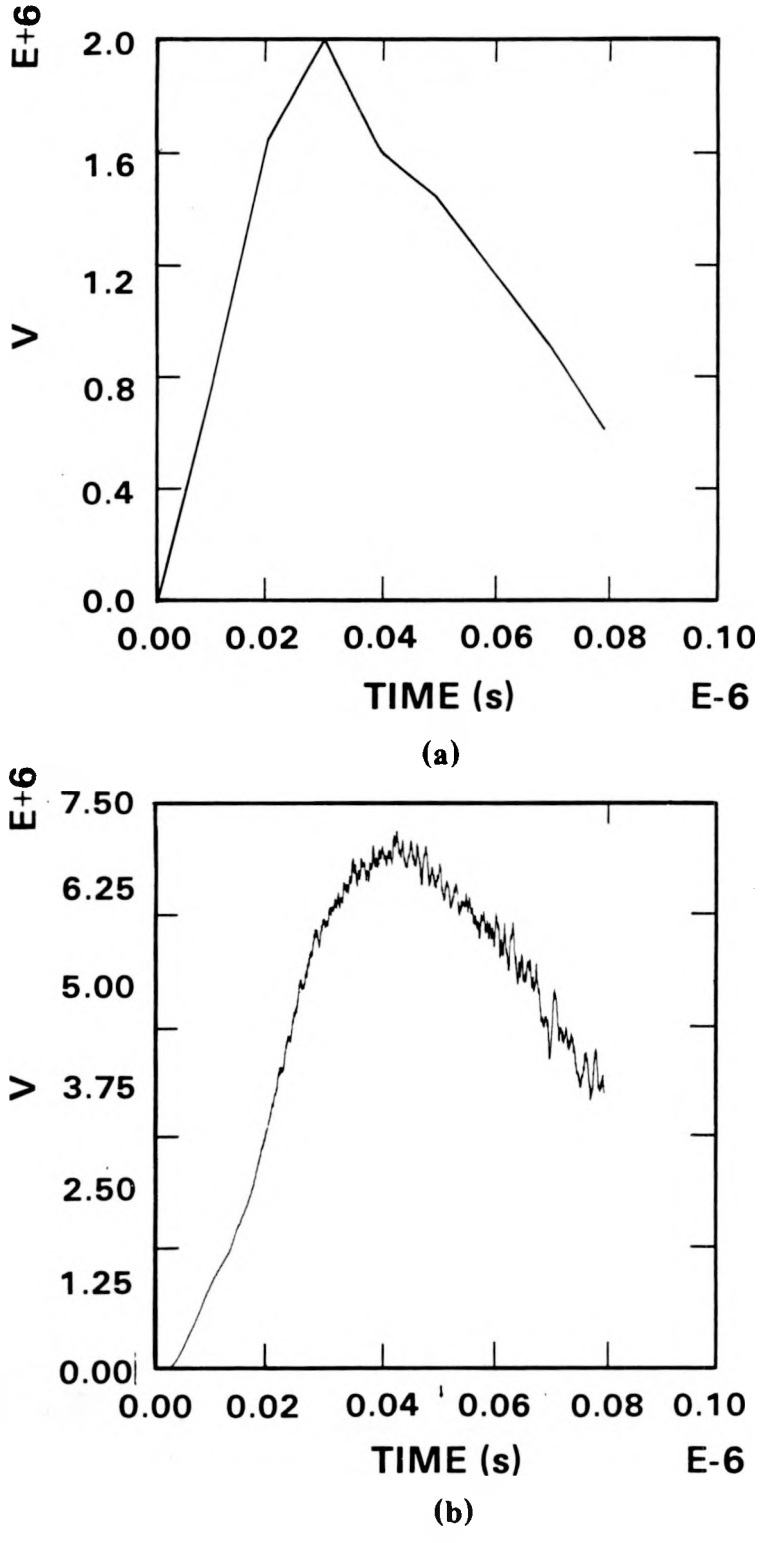

Figure 3. **Time dependence of RADLAC input voltage/feed (part a) and combined 4-feed voltage on diode gap (part b). Note that the peak total V is somewhat less than 8 MV, and occurs about 12 ns later than the peak input V. These V(t) curves apply specifically to case 4 of Table I, but are nearly correct for cases 5 and 7, also.**

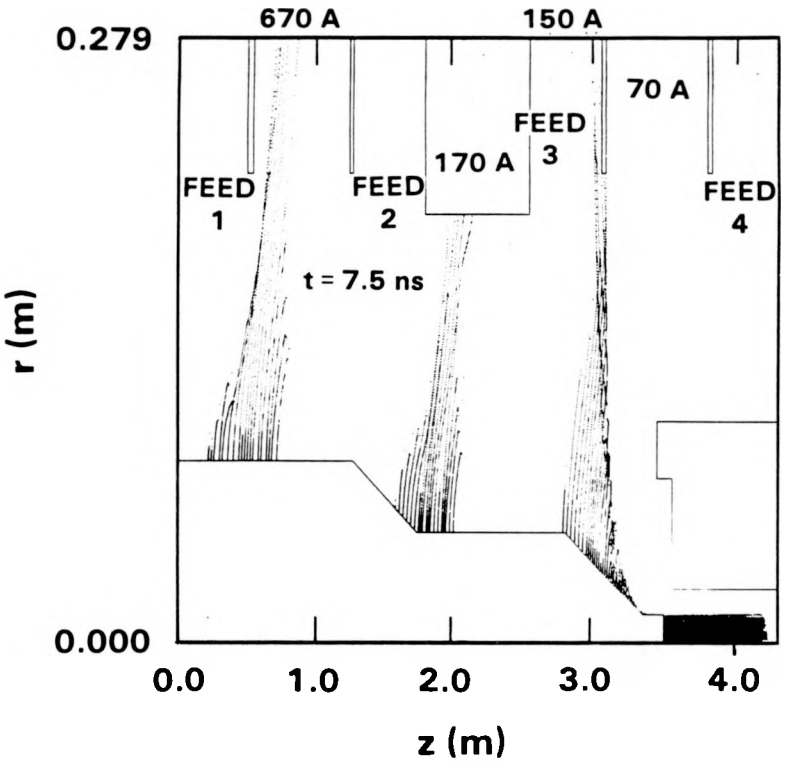

(a)

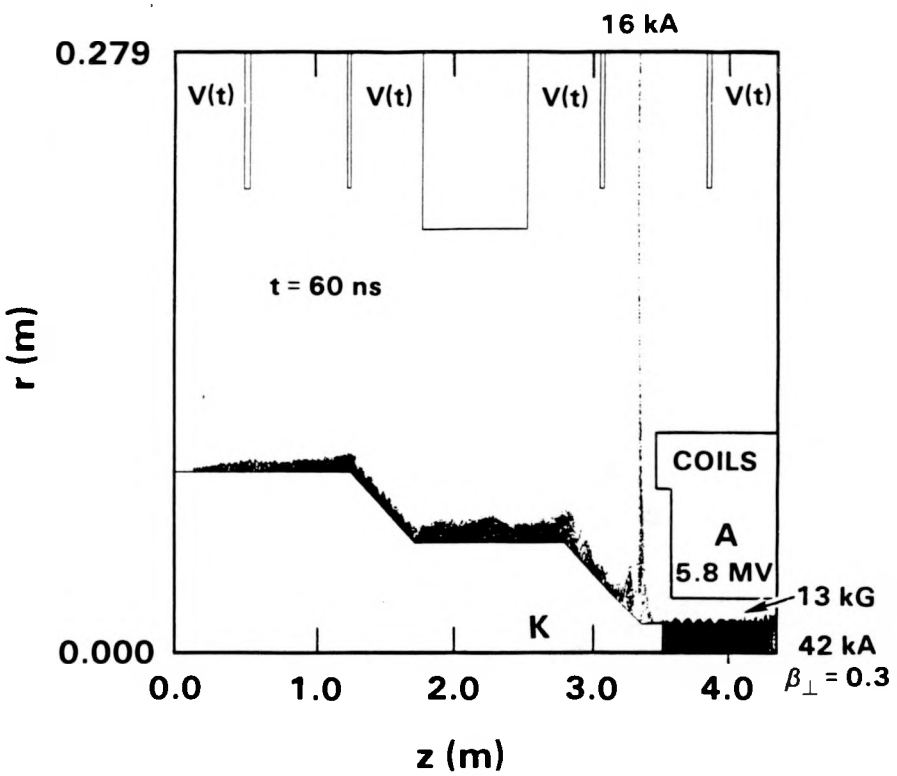

(b)

Figure 4. **Electron flow from MAGIC run of case 5, Table I (B_z = 13 kG).**
(a) Early time = 7.5 ns, showing leakages at three regions.
(b) Late time = 60 ns showing only leakage to metal divider between feeds 3 and 4.

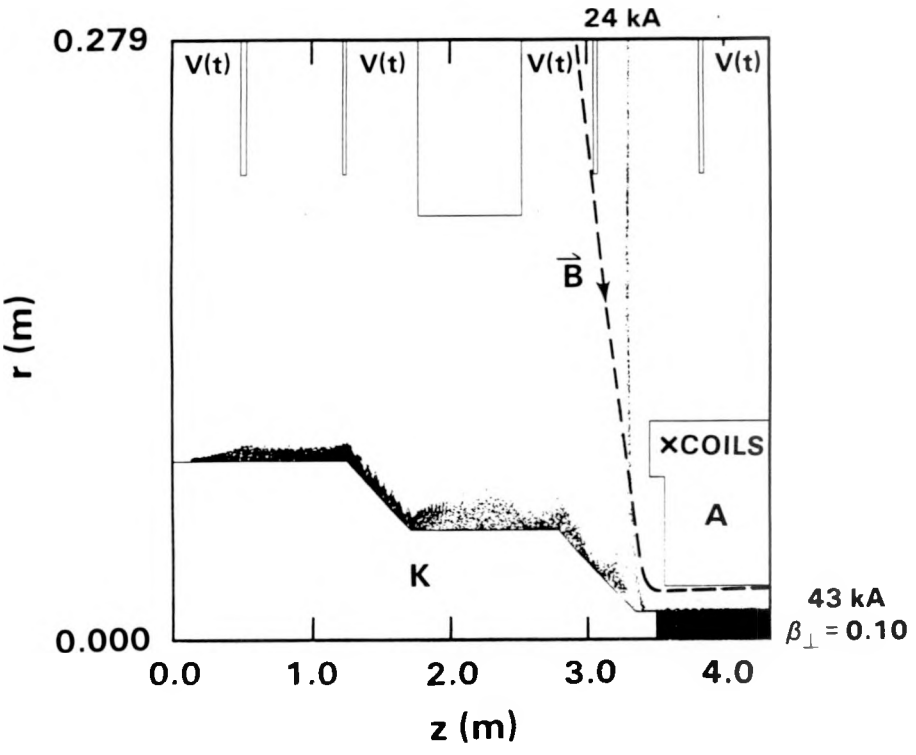

(a)

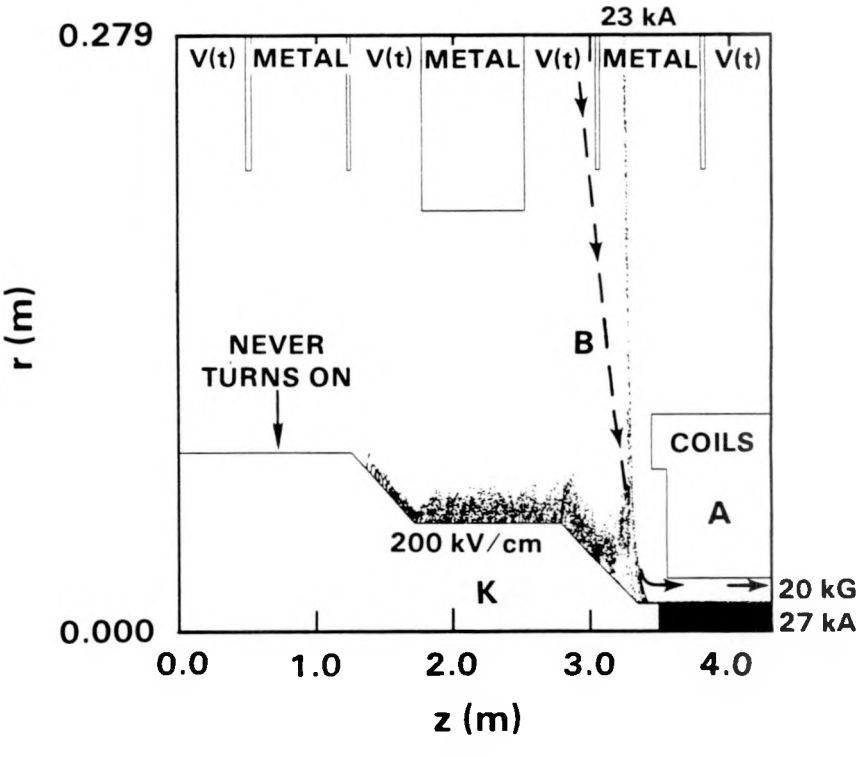

(b)

Figure 5. Electron flows for cases 4 and 7 of Table I (20 kG) for times in middle of pulse.
(a) Case 4, low emission threshold.
(b) Case 7, threshold 200 kV/cm.

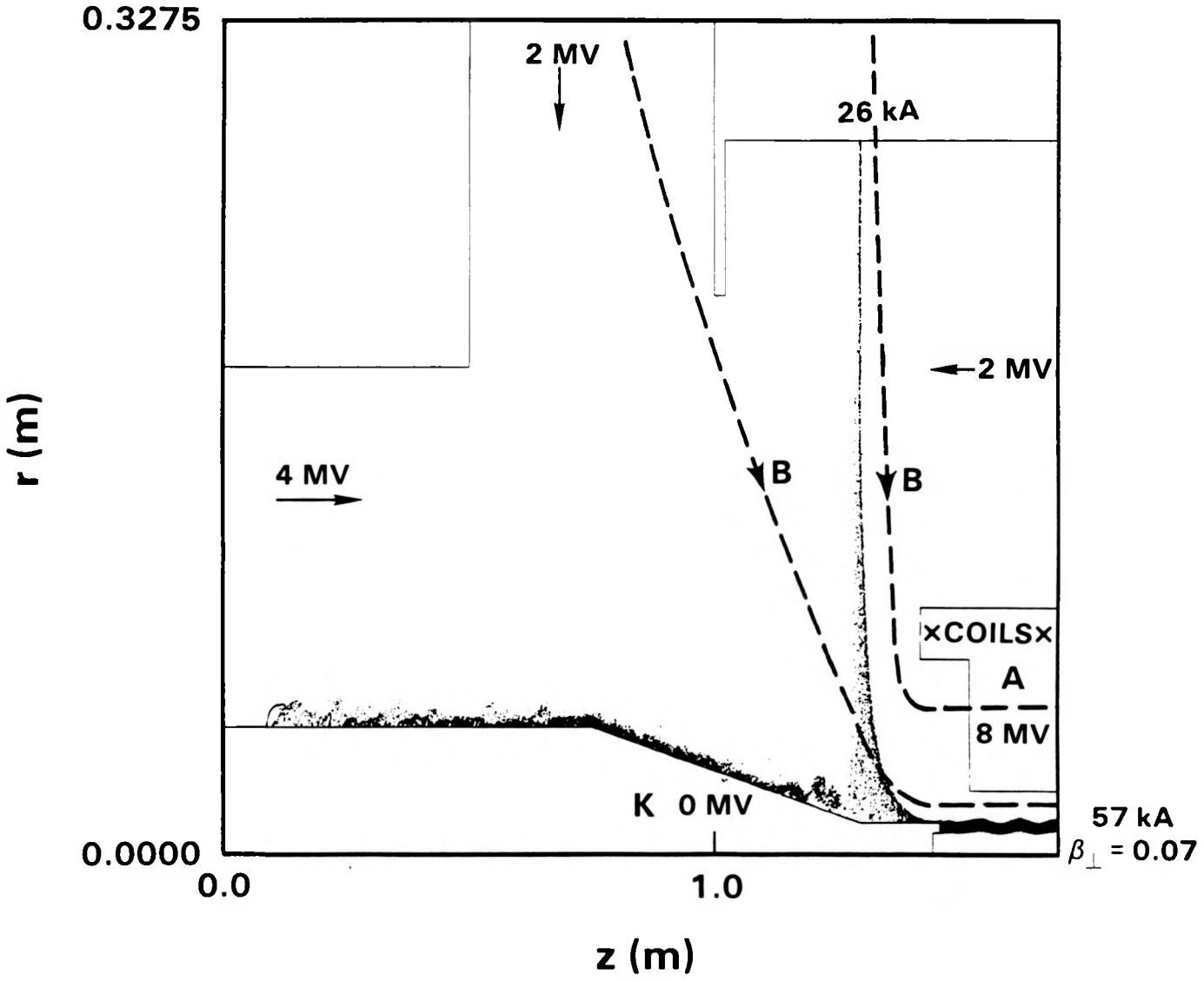

Figure 6. MAGIC run of RADLAC injector, "partial" model. Only feed #3 is included, the rest of the 8 MV is applied via TEM waves from the sides. The result (steady state) is 57 kA (beam), 26 kA (loss). This model allows us to resolve the diode better and still calculate the main leakage. Compare Fig. 5a.

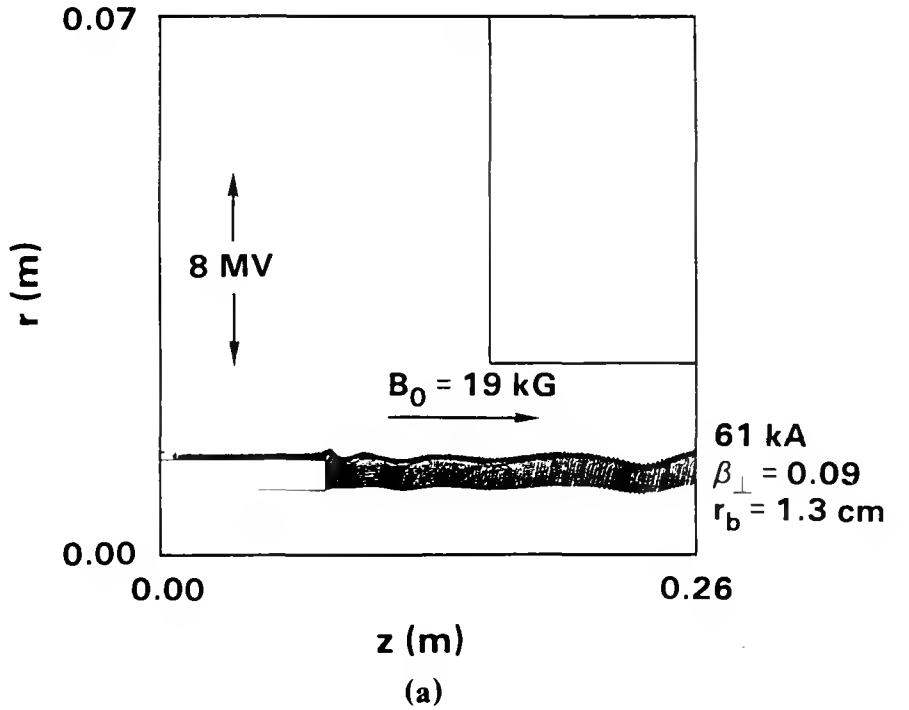

(a)

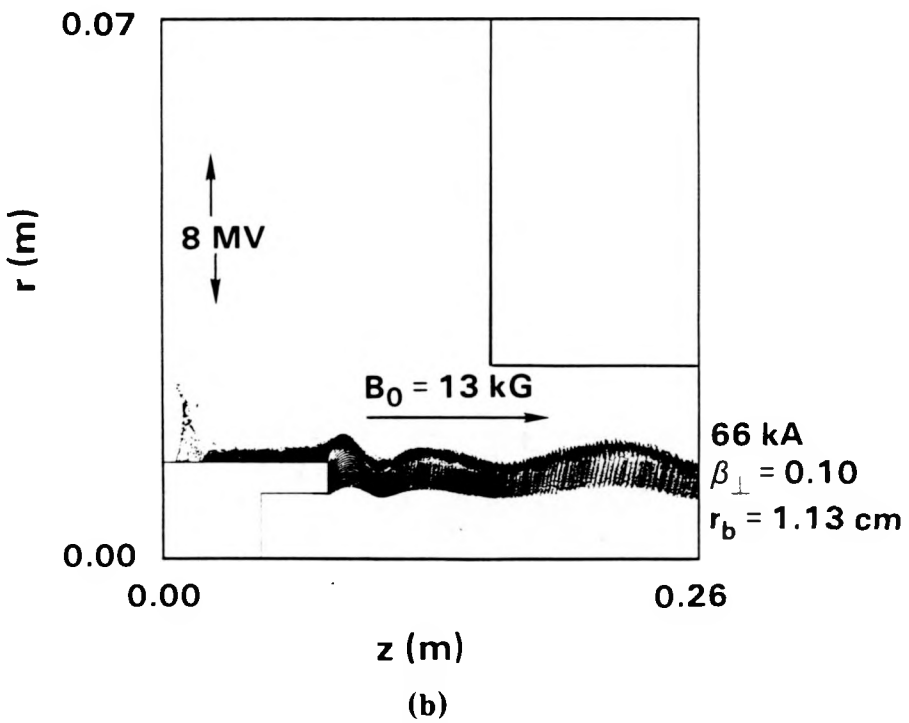

(b)

Figure 7. MAGIC runs of RADLAC diode alone at (a) B_z = 19 kG, (b) B_z = 13 kG. Applied voltage 8 MV, beam currents 61 kA (a), 66 kA (b). Note the reasonable agreement between Figs. 7a and 6, in terms of beam current and quality. Decreasing B_z from 19 to 13 kG leads to larger radial oscillations, as expected.

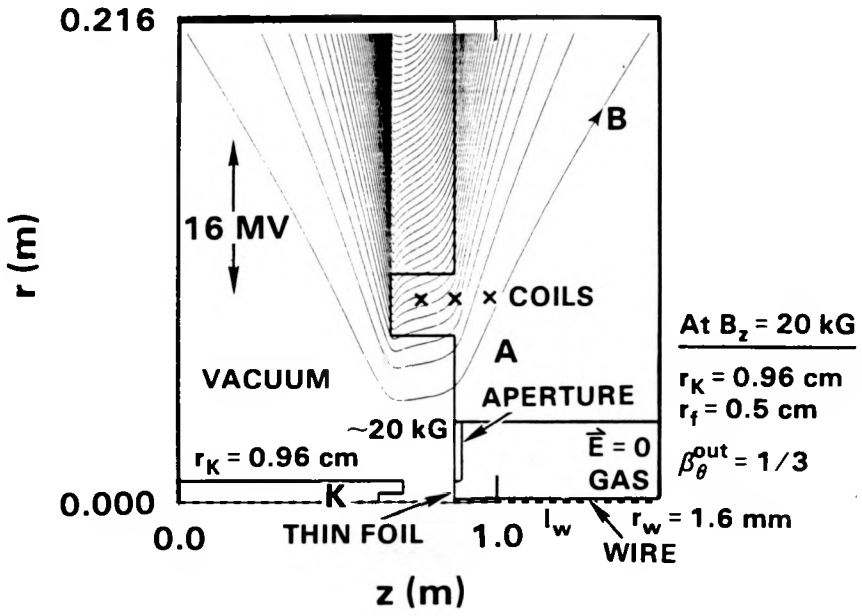

(a)

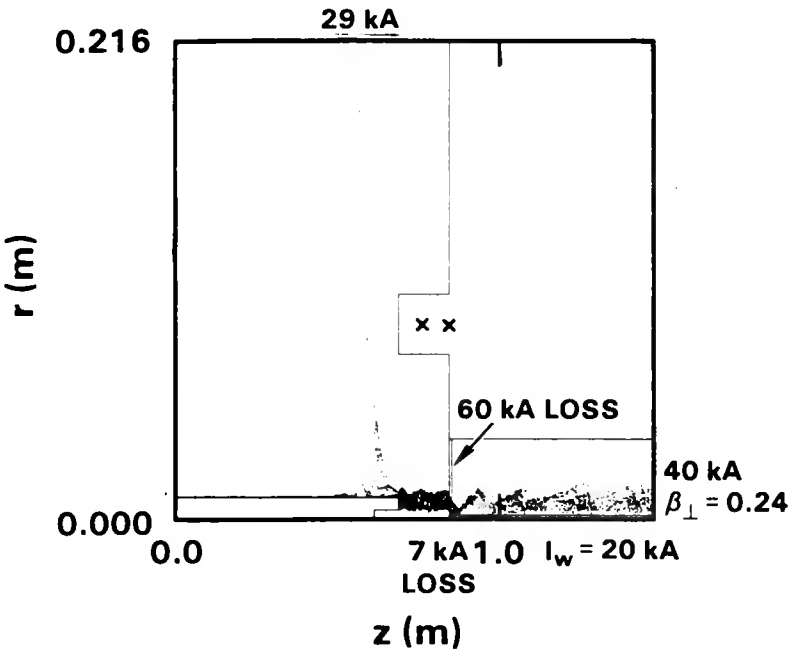

(b)

Figure 8. MAGIC simulation of 16 MV RADLAC SMILE injector plus gas/wire cell.
(a) Problem setup.
(b) Steady electron map for V = 16 MV, I(total) = 137 kA, applied B_z(gap) = 20 kG, A-K gap = 16 cm, I_w^{net} = 20 kA. We assume F_e = 1 in the gas/wire cell. About 40 kA of beam current is produced, but this can be varied easily by changing the aperture radius. The induced beam rotation keeps most of the beam from hitting the wire.

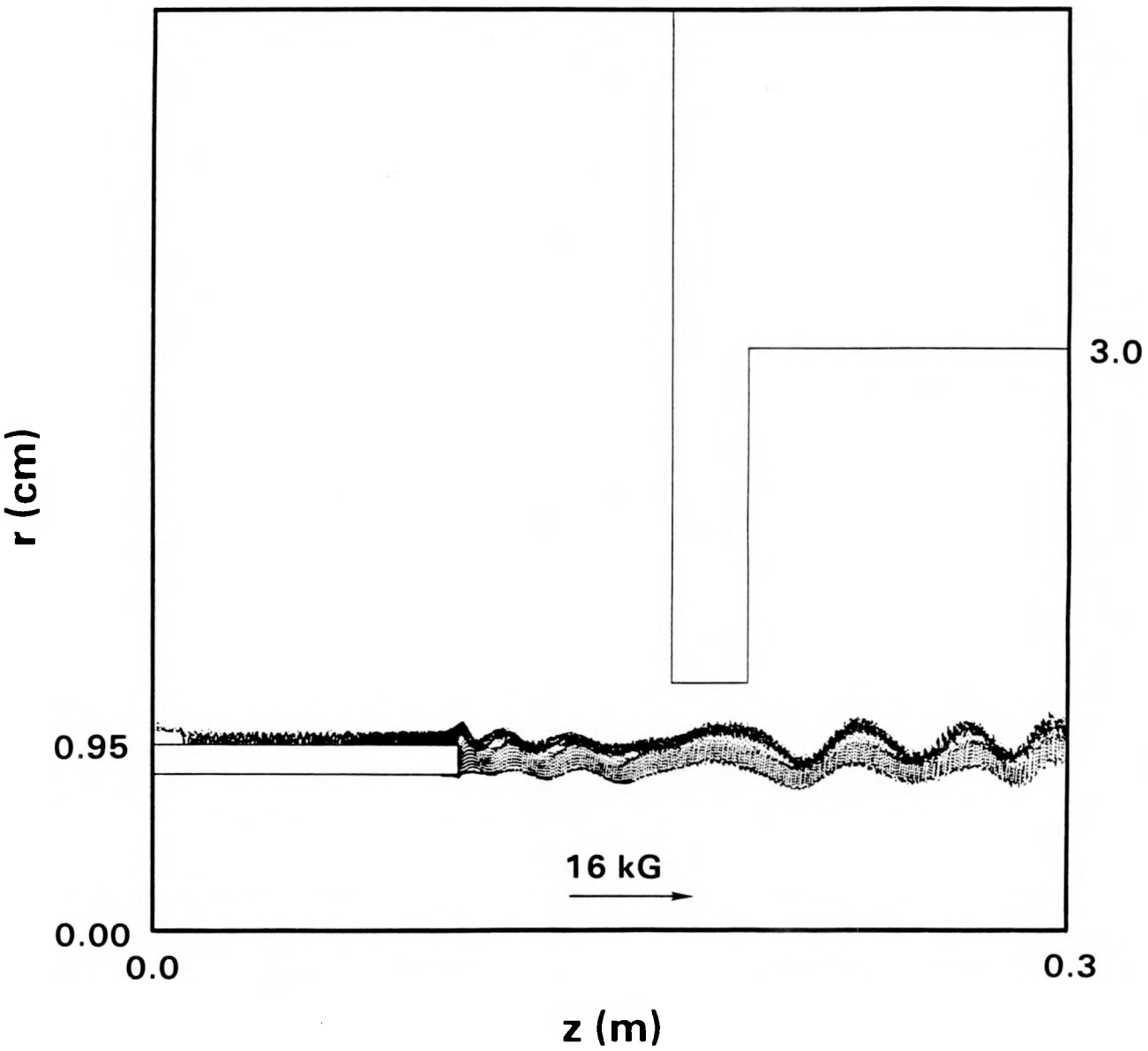

Figure 9. **MAGIC run of a large-radius IBEX diode immersed in 16 kG. At V = 3.5 MV, we find I = 23 kA. Problem: after extraction the beam in this system will be rotating at about c/2.**

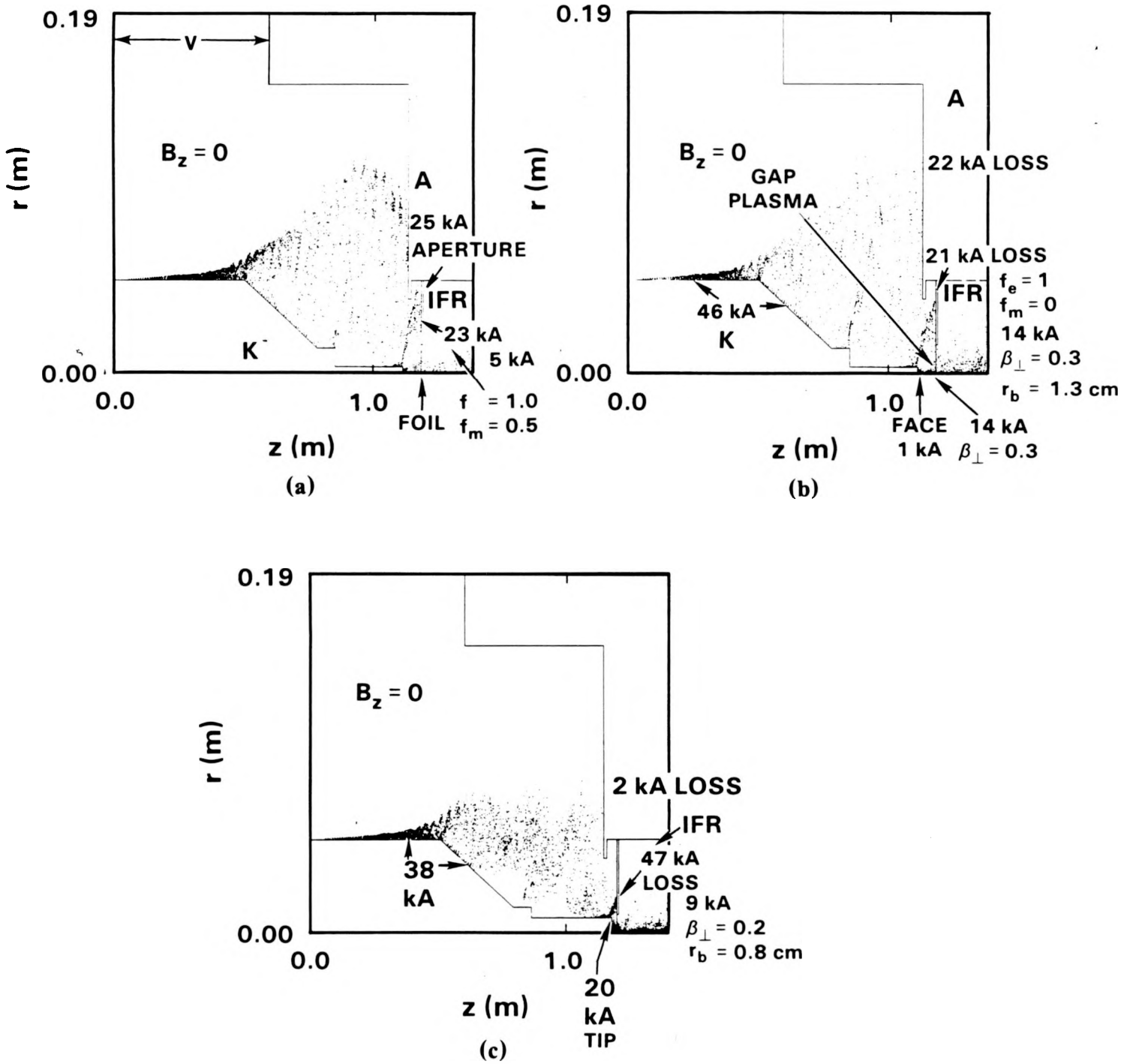

Figure 10. MAGIC runs of a Recirc/IBEX experimental injector plus IFR channel with V = 3.7 MV, A-K gap = 7 cm, I = 57 kA total, and no B_z.

(a) Vacuum diode case; only 5 kA beam is produced, unlike experiment.

(b) Add gap plasma of unknown origin, $n_{plas} = 1.5 \times 10^{12}$/cc. Now a 14 kA beam is produced, like experiment. (See Table III.)

(c) Reduce gap, use larger cathode tip. A 9 kA beam out results. No gap plasma

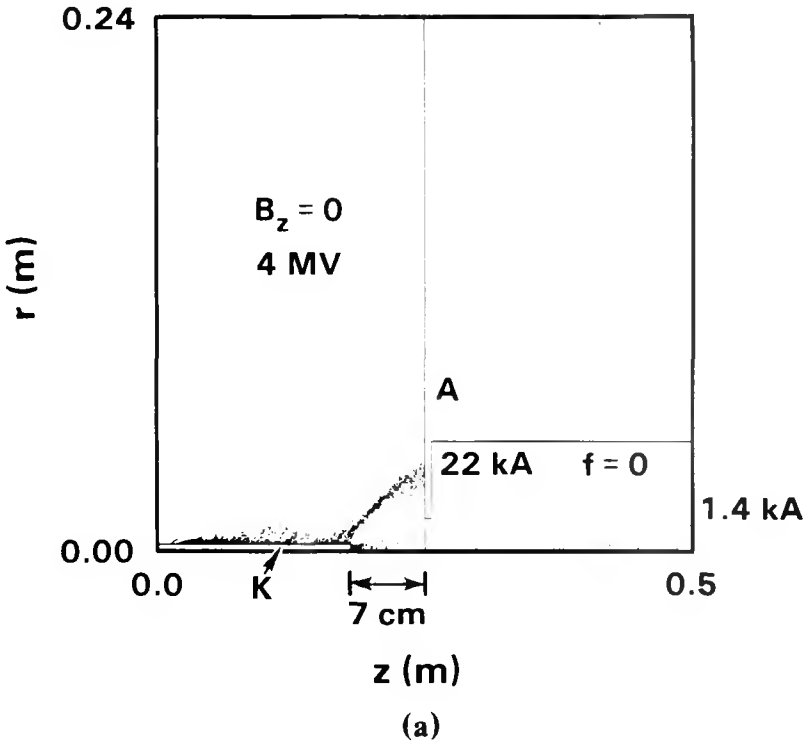

(a)

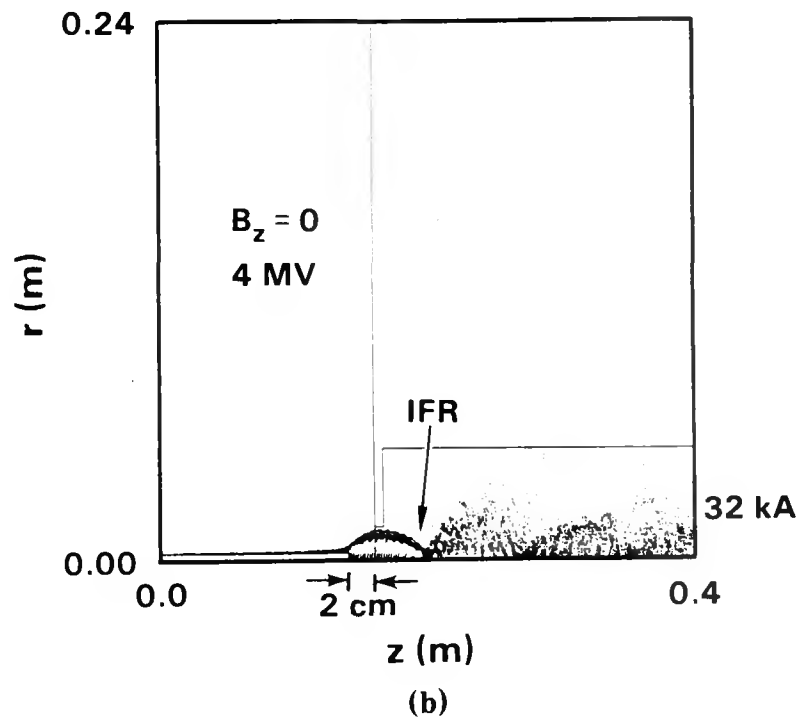

(b)

Figure 11. As in Fig. 10 but include only the cathode tip, assuming emission from the rest of the shank cannot contribute to the beam.
(a) Vacuum diode, 4 MV, no IFR channel, Total I = 23 kA, but only 1 kA out rhs.
(b) Close gap to 2 cm, yielding 32 kA, all out rhs.

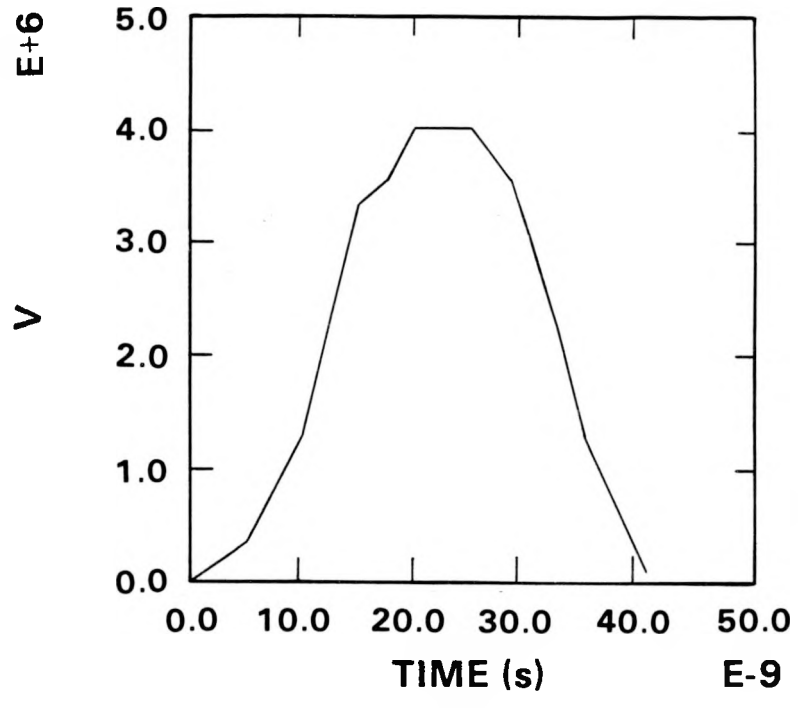

(a)

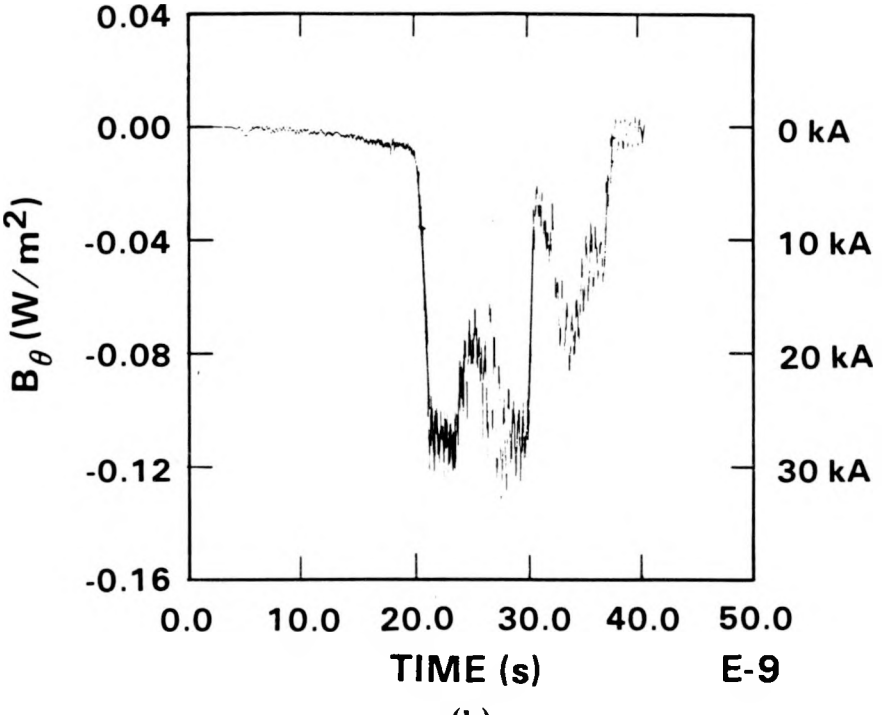

(b)

Figure 12. **(a)** **Applied voltage vs t for MAGIC Recirc diode run of Figs. 13, 14. This is the experimental input.**
(b) **Output beam current in IFR channel $I_b(t)$. Note delay with respect to V(t), and oscillations after 20 ns.**

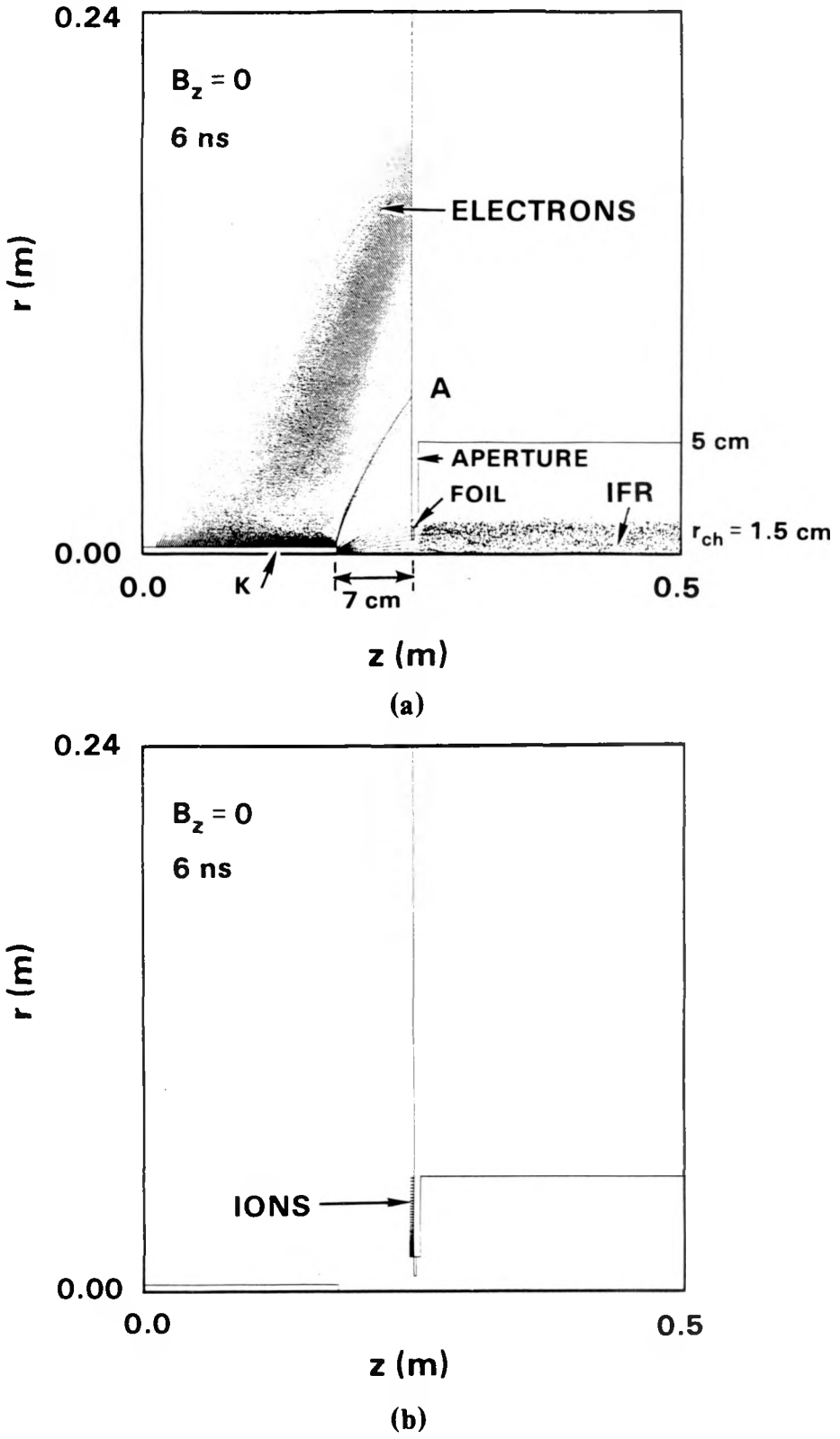

Figure 13. Early-time (6 ns) electron (a) and ion (b) maps for Recirc diode with ion emission from aperture. The emitted ions are protons, the channel ions (not shown) are infinitely massive.

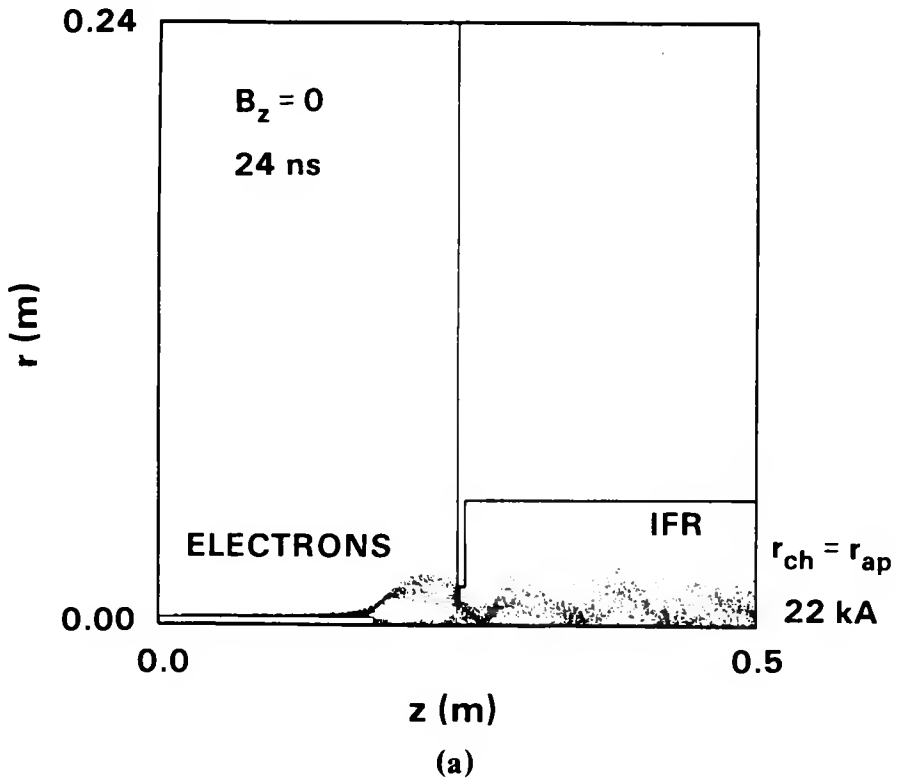

(a)

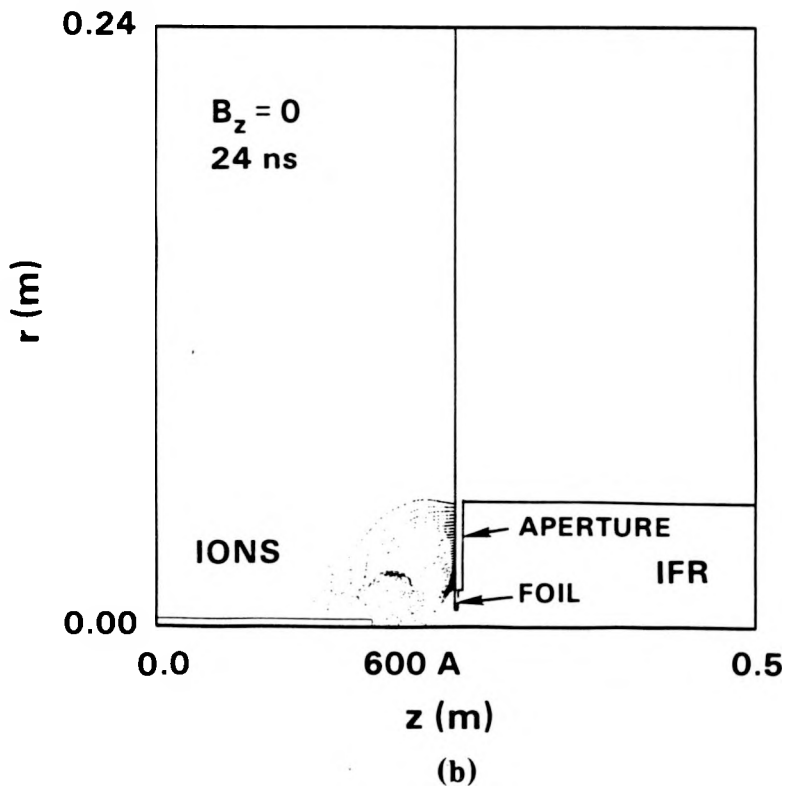

(b)

Figure 14. Electron (a) and ion (b) maps near peak V and I for Recirc diode MAGIC run. The ions in the A-K gap allow the beam to be focused into the channel.

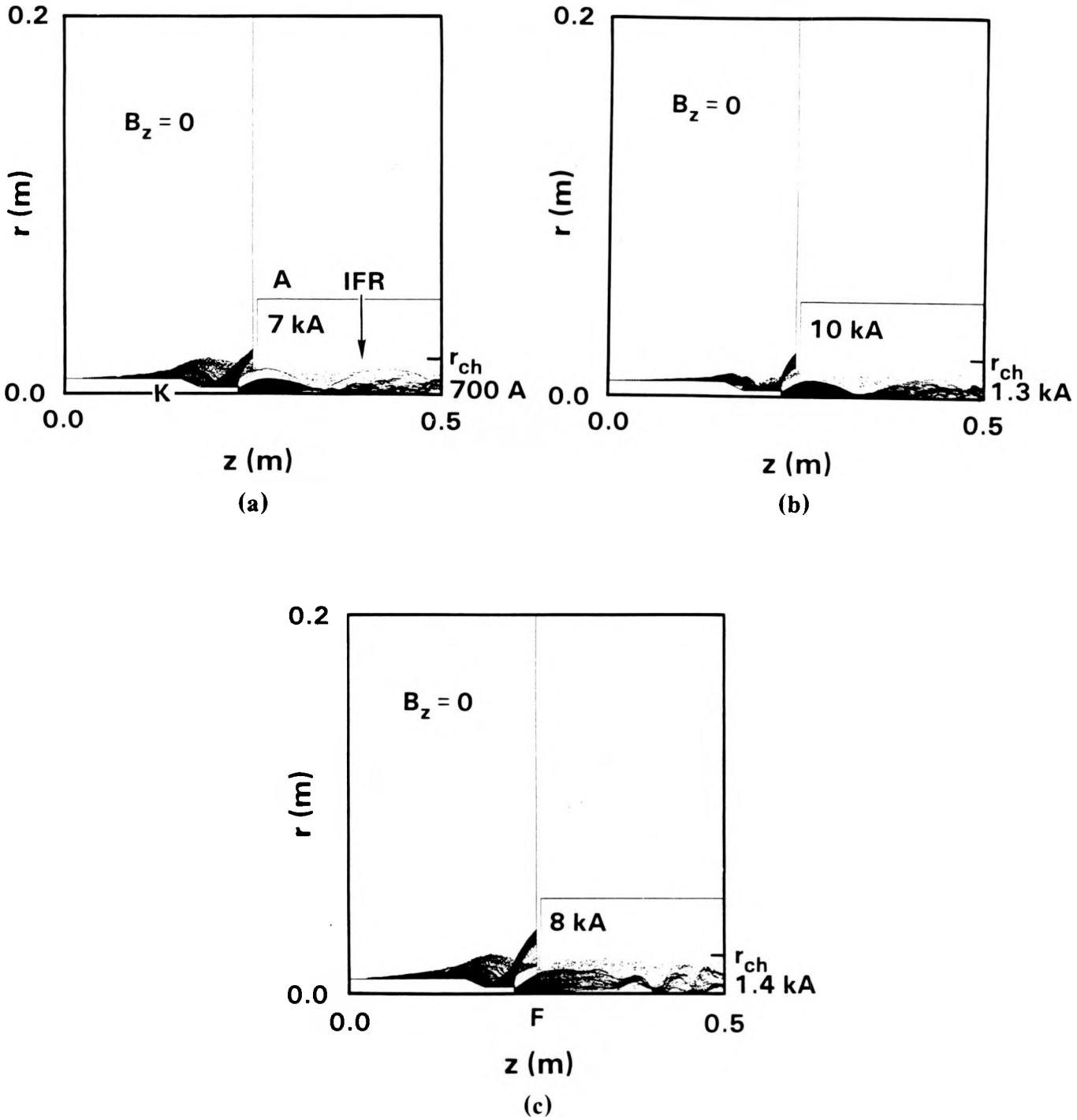

Figure 15. Little Recirc diode at V = 1 MV, no B_z, with IFR channel, showing electron maps from MAGIC for 3 cases:

(a) No ions, d = 2 cm, 8 kA total, 700 A out rhs.

(b) With ions from aperture , d = 2 cm, 11 kA total, 1.3 kA out rhs.

(c) With ions, d = 3 cm, 9 kA total, 1.4 kA out rhs, thin foil F.

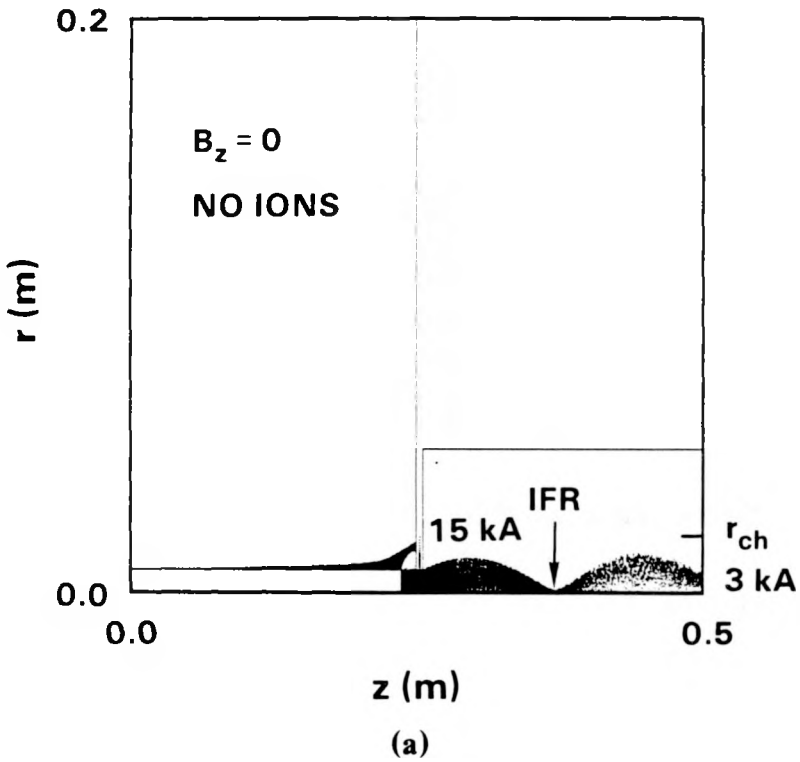

(a)

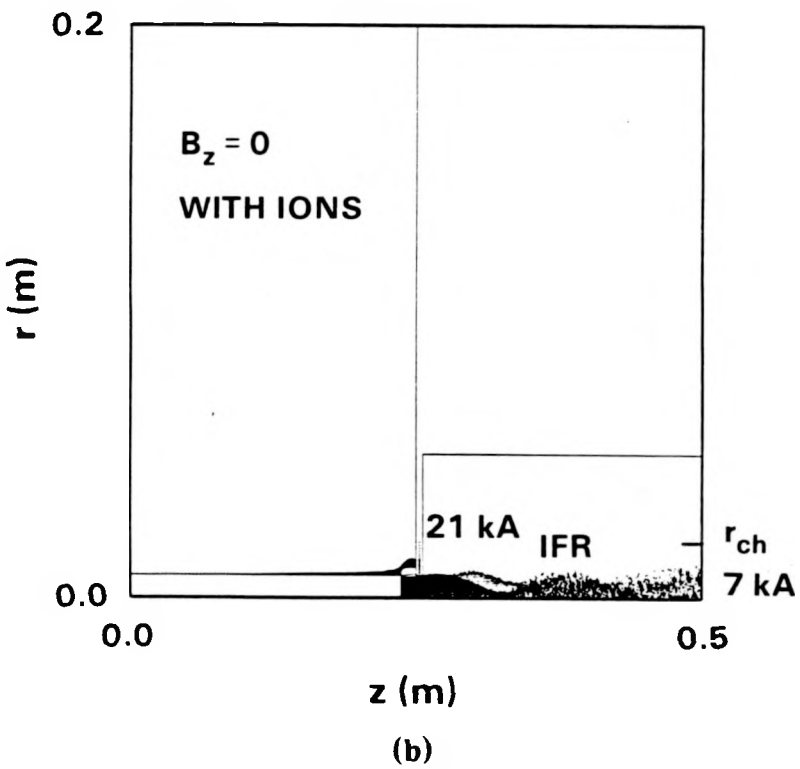

(b)

Figure 16. As in Fig. 15 but large cathode radius = 8 mm, smaller A-K gap = 1.27 cm, V = 1.2 MV, no anode foil, r_{aper} = 8 mm.
(a) No ions, 18 kA total, 3 kA out rhs.
(b) With ion emission (750 A) from aperture, 28 kA total, 7 kA out rhs.

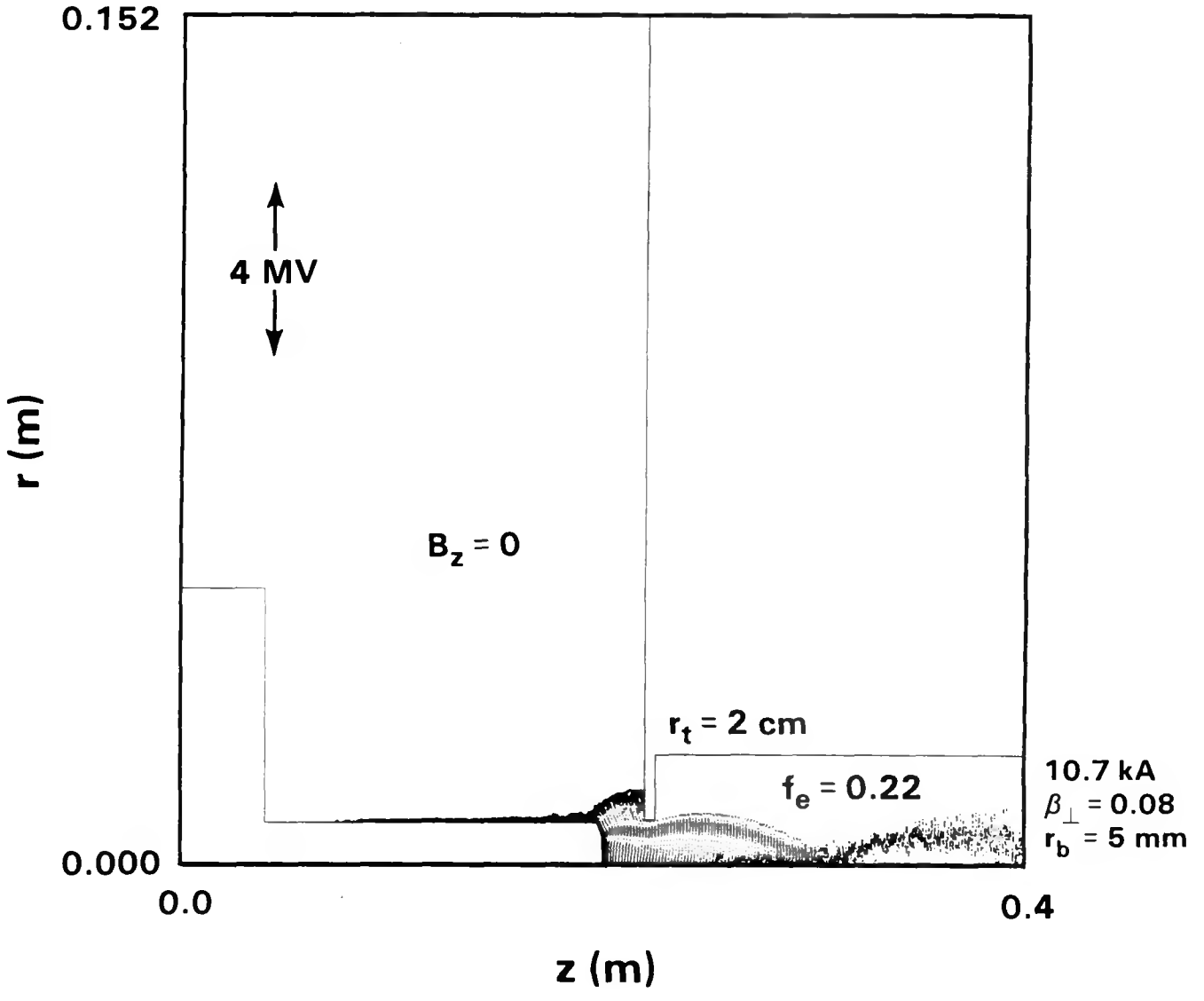

Figure 17. MAGIC (steady state) run of RLA "IFR" diode (IBEX) at 4 MV, 48 kA, d = 2 cm, an 11 kA beam is produced for $r_{aper} = r_{ch} = 8$ mm with $n_{ch} = 2.75 \times 10^{11}$ cm^{-3} ($m_i = \infty$). No applied B_z. The output beam quality is quite good (but not phase-mixed).

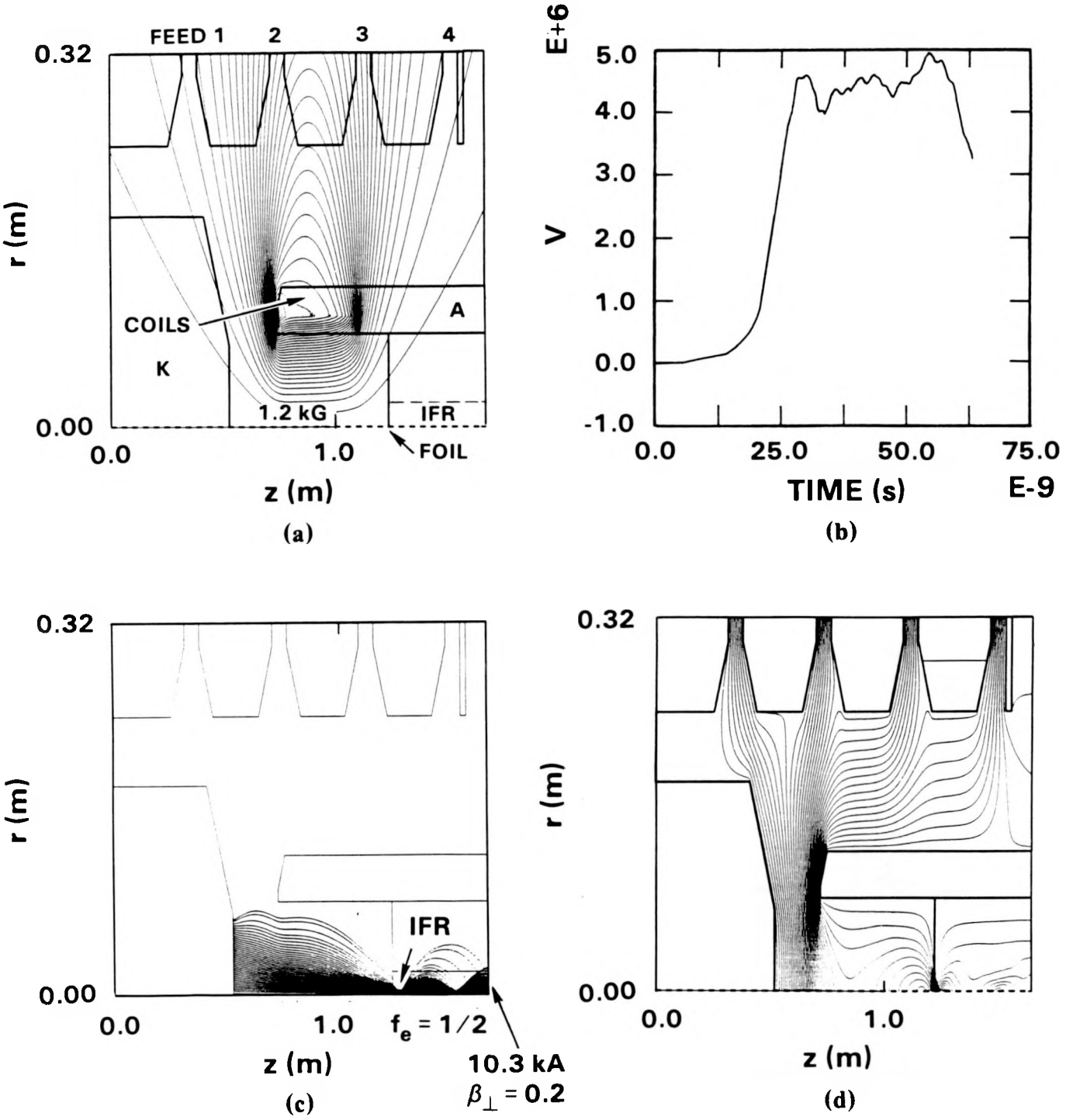

Figure 18. MAGIC simulation of the Recirc re-entrant non-immersed injector.

(a) Problem setup and B field applied.

(b) Diode voltage vs. time from the addition of the four input feed voltages.

(c) Electron flow for a 20 cm A-K gap during "flat" part of voltage pulse; for the 10 kA beam, the channel provides $f_e = 0.5$.

(d) Quasi-equipotential lines including beam space charge.

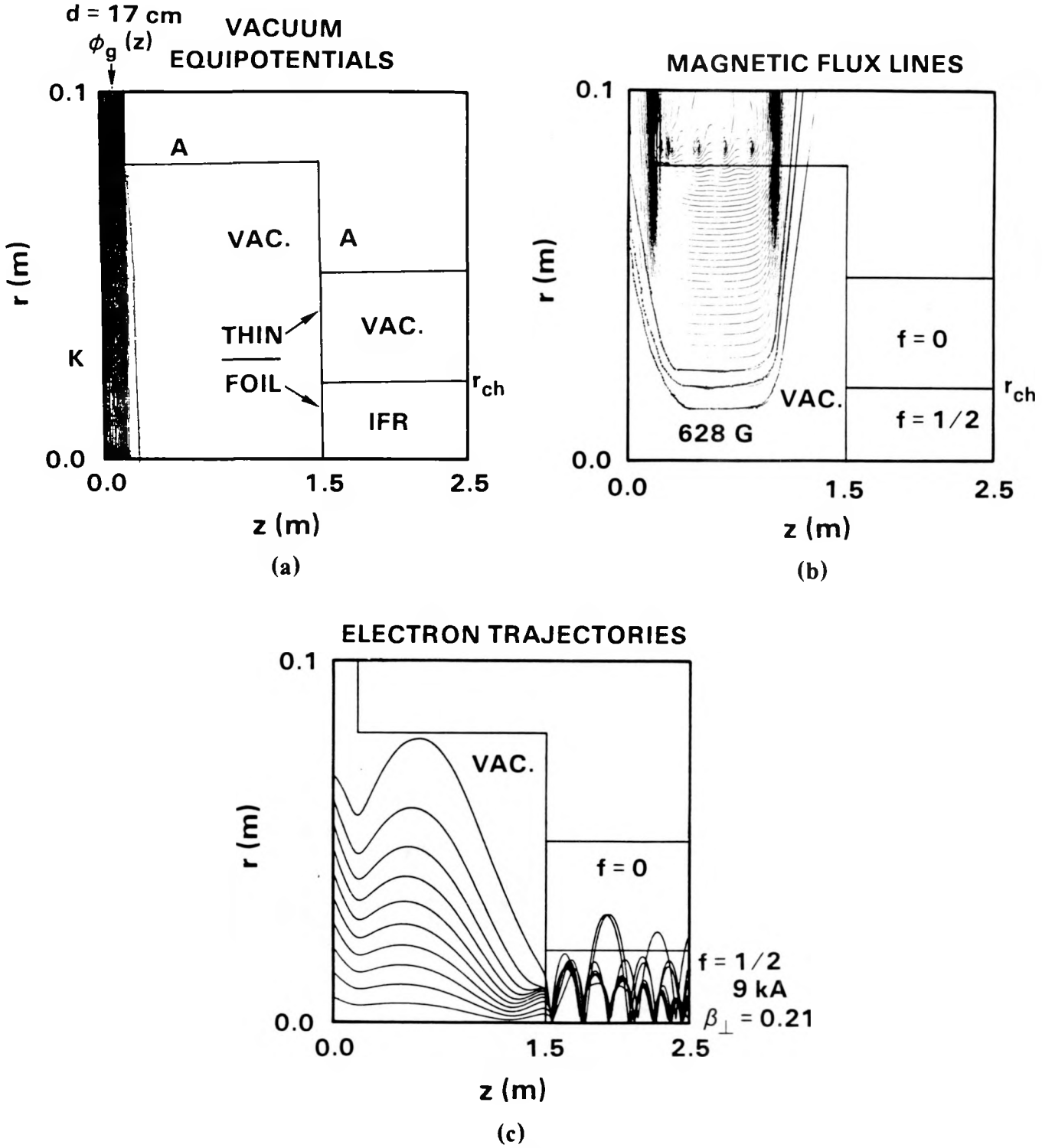

Figure 19. TRAJ run of a Recirc diode plus IFR channel (f_e = 1/2).
(a) Applied potential lines and problem geometry; A-K gap = 17 cm.
(b) Applied B lines; B_z(K) = 33 G.
(c) Electron trajectories for V = 4 MV, I = 9 kA. The output beam is mostly within the channel; $\beta_\perp$ = 0.21.

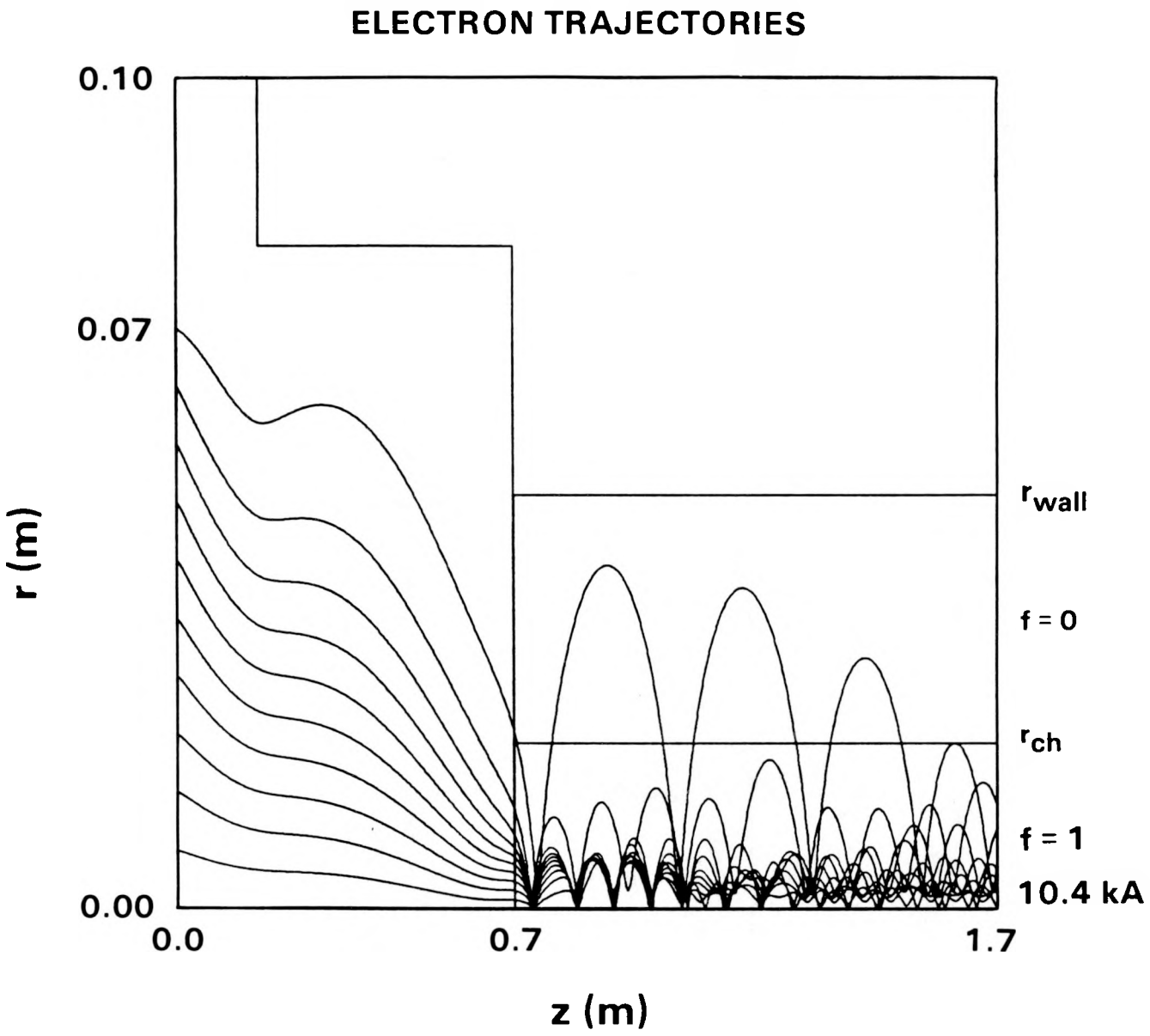

Figure 20. TRAJ run of Recirc diode, as in Fig. 19 but shorter cathode-foil distance, stronger applied B, f_e = 1 in IFR channel. Output at 4 MV: 10kA, $\beta_\perp$ = 0.25.

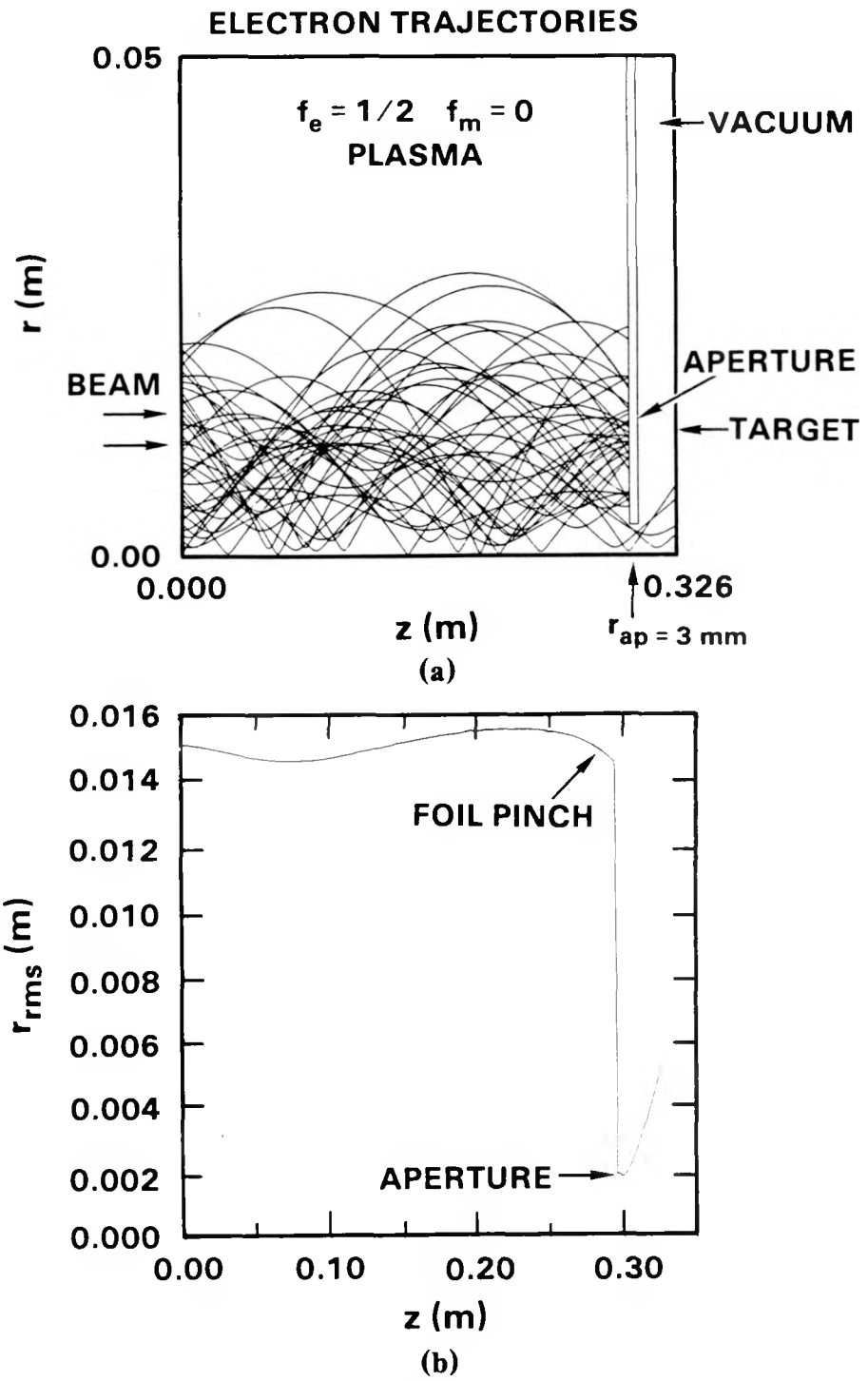

Figure 21. **TRAJ run of beam-aperture problem. The input (lhs) beam is in equilibrium in an IFR channel ($f_e = 1/2$), with $\gamma = 8$, $I_b = 10$ kA, $\beta_\perp = 0.18$, and uniform $j_z(r)$. There is no B_z or net rotation. Only 10 trajectories out of 200 pass through the hole into the vacuum expansion region. This expansion can be used to roughly deduce $\beta_\perp$ of the beam near the axis, but the uncertainty is too large and large $-V_\theta$ electrons are not included.**

(a) Trajectories.

(b) r_{rms} vs. z.

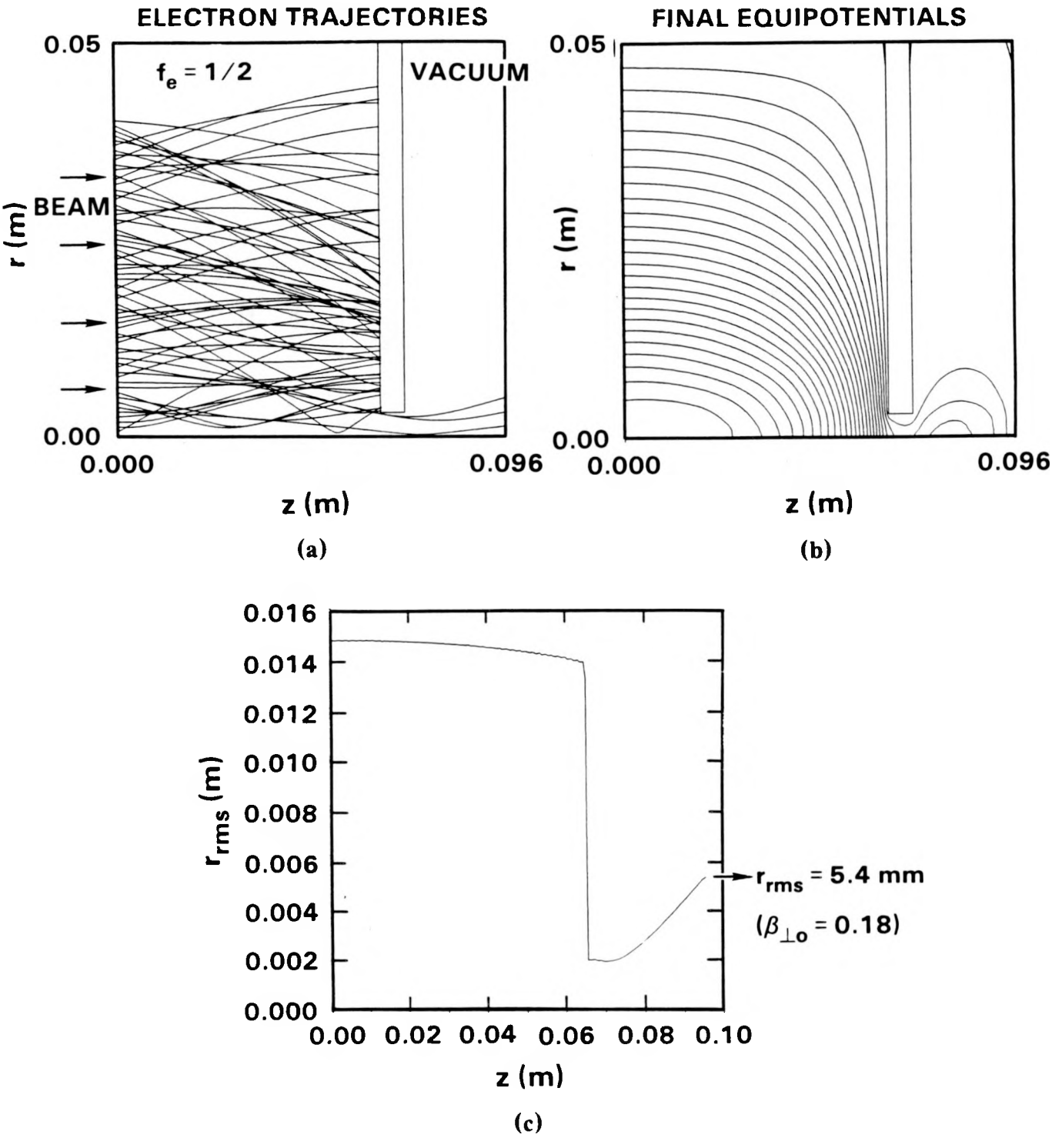

Figure 22. As in Fig. 21 but shorter system and Gaussian (radial profile) beam. On the left of the aperture, the beam is in equilibrium; on the right, 576 A expands in vacuum.
(a) Trajectories.
(b) Equipotentials.
(c) r_{rms} vs. z.

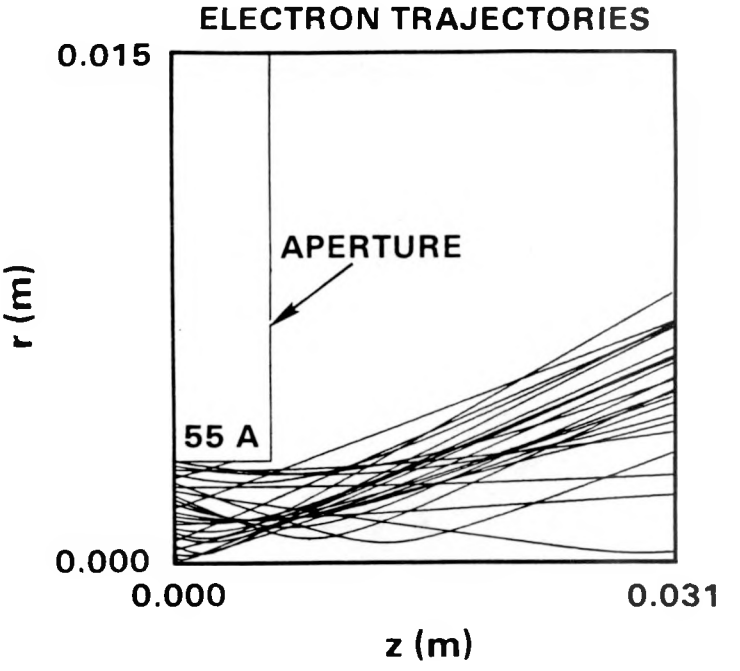

(a)

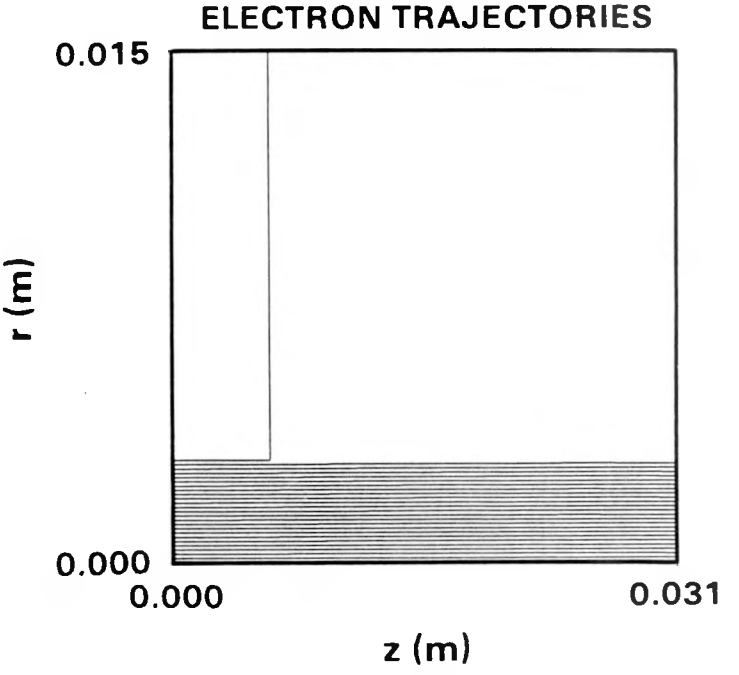

(b)

Figure 23. **TRAJ run of aperture-only emittance calculation. The input beam is 395 A with $\gamma = 8$ and uniform profile. The precise value of current is not relevant, provided it is not too large, because comparing (a) with $\beta_\perp = 0.18$ and (b) with $\beta_\perp = 0$ shows that space charge and B_θ effects play no role; the expansion in (a) is emittance driven and agrees with eq. (1) to better than 2%. Note 55 A scrape-off on aperture in (a).**

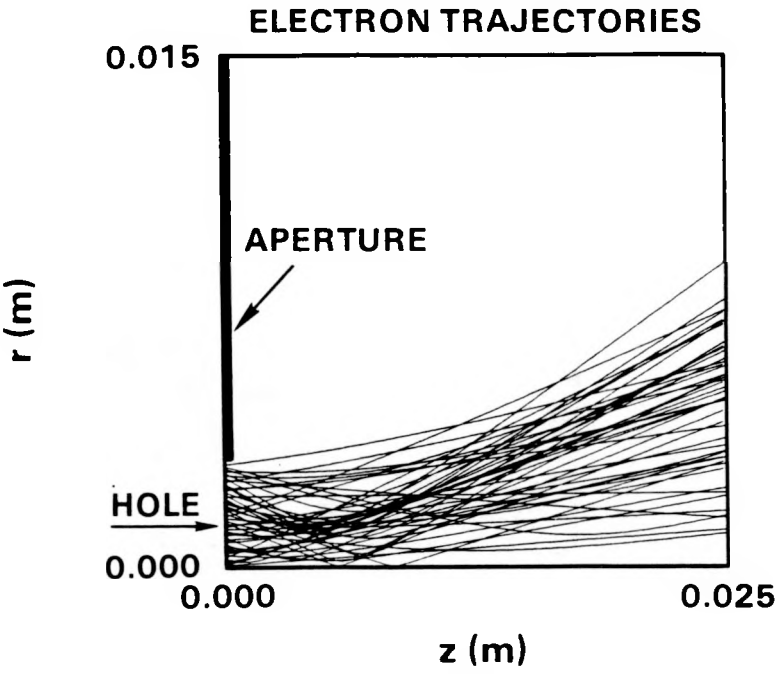

(a)

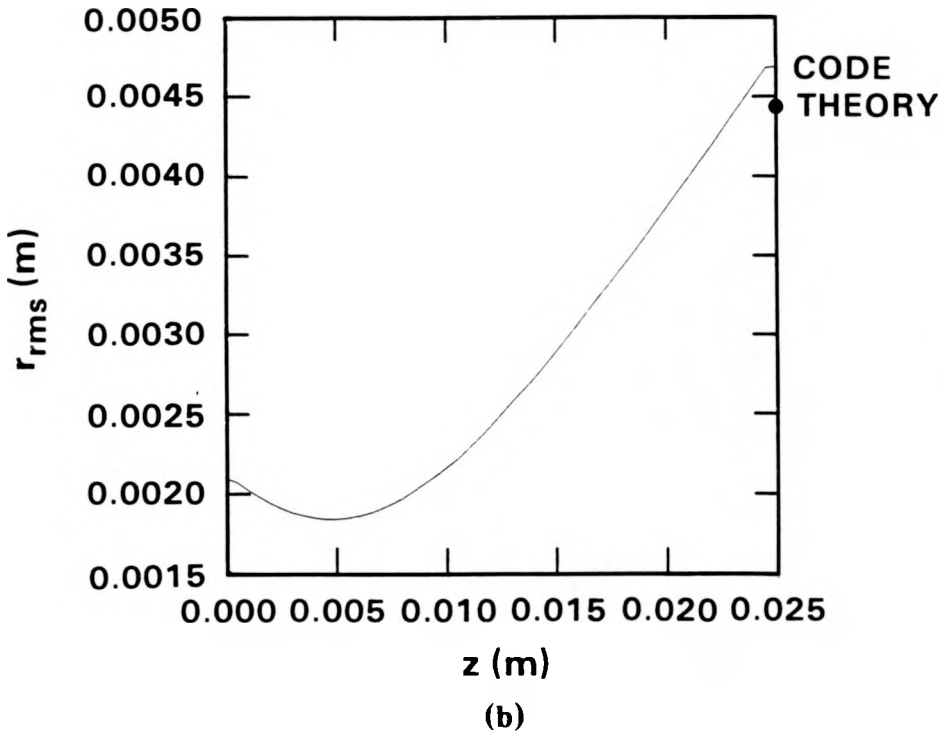

(b)

Figure 24. As in Fig. 23 except use thin aperture and include an initial convergence of the beam to simulate a foil-pinch effect. Input: 394 A, γ = 8, $\beta_\perp$ (random) = 0.174, $\overline{\beta}_r = -0.15\ r/r_{ap}$.
(a) Trajectories (every fifth plotted).
(b) r_{rms} (z) showing slight initial decrease in r_{rms}.

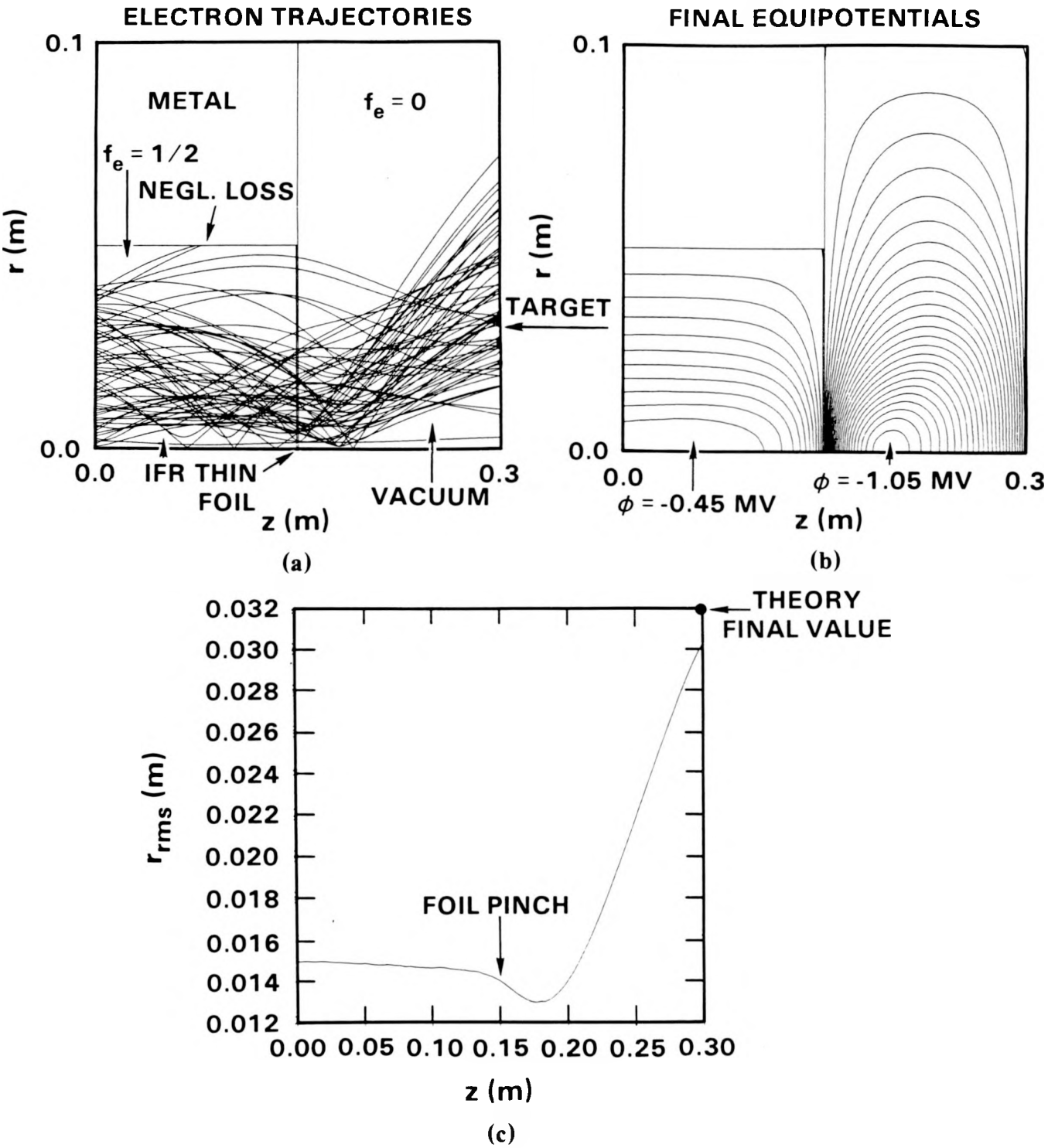

Figure 25. **TRAJ simulation of whole beam expansion to measure emittance for Recirc/IBEX beam of 10 kA, $\gamma = 8$, $\beta_{\perp o} = 0.18$, $B_z = 0$, $r_0 = 1.5$ cm.**

(a) Trajectories (every fifth of 320 is plotted).

(b) Equipotentials showing non-negligible electric fields but no virtual cathode problem.

(c) r_{rms} vs. z showing equilibrium (lhs), small foil pinch, vacuum expansion agreeing with theory.

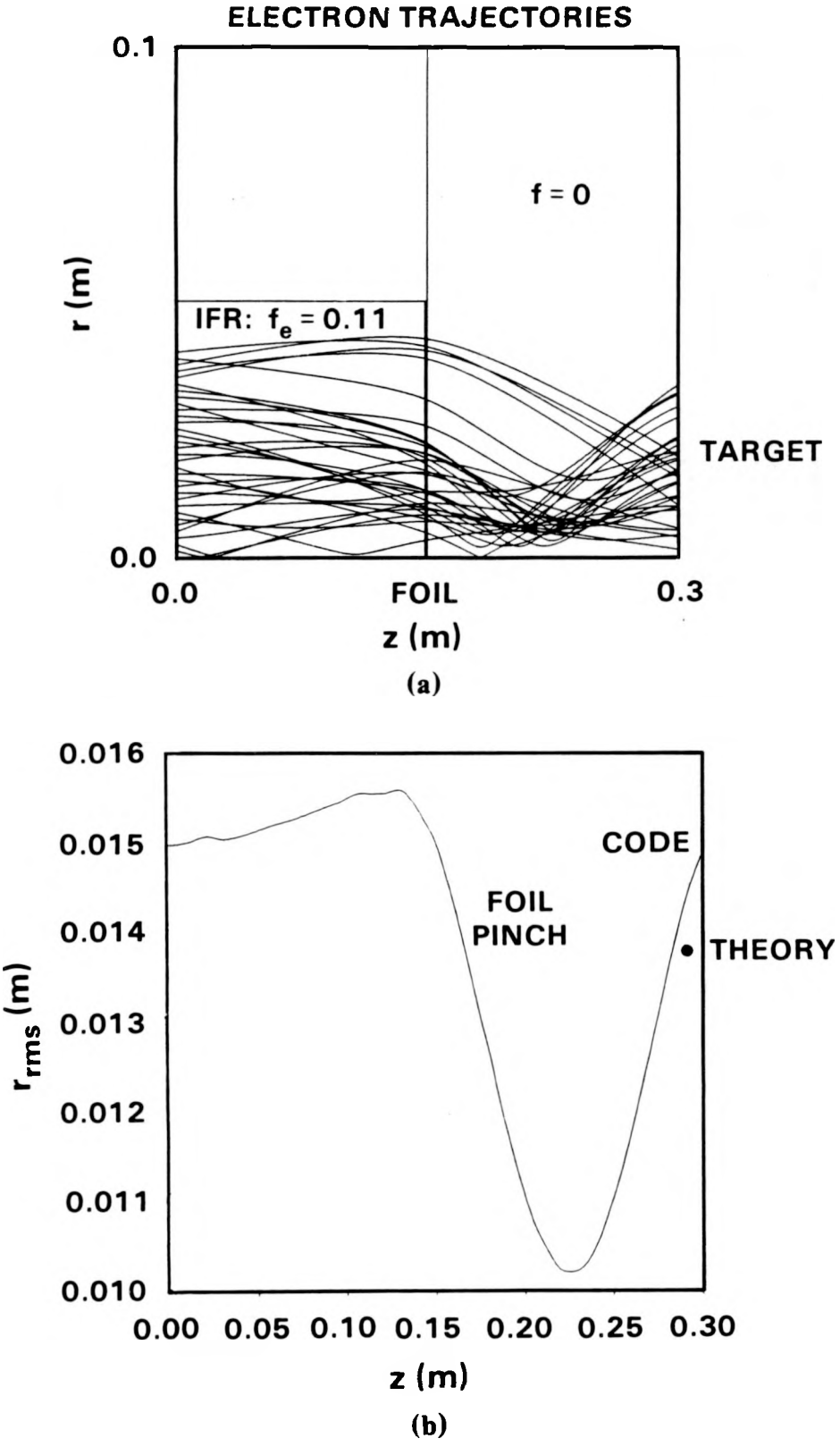

Figure 26. As in Fig. 25 but cooler beam $\beta_{\perp o}$ = 0.09, f_e = 0.11 on lhs of foil.
(a) Trajectories (total 160 used).
(b) r_{rms} vs. z; note huge foil pinch effect.

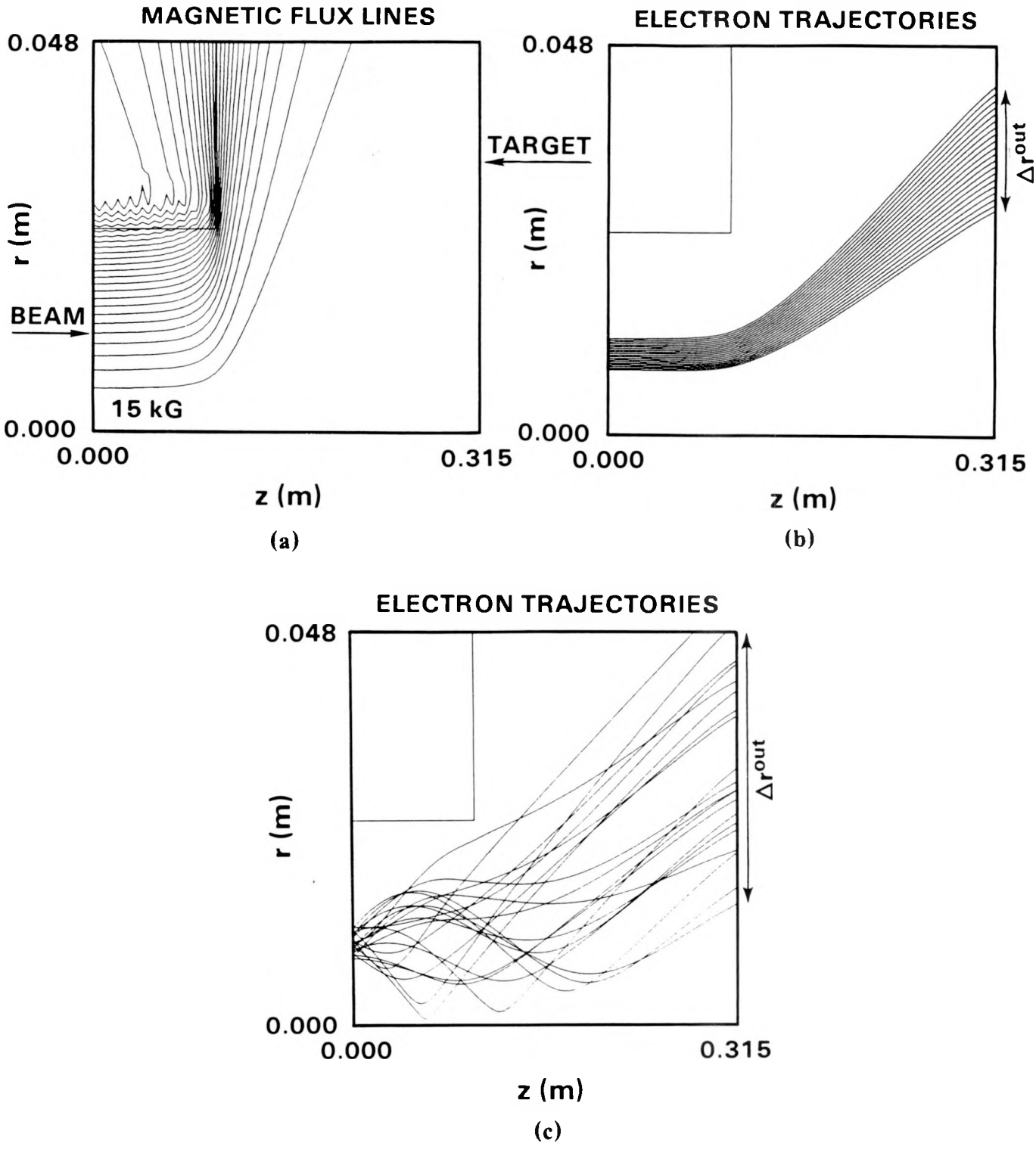

Figure 27. TRAJ calculation of RADLAC beam emittance in the full B_z guide field using the differential expansion method.

(a) Applied B lines in extraction region; B_0 = 15 kG.

(b) Trajectories for cold input beam.

(c) Trajectories for warm input beam, $\beta_{\perp o}$ = 0.156.

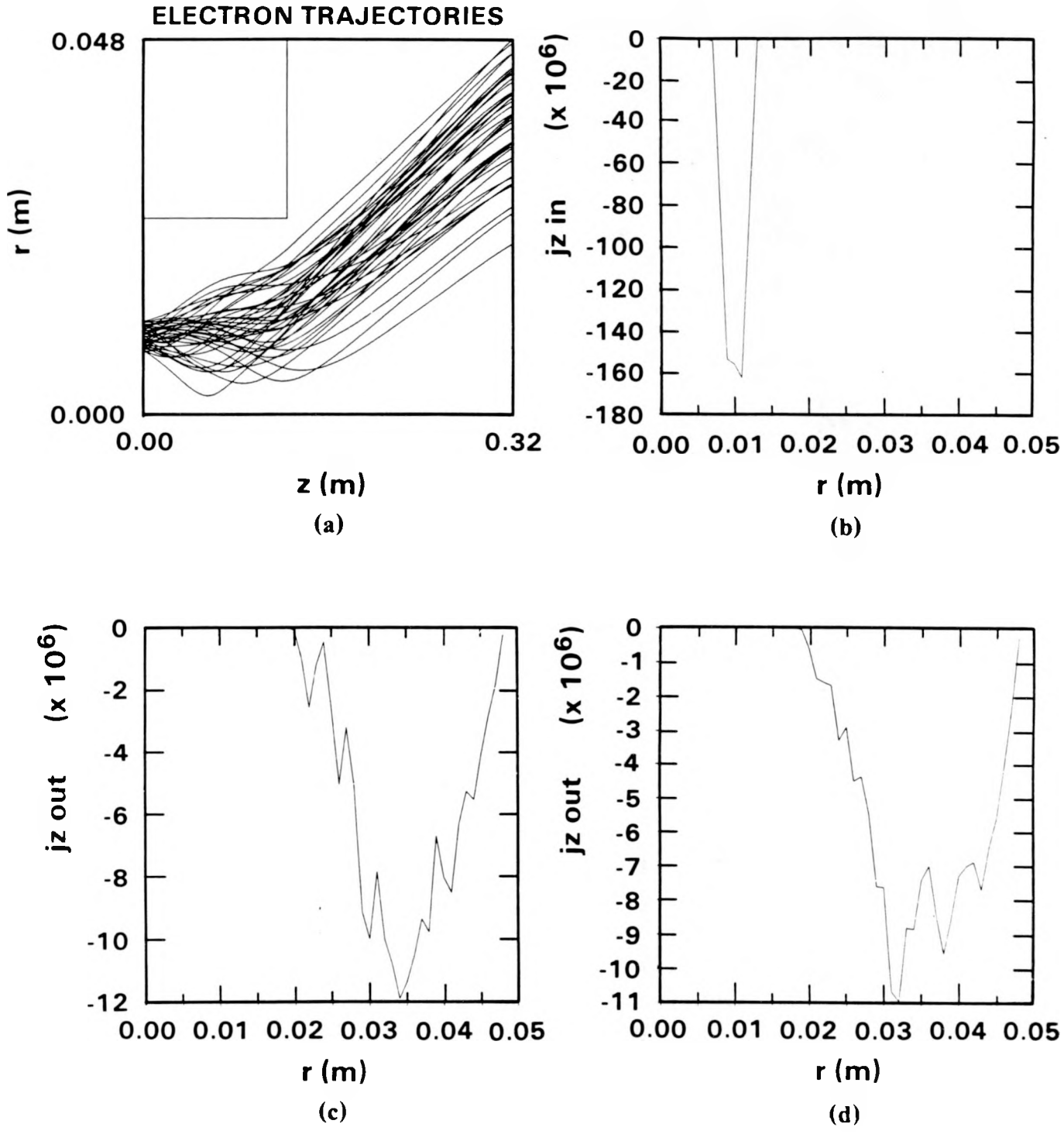

Figure 28. As in Fig. 27 but $\beta_{\perp_o} = 0.08$.
(a) Trajectories (200 total).
(b) $j_z(r)$ input.
(c) $j_z(r)$ output (200 trajectories).
(d) $j_z(r)$ output (400 trajectories).

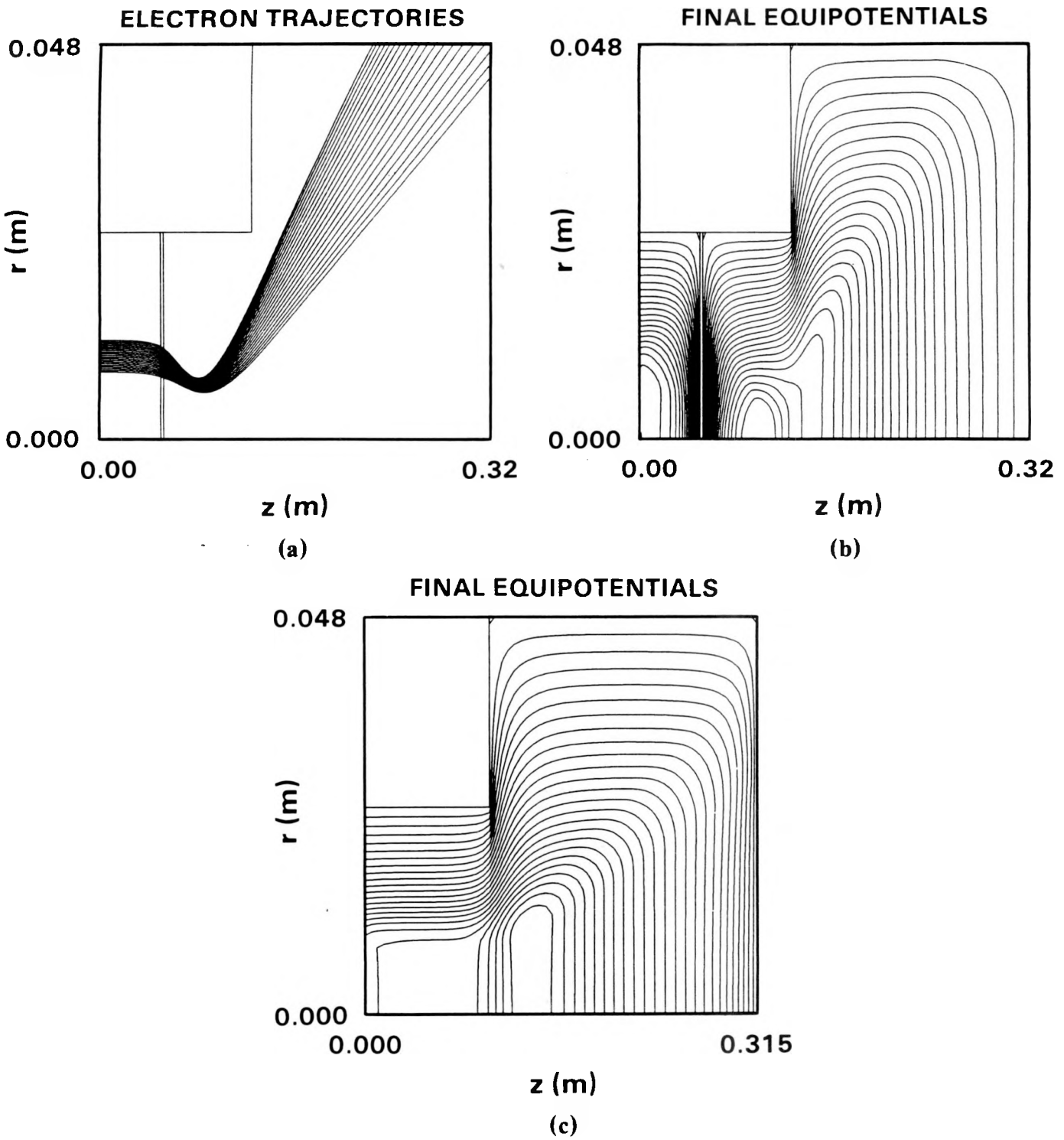

Figure 29. As in Fig. 27b but add thin foil in full-B_z region to measure beam parameters (input and output) all on one shot.
(a) Trajectories.
(b) Equipotentials, showing large E_z near foil and shorting of E_r.
(c) Equipotentials without foil (for case in Fig. 27b).

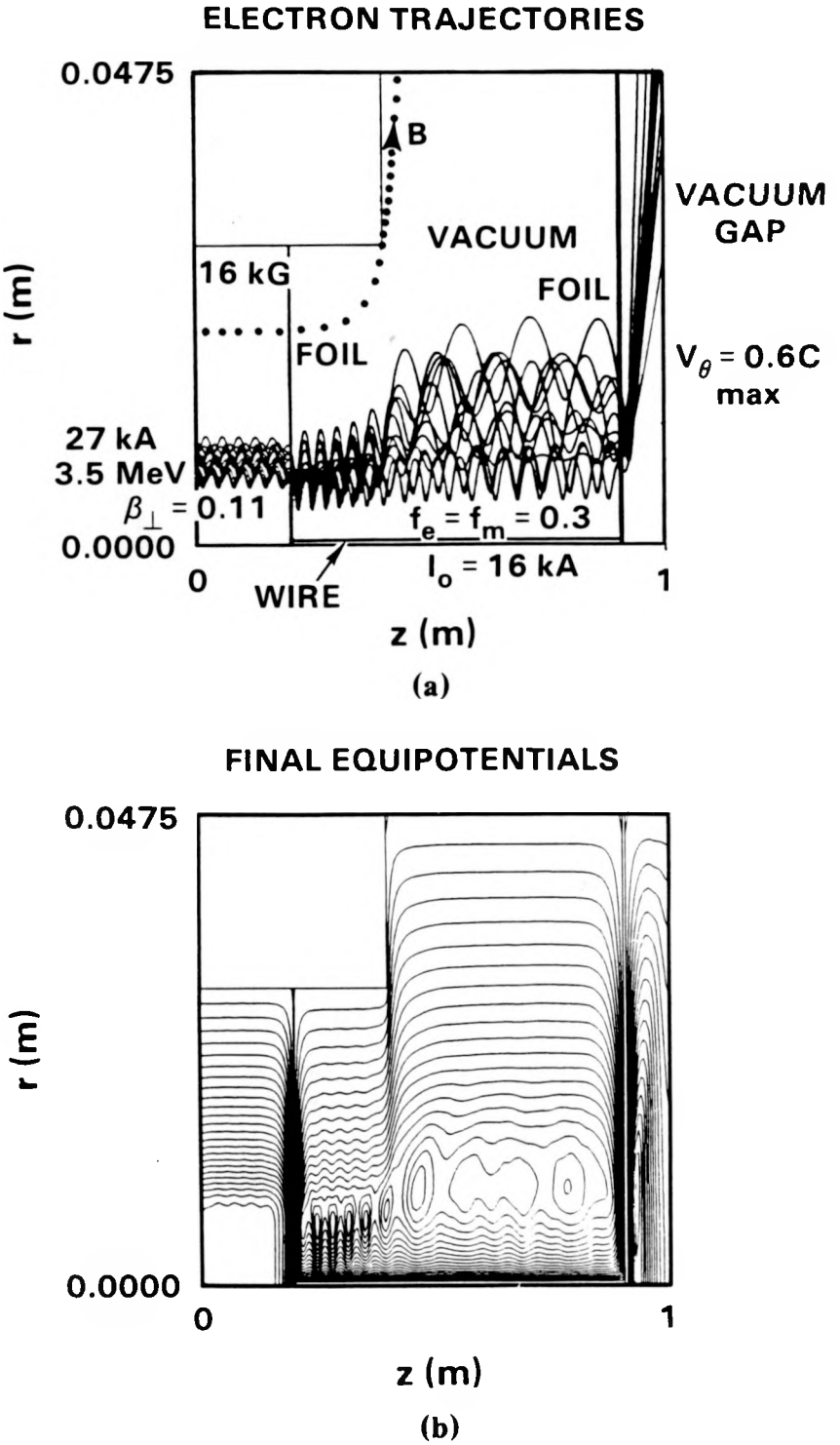

Figure 30. **TRAJ model of the IBEX B_θ-cell experiment. The input beam (lhs) has I_b = 27 kA, total energy = 3.5 MeV, $\beta_\perp$ = 0.11, annulus 7, 10 mm, and is extracted from 16 kG. The wire carries 16 kA (applied), but the wire charge and current neutralization fractions are 0.3.**
(a) Trajectories, showing rhs blowup in vacuum gap.
(b) Equipotentials.

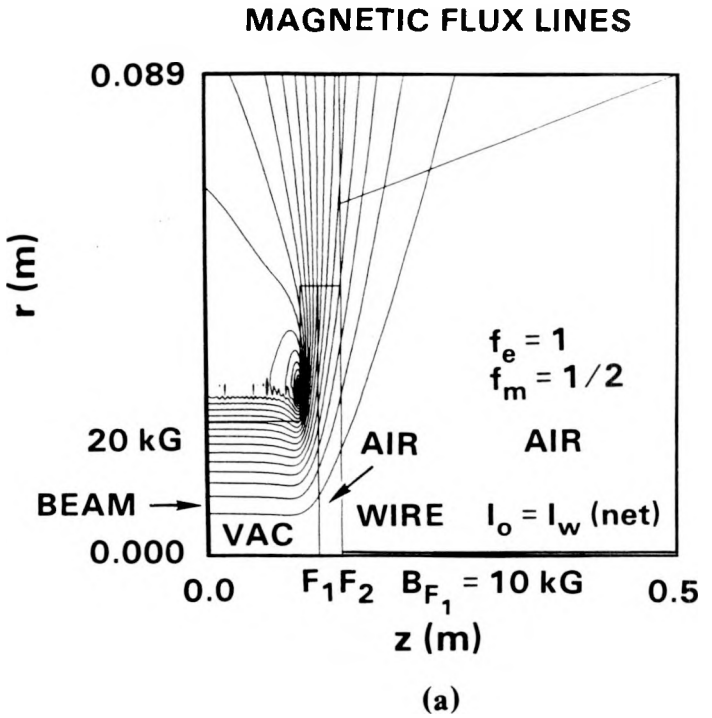

(a)

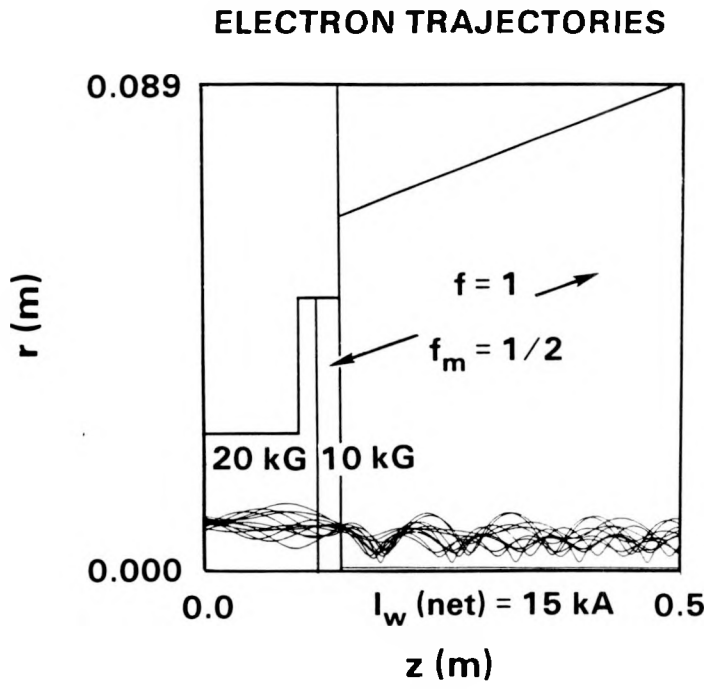

(b)

Figure 31. TRAJ model of the RADLAC B_θ/gas-cell system. There are 2 foils, F_1 and F_2, about an inch apart; this gap and the wire cell are filled with air, which we model using empirical neutralization fractions.

(a) B field (applied) and problem setup, foil F_1 in standard position.

(b) Electron trajectories for γ = 30, 30 kA, $\beta_{\perp_o}$ = 0.08, r_0 = 0.87 cm rms; output r_b = 0.63, $\beta_\perp$ = 0.30. The net wire current is 15 kA.

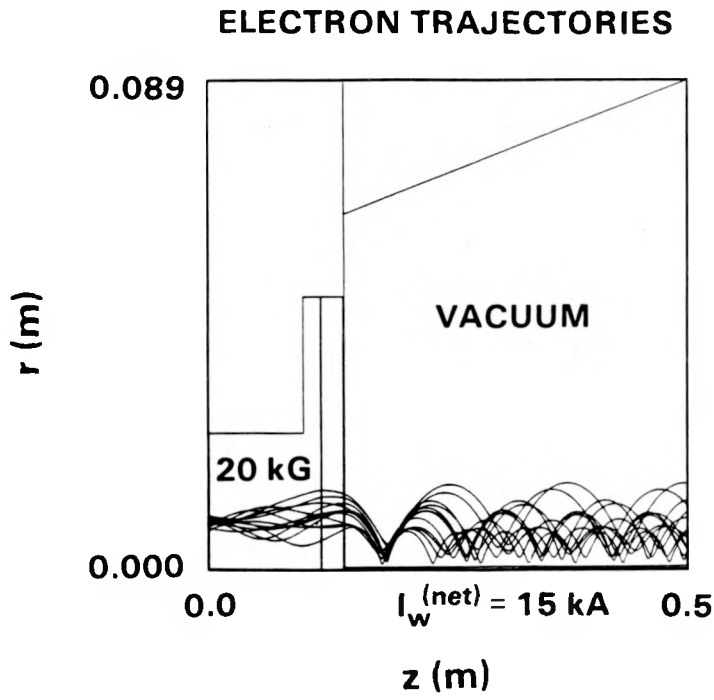

(a)

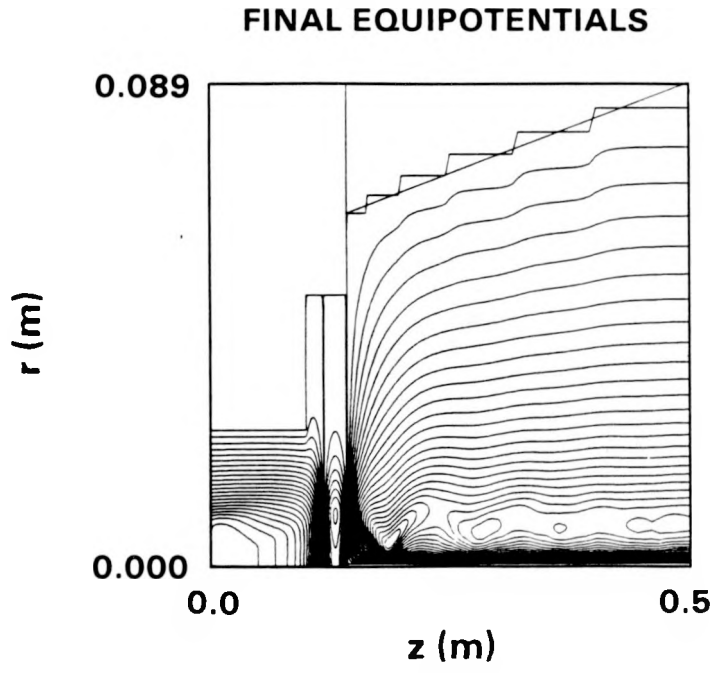

(b)

Figure 32. As in Fig. 31 but no gas (i.e., vacuum everywhere).
(a) Trajectories, with output rms $\beta_\perp$ = 0.33, r_b = 0.90 cm.
(b) Equipotentials corresponding to (a).

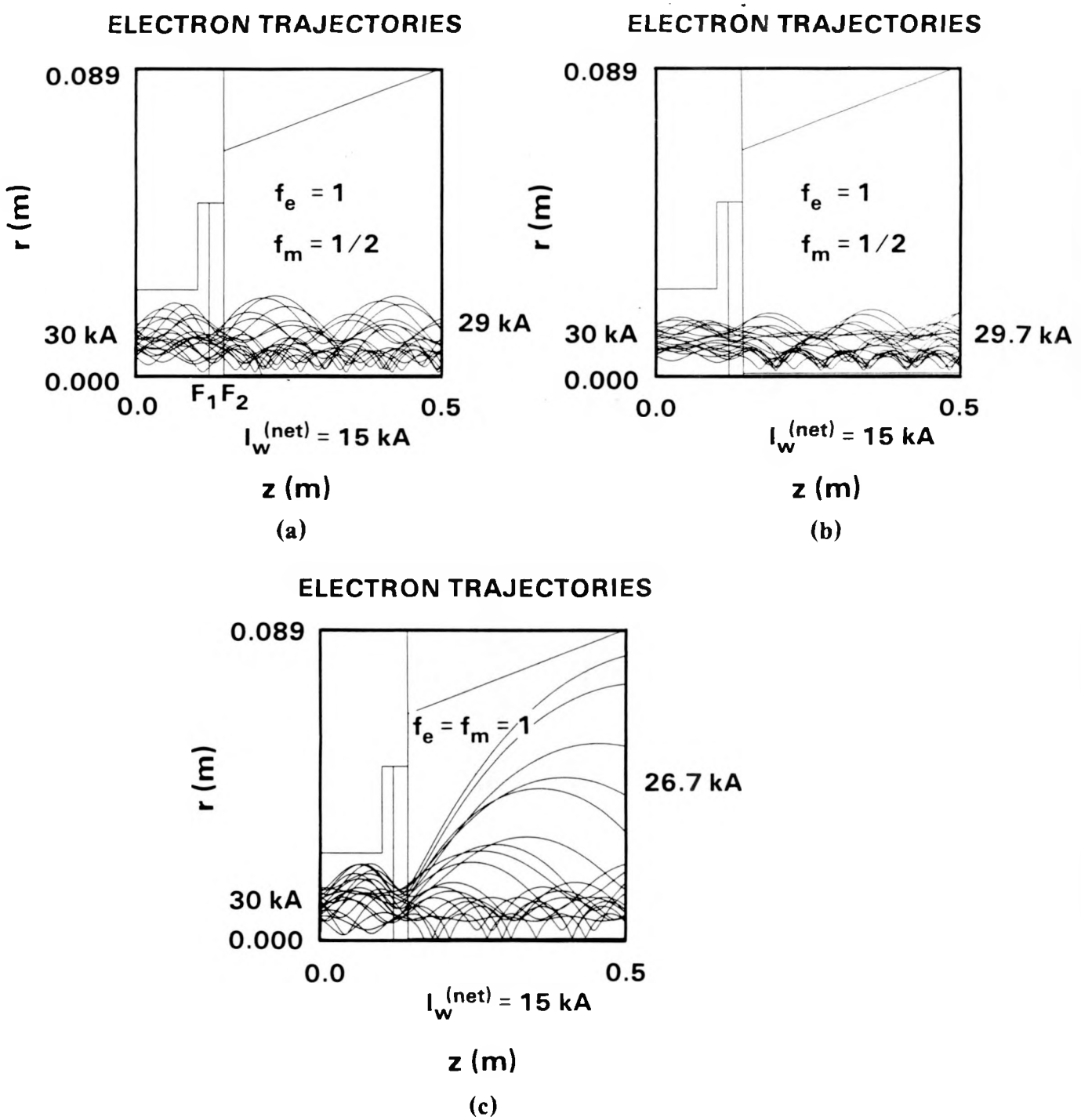

Figure 33. As in Fig. 31 but fatter-annulus input beam. Net wire current is still 15 kA.
(a) $\beta_{\perp o}$ = 0.16 giving output $\beta_\perp$ = 0.30, r_b = 1.1 cm, 1 kA loss to wire.
(b) $\beta_{\perp o}$ = 0.08, giving output $\beta_\perp$ = 0.29, r_b = 1.05 cm.
(c) $\beta_{\perp o}$ = 0.16, f_m^{gas} = 1 (complete current neutralization by the gas), giving output $\beta_\perp$ = 0.24, r_b = 2.5 cm, 3 kA loss to wire.

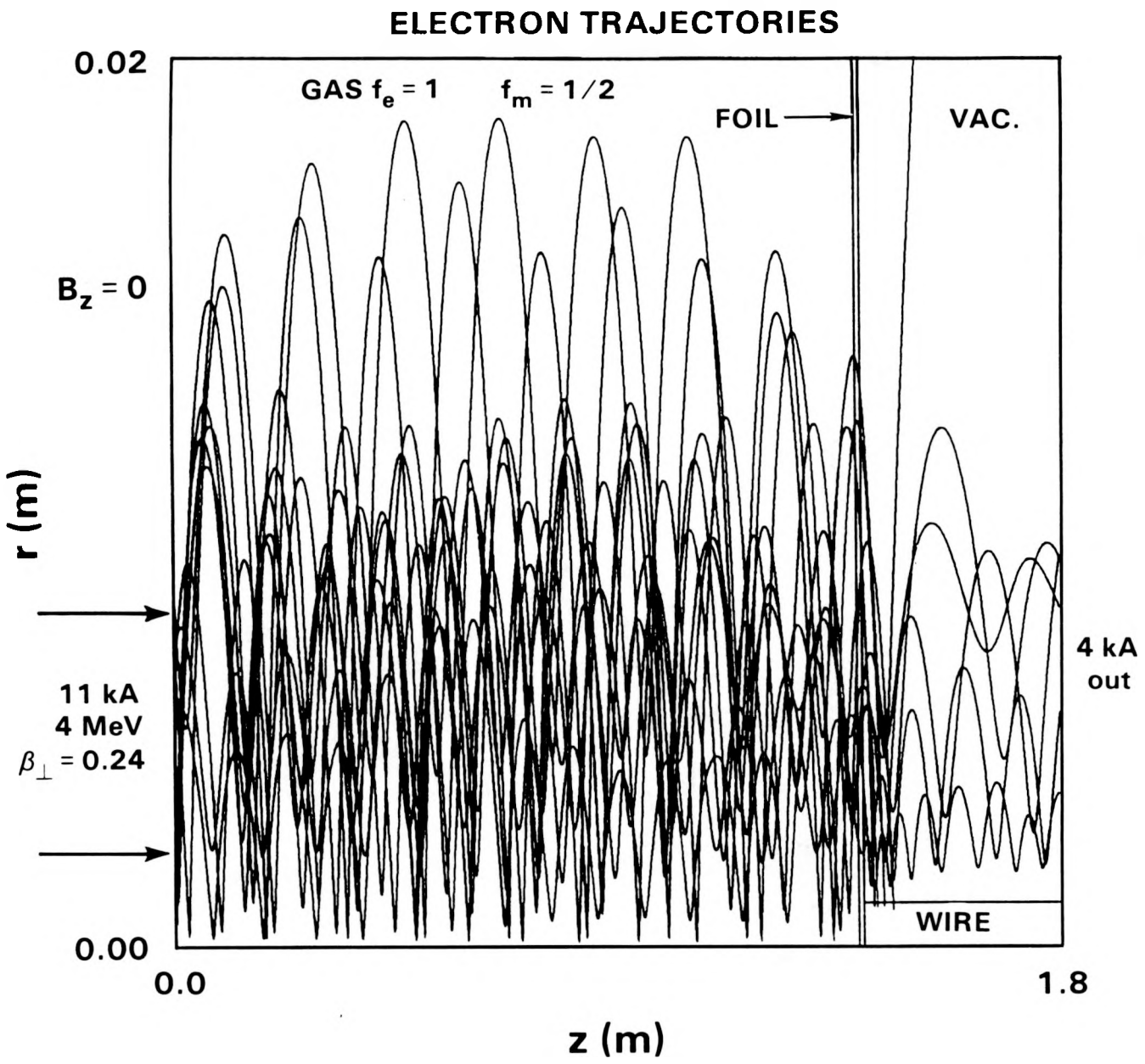

Figure 34. TRAJ run of IFR cell plus B_θ cell for Recirc parameters. The main problem is that the lack of net rotation allows most of the beam to hit the wire.

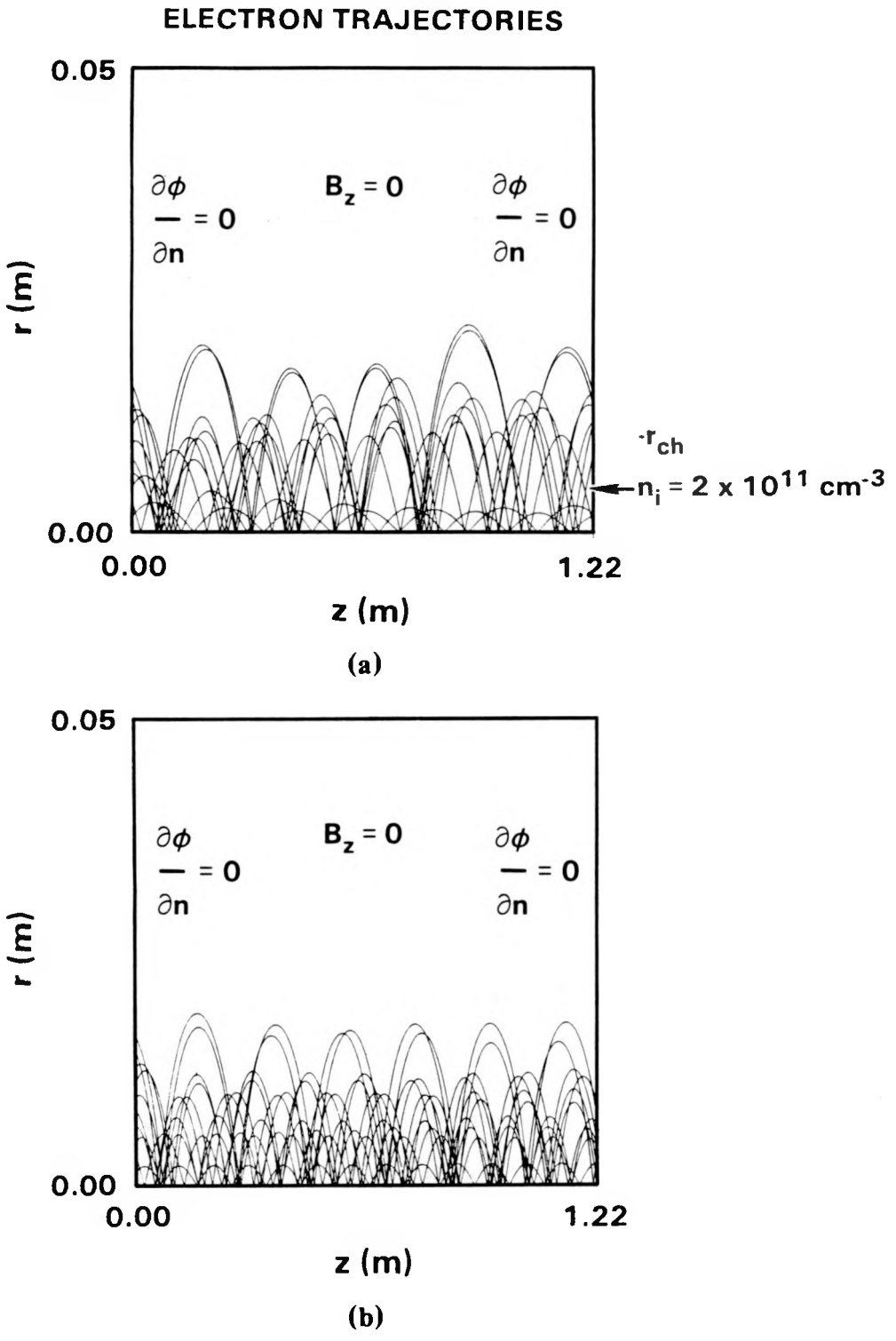

Figure 35. TRAJ runs of beam equilibria in IFR channels. Beam: 4 MeV, 10 kA, $\beta_{\perp o} = 0.08$. Both ends are "open" electrically (no foils). There is no B_z. Both cases have $f_e = 0.3$, $f_m = 0$.

(a) Uniform channel, $n_i = 2 \times 10^{11}$ cm^{-3} ($r < 1$ cm).

(b) Peaked channel, $n_i = 6 \times 10^{11}$ cm^{-3} ($r < 0.4$ cm), 1.24×10^{11} cm^{-3} ($0.4 < r < 1$ cm).

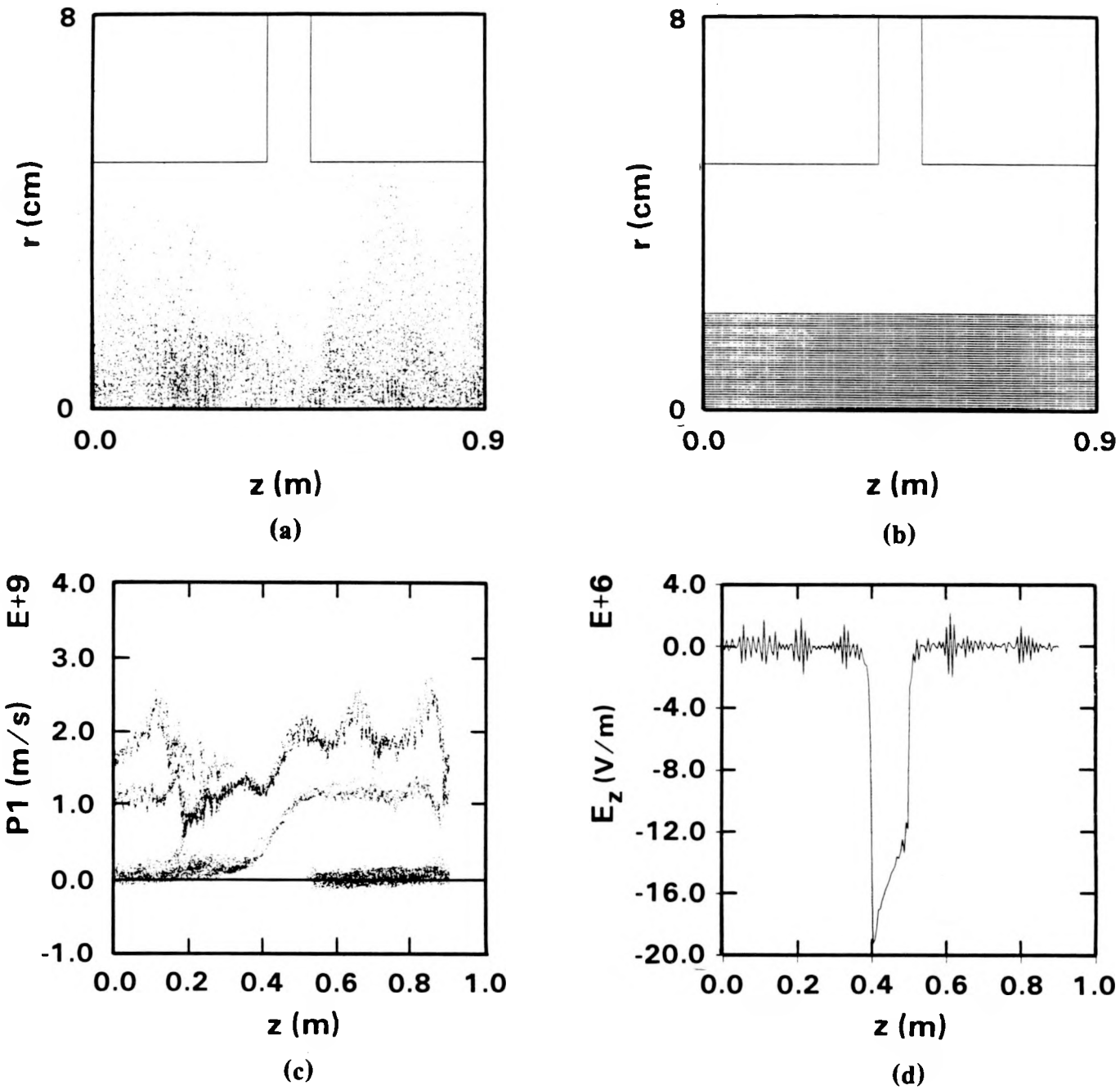

Figure 36. MAGIC simulation of IFR gap (no beam) for Recirc with periodic boundary conditions. Time = 7.5 ns. Applied gap voltage 1.5 MV (2 ns rise). Channel: r_{ch} = 2 cm, $n_{ch} = 8 \times 10^{10}$/cc.

(a) Electrons.

(b) Ions ($m_i = \infty$).

(c) γV_z vs. z phase space.

(d) $E_z(z)$ outside channel.

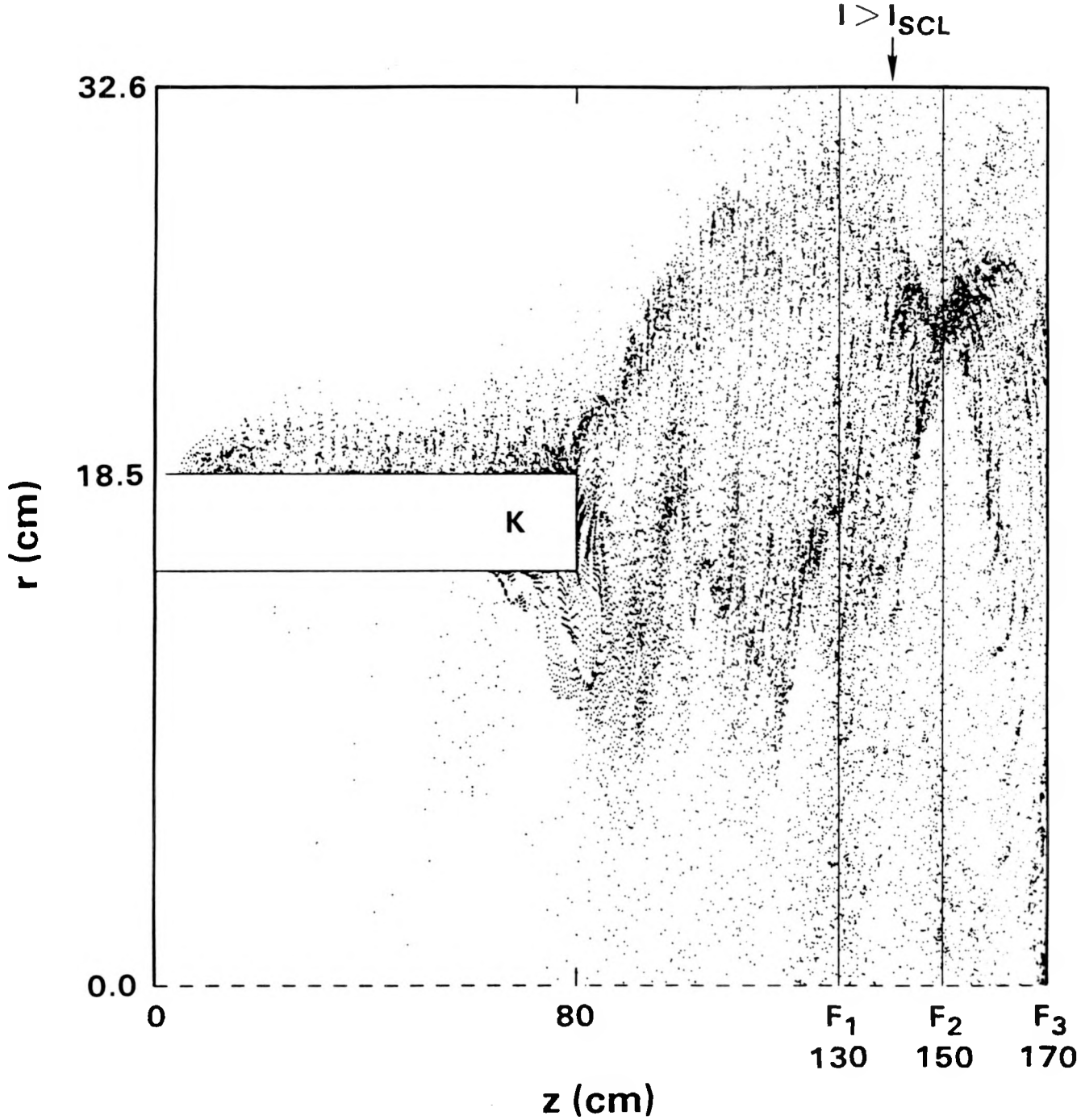

Figure 37. **MAGIC run of Hermes III diode plus foil-focus system. For V = 20 MV, the diode current is 700 kA. The foils (spacing 20 cm) perturb the beam, in fact a VK forms past F_1, because the space charge limit is exceeded.**

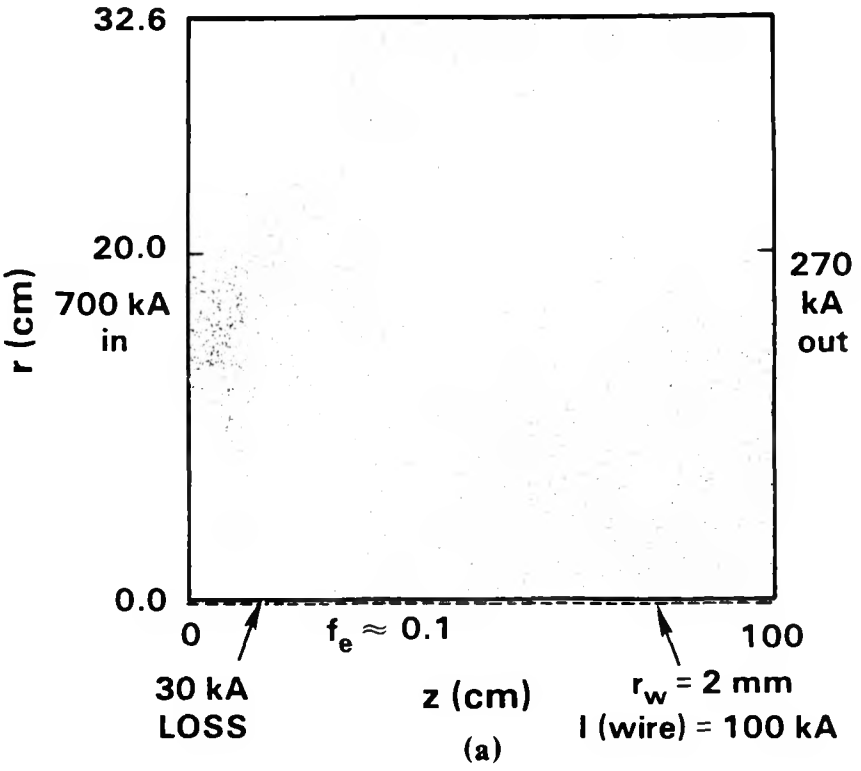

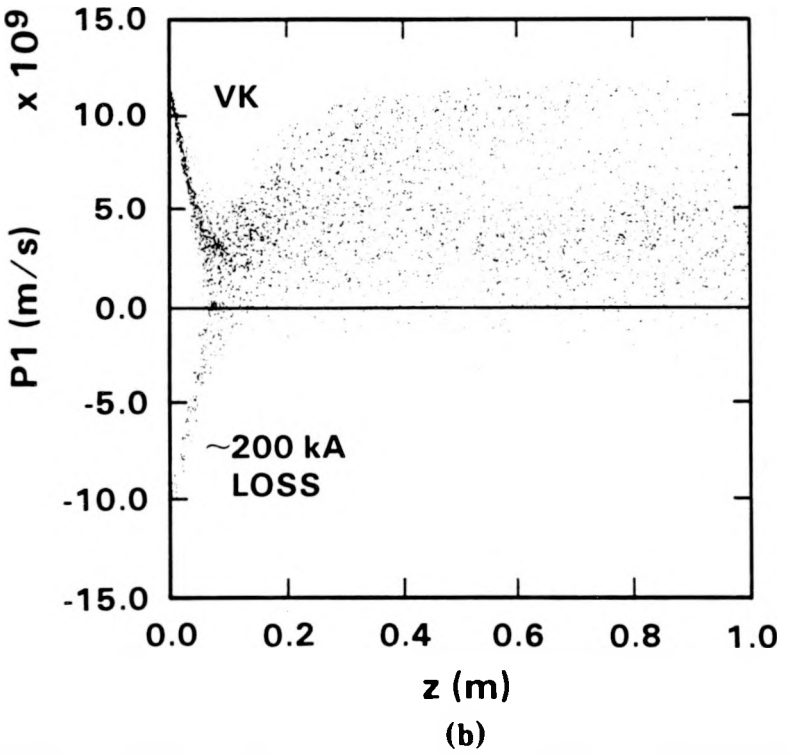

Figure 38. MAGIC run of Hermes III vacuum B_θ cell. Injected beam: 700 kA, 20 MeV, $\beta_{\perp o} = 0.3$, annulus (11, 20 cm); no B_z or rotation. Wire: 2 mm radius, carrying 100 kA. There is a big loss to the wall, a small loss to the wire, so only 270 kA emerges from the cell with poor quality. Problem: the space-charge-limit is exceeded.

(a) Electron map in quasisteady state.

(b) γV_z vs. z phase space showing VK in agreement with 1-D theory.

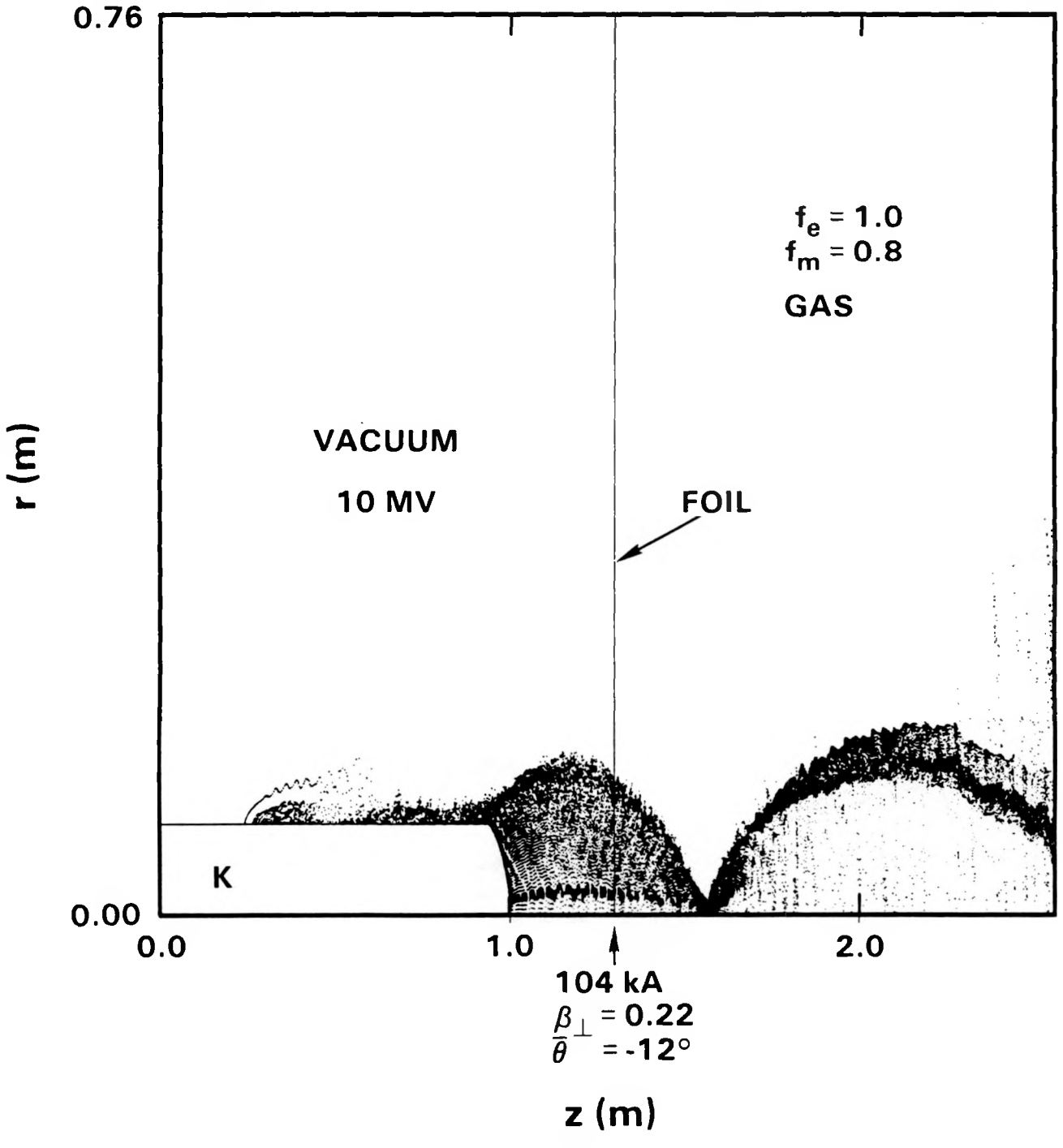

Figure 39. MAGIC run of Hermes II diode plus a short gas cell, characterized by $f_e = 1, f_m = 0.8$. This setup is similiar to the typical experimental one, and yields the expected 100 kA at 10 MV. There is no B_z.

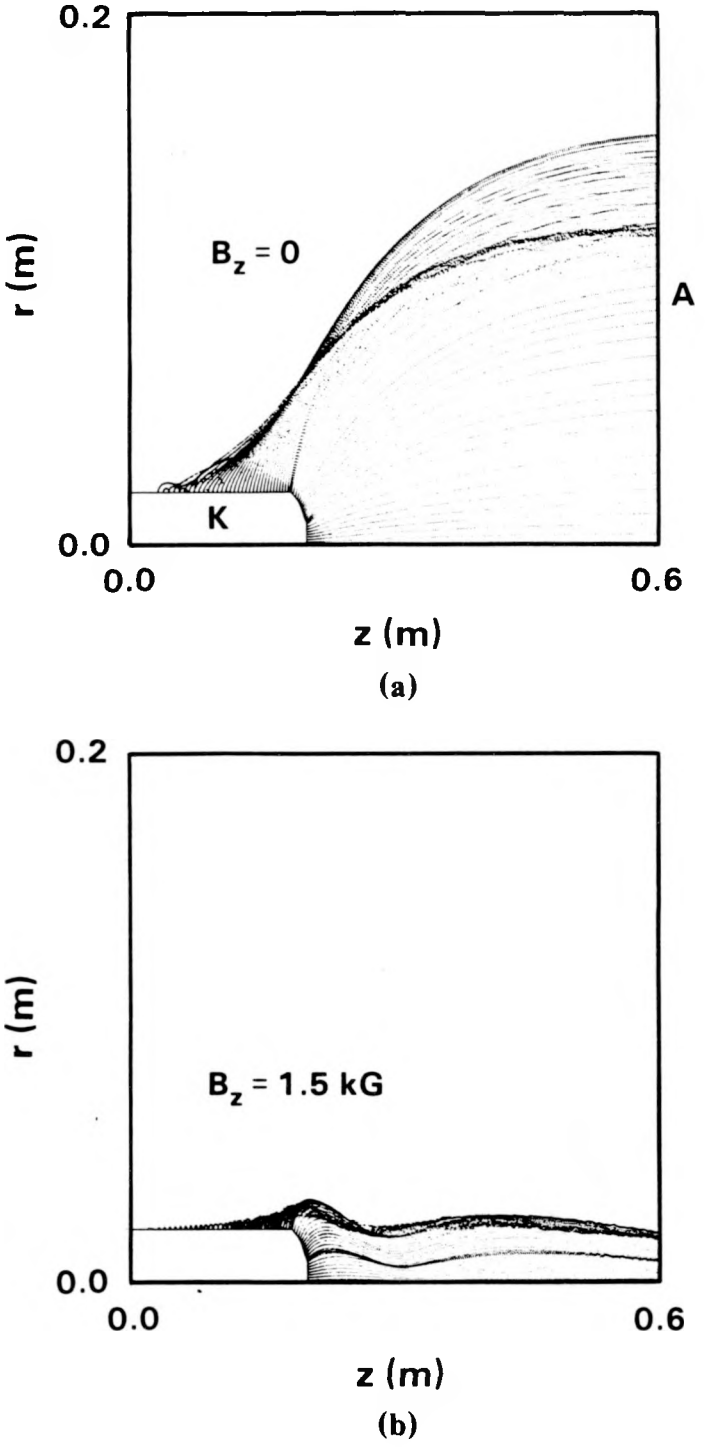

Figure 40. MAGIC runs of RHEPP diode without (a) and with (b) B_z = 1.5 kG. The gap is 40 cm with r_K = 2 cm. The voltage wave is applied from the top (Z_0 = 180 Ω). In (a) we obtain 7.0 kA at 4.45 MV and a large beam normally incident on the anode convertor. In (b) we find 5.5 kA at 4.75 MV and a very small beam.

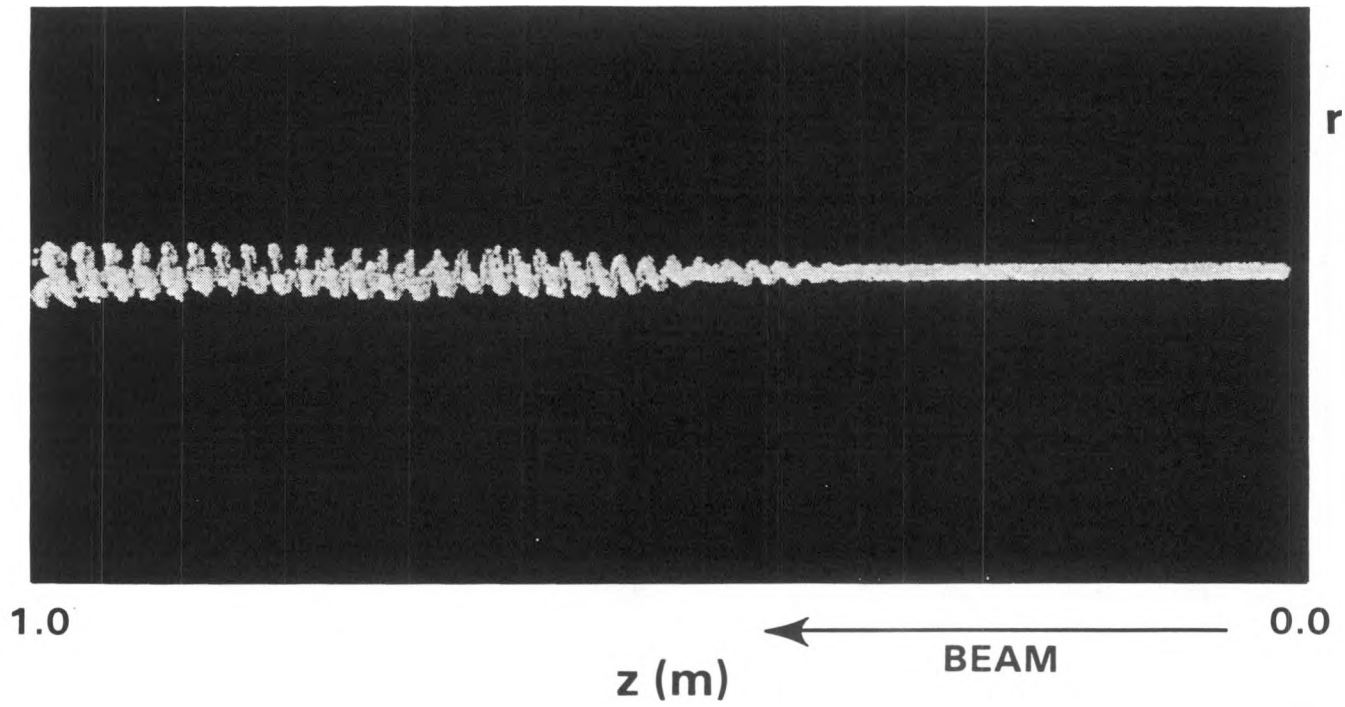

Figure 41. Quicksilver electron map (25,000 electrons) for a 10 kA, γ = 20, r_b = 0.5 cm beam, being guided by a 2 mm wire carrying 15 kA. The initial beam (rhs) is offset by ~1 cm and rotating with β_θ(max) = 0.4. A 5 kA return current is induced. Neither wire nor wall (R = 3.2 cm) are visible. Note the beam evolves into a "corkscrew" mode near the output (lhs); 2 kA are lost. Boundary conditions: perfectly conducting wire, wall, and rhs endplate. The lhs is open.

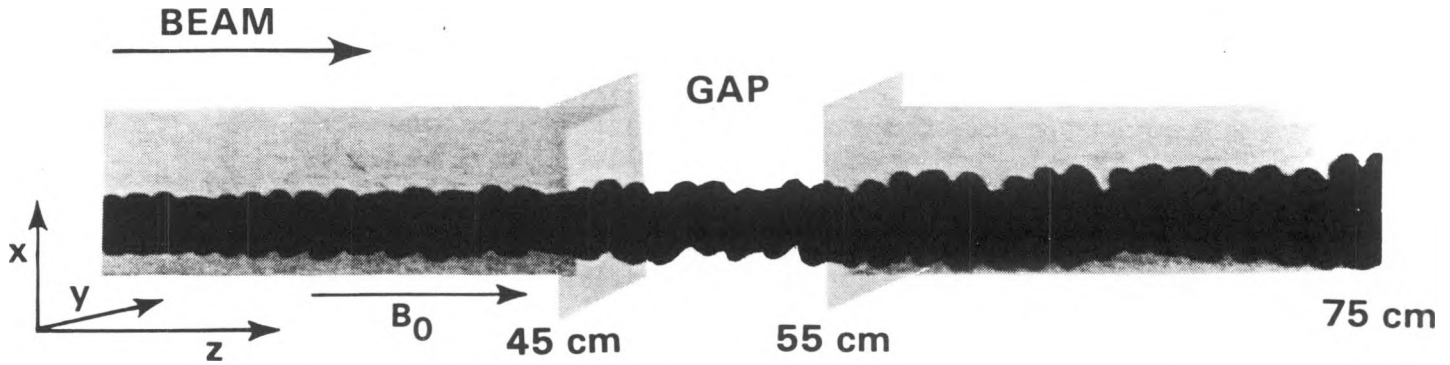

Figure 42. Quicksilver simulation of off-center beam passing through an accelerating gap in B_0 = 15 kG. Beam: 20 kA, 5 MeV, cold, square initial cross-section, offset 1 cm in X. Gap: d = 10 cm, 5.2 MV. Result: beam scrapes wall near output (rhs) end, 1 kA loss.

DISTRIBUTION:
Unlimited Release

Air Force Weapons Laboratory
Kirtland Air Force Base
Albuquerque, NM 87117
Attn: Dr. W. Baker, AWP
Dr. B. B. Godfrey

Applied Physics Branch
Ballistic Modeling Division
Department of the Army
U.S. Army Ballistic Research Lab.
Aberdeen Proving Ground, MD 21005
Attn: D. Eccleshall

Austin Research Associates
1901 Rutland Drive
Austin, TX 78758
Attn: M. L. Sloan

Defense Advanced Research Projects Agency
1400 Wilson Blvd.
Arlington, VA 22209
Attn: H. L. Buchanan
B. Hui

Lawrence Livermore National Laboratory
P. O. Box 808
Livermore, CA 94550
Attn: Simon Yu

Los Alamos National Laboratory
University of California
P.O. Box 1663
Los Alamos, NM 87544
Attn: H. O. Dogliani, H818
J. Mack, P940
T. P. Starke, P942

Mission Research Corporation
1720 Randolph Road, SE
Albuquerque, NM 87106
Attn: D. Welch

Mission Research Corporation
5503 Cherokee Avenue
Alexandria, VA 22312
Attn: Bruce Goplen
Khanh Nguyen

Naval Research Laboratory
Department of the Navy
Washington, D. C. 20375
Attn: M. Lampe
R. Hubbard

Naval Surface Weapons Center
White Oak Laboratory
Silver Spring, MD 20910
Attn: E[illegible]ene [illegible] No[illegible]ing ([illegible])

Pulse Sciences, Inc.
600 McCormick Street
San Leandro, CA 94577-1110
Attn: S. D. Putnam

Science Applications Int'l Corp.
5150 El Camino Real, Suite B-31
Los Altos, CA 94022
Attn: L. Feinstein

Science Applications Int'l Corp.
1710 Goodridge Drive
McLean, VA 22102
Attn: W. Reinstra

Commander
Space & Naval Warfare Systems Command
PMW-145
Washington, DC 20363
Attn: Lt. Bill Fritchie

Titan Technologies-Spectron Division
2017 Yale Blvd., SE
Albuquerque, NM 87106
Attn: R. B. Miller

Internal Distribution:

1000 V. Narayanamurti
1200 J. P. VanDevender
1201 M. J. Clauser
1230 J. J. Ramirez
1231 J. R. Lee
1240 K. R. Prestwich
1241 J. R. Freeman
1241 R. W. Lemke
1241 B. M. Marder
1241 K. J. O'Brien
1241 C. L. Olson
1241 J. W. Poukey (10)
1241 D. B. Seidel
1241 J. S. Wagner
1242 B. N. Turman
1242 C. A. Frost
1242 M. G. Mazarakis
1242 S. L. Shope
1244 J. M. Hoffman
1244 P. D. Coleman
1248 M. T. Buttram
1251 R. J. Lipinski
1260 D. L. Cook
1265 J. P. Quintenz
1270 J. K. Rice
1275 R. A. Gerber
1290 T. H. Martin
3141 S. A. Landenberger (5)
3151 W. I. Klein (3)
3141-1 C. L. Ward for DOE/OSTI (8)
8524 J. A. Wackerly